

**DNA/Metal Oxide Nanoconjugates: Fundamental
Understandings and Analytical Applications**

by

Biwu Liu

A thesis

presented to the University of Waterloo

in fulfilment of the

thesis requirement for the degree of

Doctor of Philosophy

in

Chemistry

Waterloo, Ontario, Canada, 2016

© Biwu Liu 2016

Author's Declaration

I hereby declare that I am the sole author of this thesis. This thesis consists of material all of which I authored or co-authored: see Statement of Contributions included in the thesis. This is a true copy of the thesis, including any required final revisions, as accepted by my examiners. I understand that my thesis may be made electronically available to the public.

Statement of Contributions

The work presented in this thesis is the result of work performed by the author and several scientific collaborations. Contributions from each scientist and the resulting publications are listed in detail below.

The work in Chapter 2 has been accepted as: Biwu Liu and Juewen Liu, DNA Adsorption by Indium Tin Oxide (ITO) Nanoparticles. *Langmuir*, 31, 371-377, 2015. All of experiments were performed by the first author. The manuscript were written by two authors.

The work in Chapter 3 has been accepted as: Biwu Liu and Juewen Liu, DNA Adsorption by Magnetic Iron Oxide Nanoparticles and Its Application for Arsenate Detection. *Chemical Communications*, 50, 8568-8570, 2014. All of experiments were performed by the first author. The manuscript were written by the two authors.

The work in Chapter 4 has been accepted as: Biwu Liu and Juewen Liu, A Comprehensive Screen of Metal Oxide Nanoparticles for DNA Adsorption, Fluorescence Quenching, and Anion Discrimination. *ACS Applied Materials & Interfaces*, 7, 24833-24838, 2015. All of experiments were performed by the first author. The manuscript were written by the two authors.

The work in Chapter 5 is has been accepted as: Biwu Liu, Ziyi Sun, Po-Jung Jimmy Huang and Juewen Liu, Hydrogen Peroxide Displacing DNA from Nanoceria: Mechanism and Detection of Glucose in Serum. *Journal of the American Chemical Society*, 137, 1290-1295, 2015. Ziyi and Jimmy performed the gel electrophoresis experiment. All other experiments were carried out by the first author. The manuscripts were written by the first author and the corresponding author.

The work in Chapter 6 is has been accepted as: Biwu Liu and Juewen Liu, Accelerating Peroxidase Mimicking Nanozymes Using DNA. *Nanoscale*, 33, 13831-13835, **2015**. All of experiments were performed by the first author. The manuscript were written by the two authors.

Abstract

DNA-functionalized nanomaterials have shown versatile applications in biosensor development, biomedical diagnostics, therapy, and catalysis. DNA is attractive for this purpose for its programmable structure, molecular recognition function, and ease of modification. Various nanomaterials, including noble metals, carbons, metal oxides, soft polymeric nanostructures, and metal organic frameworks have been conjugated with DNA. Among them, metal oxide nanoparticles (MONPs) exhibit unique magnetic, catalytic, and surface properties. Most previously reported DNA/MONP conjugates were prepared with the help of surface coating layers or linkers. While such conjugation provides stable hybrid materials, the intrinsic surface properties of MONPs are often masked. The primary focus of this thesis is to interface DNA oligonucleotides with pristine MONPs to provide critical insights into the fundamental understandings at these bio-nano interfaces and to design functional biosensors towards environmentally and biologically important analytes.

In Chapter 2 the interaction between indium-doped tin oxide nanoparticles (ITO NPs) and fluorescently labeled single-stranded DNA (ssDNA) is systematically studied. While electrochemical and photochemical biosensors based on ITO for DNA detection have been developed, little is known about the biointerface chemistry. The DNA adsorption and fluorescence quenching capability of ITO NPs is first confirmed. Salt concentration, pH, DNA sequence and length affect DNA adsorption. The adsorption mechanism is found to be through the phosphate backbone using displacement assays. ITO NPs but not In_2O_3 can discriminate ssDNA and double stranded DNA (dsDNA) based on the difference in their chain flexibility.

In Chapter 3, the interaction between fluorescently labeled DNA and iron oxide nanoparticles is investigated. Fe_3O_4 NPs adsorb DNA via the phosphate backbone and quench the fluorescence. With the strong affinity between arsenate and Fe_3O_4 , a highly sensitive arsenate sensor is demonstrated based on the displacement of fluorescently labeled DNA by arsenate. Arsenate displaces adsorbed DNA to increase fluorescence, allowing the detection of arsenate down to 300 nM. The sensor design represents a new way of using DNA: analyte recognition relying on metal oxide while DNA is used only as a signaling molecule.

In Chapter 4, following the work in Chapter 2 and 3, a total of 19 MONPs are screened for their ability to adsorb DNA, quench fluorescence, and release adsorbed DNA in the presence of a few common anions. These MONPs have different fluorescence quenching properties, DNA adsorption affinity, and different sensitivity toward anions probed by DNA desorption. Finally, CeO_2 , Fe_3O_4 , and ZnO are used to form a sensor array to discriminate phosphate, arsenate, and arsenite from the rest using the linear discriminant analysis method. The study not only provides a solution for anion discrimination using MONPs and DNA but also insights into the interface of metal oxides and DNA.

In Chapter 5, a fluorescently labeled DNA is used as a probe to investigate the interaction between a biologically important molecule, H_2O_2 , and a nanozyme, nanoceria. Nanoceria has been previously reported to bind DNA strongly. I demonstrate that the adsorbed DNA can be readily displaced by H_2O_2 , resulting in over 20-fold fluorescence enhancement. The displacement mechanism instead of oxidative DNA cleavage is confirmed by denaturing gel electrophoresis and surface group pK_a measurements. This system can sensitively detect H_2O_2 down to 130 nM. When coupled with glucose oxidase,

glucose is detected down to 8.9 μM in buffer. Detection in serum is also achieved with results comparable with that from a commercial glucose meter. With an understanding of the ligand role of H_2O_2 , new applications in rational materials design, sensor development, and drug delivery can be further exploited.

In Chapter 6, I demonstrate the feasibility of using DNA in promoting the peroxidase activity of iron oxide nanoparticles. The effect of DNA length, sequence, surface coating are systematically studied. The rate enhancement is more significant with longer DNA. The negatively charged phosphate backbone and bases of DNA can increase the substrate binding, thus facilitating the oxidation reaction in the presence of H_2O_2 . The role of DNA in modulating the peroxidase activity of iron oxide provides insights into the mechanism the nanozymes.

Overall, the adsorption mechanism of DNA by various oxides, the controlling of the catalytic activity of oxides, and the related biosensor applications have been extensively studied in this thesis.

Acknowledgements

I would like to thank my supervisor, Dr. Juewen Liu, for his guidance in the past four years. It was quite risky for him to accept me as his first international graduate student. He would never realize how important it was for me at that moment. All I can do was working hard every day in the past four years. I would also like to extend my gratitude to my PhD committee: Dr. V. Maheshwari, Dr. D. Thomas, and Dr. M. Pope for their guidance at the University of Waterloo. I would also like to thank my external examiner, Dr. Maria DeRosa, for taking time to attend my examination. I would also like to thank Sue Stathopoulos, Howard Siu, and Dara Gilbert for their guidance in my TA terms. I would also like to acknowledge Cathy van Esch and Kim Rawson for their patience and support.

I would also like to thank all my colleagues in the Liu lab for all the happy moments we have experienced together: Dr. Xu Zhang, Dr Hao Liang, Dr Feng Wang, Dr. Jimmy Huang, Imran Khimji, Alex Ip, Jing Cao, Wenhui Zhou, Zijie Zhang, Mahsa Vazin, Runjhun Saran, Howard Tsai, Michael Hoang, Qingyun Chen, James Yu, Yibo Liu, Lingzi Ma, Zhicheng Huang, Xiao Han and Ziyi Sun. I would also like to thank Quan Pang, He Huang, Juntao Tang, Dr. Xiao Liang, and all my friends in Waterloo for making the life so enjoyable.

I would also like to express my gratitude to Prof. Bozhong Mu at the East China University of Science and Technology for his guidance during the three years, and for his supporting me pursuing PhD abroad. I would also like to thank Prof. Shizhong Yang, Dr. Chuanshi Shao, Dr. Xinyu Bian, Dr. Qiqi Zhang, Dr. Yong Meng, Dr. Lei Lv, Dr. Jia You, Yuanyang Rong, and all other members in the Mu lab for their support during the beginning of my graduate study.

To my sisters, Fen Liu and Jing Liu, I would like to say thank-you for taking care of mom and dad, for always being proud of your brother, for supporting all my decisions, and for waiting for my growing up. To my mama and baba, I would like to say thank-you for supporting me finishing this endless graduate study. You may have no idea about what your son is doing in the lab. You may have no idea about a single word in this thesis. But without your love, I cannot get through all of the difficult periods.

Dedication

I would like to dedicate this thesis to my family for their encouragement and support.

Table of Contents

| | |
|--|------|
| Author’s Declaration..... | ii |
| Statement of Contributions | iii |
| Abstract..... | v |
| Acknowledgements..... | viii |
| Dedication..... | x |
| Table of Contents..... | xi |
| List of Figures..... | xvii |
| List of Tables | xx |
| List of Abbreviations | xxi |
| Chapter 1 Introduction | 1 |
| 1.1 DNA as a Functional Molecule..... | 1 |
| 1.1.1 The structure of DNA | 1 |
| 1.1.2 Functional DNA..... | 5 |
| 1.2 DNA in Bionanotechnology | 9 |
| 1.2.1 Interfacing AuNPs with thiolated DNA..... | 10 |
| 1.2.2 Interfacing AuNPs with non-thiolated DNA | 16 |
| 1.3 Metal Oxide Nanomaterials | 19 |
| 1.3.1 Metal oxide-solution interface | 19 |
| 1.3.2 Interfacing metal oxides with DNA..... | 20 |
| 1.3.3 Interfacing metal oxides with arsenic | 24 |
| 1.3.4 Metal oxides with enzyme-like activities | 29 |
| 1.4 Research Goals and Thesis Outline | 37 |

| | |
|---|----|
| 3.2.3 Sensor performance | 63 |
| 3.2.4 Improved sensitivity | 66 |
| 3.3 Materials and Methods..... | 67 |
| 3.3.1 Chemicals..... | 67 |
| 3.3.2 Characterization of Fe ₃ O ₄ NPs | 67 |
| 3.3.3 DNA adsorption by Fe ₃ O ₄ NPs | 68 |
| 3.3.4 Arsenate detection (method 1)..... | 68 |
| 3.3.5 Arsenate detection (method 2)..... | 69 |
| 3.3.6 Arsenate removal | 69 |
| 3.4 Summary | 69 |
| Chapter 4 A Comprehensive Screen of Metal Oxide Nanoparticles for DNA Adsorption, Fluorescence Quenching, and Anion Discrimination | 71 |
| 4.1 Introduction..... | 71 |
| 4.2 Results and Discussions..... | 72 |
| 4.2.1 Rationale of sensor design | 72 |
| 4.2.2 Screen for DNA adsorption | 75 |
| 4.2.3 Screen for DNA desorption | 77 |
| 4.2.4 Sensor optimization | 81 |
| 4.2.5 Array-based anion sensing..... | 82 |
| 4.3 Materials and Methods..... | 86 |
| 4.3.1 Chemicals..... | 86 |
| 4.3.2 Instrumentation | 86 |
| 4.3.3 DNA adsorption capability of MONPs..... | 87 |

| | |
|--|-----|
| 4.3.4 DNA desorption by anions. | 87 |
| 4.4.5 Effect of DNA sequence on desorption. | 88 |
| 4.4.6 Sensor array for anion discrimination..... | 88 |
| 4.4 Summary..... | 89 |
| Chapter 5 DNA/Cerium Oxide Nanoparticles with Catalase-like Activity: Detection of H ₂ O ₂ and Glucose | 90 |
| 5.1 Introduction..... | 90 |
| 5.2 Results and Discussions | 92 |
| 5.2.1 Sensor rationale and proof of concept | 92 |
| 5.2.2 Effect of ionic strength | 94 |
| 5.2.3 Effect of pH | 95 |
| 5.2.4 Effect of DNA sequence and length | 96 |
| 5.2.5 Mechanistic investigations..... | 97 |
| 5.2.6 Detection of H ₂ O ₂ and glucose | 102 |
| 5.3 Materials and Methods..... | 106 |
| 5.3.1 Chemicals..... | 106 |
| 5.3.2 Washing CeO ₂ nanoparticles | 107 |
| 5.3.3 Transmission electron microscopy and UV-vis spectroscopy..... | 107 |
| 5.3.4 Kinetics of H ₂ O ₂ decomposition..... | 107 |
| 5.3.5 Dynamic light scattering (DLS) measurement | 108 |
| 5.3.6 DNA adsorption kinetics and capacities | 108 |
| 5.3.7 H ₂ O ₂ -induced DNA desorption | 108 |
| 5.3.8 Potentiometric and Conductometric Titration. | 109 |

| | |
|---|-----|
| 5.3.9 Gel Electrophoresis..... | 110 |
| 5.3.10 pH monitoring..... | 110 |
| 5.3.11 Detection of glucose in buffer and in serum..... | 110 |
| 5.4 Summary..... | 111 |
| Chapter 6 DNA/Iron Oxide Conjugates with Enhanced Peroxidase-like Activity..... | 112 |
| 6.1 Introduction..... | 112 |
| 6.2 Results and Discussions..... | 113 |
| 6.2.1 Characterization of Fe ₃ O ₄ NPs | 113 |
| 6.2.2 Proof of concept..... | 115 |
| 6.2.3 Effect of DNA sequence, length, and concentration..... | 117 |
| 6.2.4 Effect of pH | 119 |
| 6.2.5 Mechanistic investigation | 120 |
| 6.3 Materials and Methods..... | 126 |
| 6.3.1 Chemicals..... | 126 |
| 6.3.2 Modification of iron oxide NPs | 127 |
| 6.3.3 Transmission Electron Microscopy (TEM) and UV-vis spectroscopy..... | 127 |
| 6.3.4 ζ-potential measurement | 128 |
| 6.3.5 Inhibition of DNA adsorption..... | 128 |
| 6.3.6 Peroxidase activity assays of Fe ₃ O ₄ NPs | 128 |
| 6.3.7 Activity of CeO ₂ NPs..... | 129 |
| 6.3.8 Gel electrophoresis | 129 |
| 6.4 Summary..... | 130 |
| Chapter 7 Conclusions and Future Work..... | 131 |

| | |
|----------------------------------|-----|
| 7.1 Conclusions..... | 131 |
| 7.2 Original Contributions | 133 |
| 7.2 Future Work..... | 135 |
| References..... | 137 |

List of Figures

| | |
|--|----|
| Figure 1.1 Chemical structures of DNA.. | 2 |
| Figure 1.2 Interaction forces between DNA bases.. | 3 |
| Figure 1.3 Typical structures formed by non-canonical base pairing.. | 6 |
| Figure 1.4 Examples of DNA aptamers.. | 7 |
| Figure 1.5 DNA as building blocks to form nanostructures.. | 9 |
| Figure 1.6 Schematics of conjugating thiolated DNA with AuNPs.. | 12 |
| Figure 1.7 Cooperative effect in the DNA/AuNPs assembly/melting process.. | 15 |
| Figure 1.8 Interaction between DNA bases and AuNPs.. | 17 |
| Figure 1.9 Schematics of DNA detection using AuNPs.. | 18 |
| Figure 1.10 Surface properties of metal oxides in aqueous solutions.. | 20 |
| Figure 1.11 Schematics of interaction mechanisms of anion with iron oxides.. | 28 |
| Figure 1.12 Nanoceria with oxidase-like activity.. | 32 |
| Figure 1.13 Schematics of sensing H ₂ O ₂ and glucose using nanozymes with peroxidase-like activity and GOx.. | 34 |
| Figure 2.1 TEM micrographs of NPs used in this work.. | 42 |
| Figure 2.2 Dynamic light scattering measurement of three NPs.. | 43 |
| Figure 2.3 Effect of pH on DNA adsorption by ITO NPs.. | 44 |
| Figure 2.4 Effect of ionic strength on DNA adsorption and desorption by ITO NPs..... | 47 |
| Figure 2.5 DNA (FAM-DNA2) adsorption isotherm by ITO NPs.. | 48 |
| Figure 2.6 DNA adsorption as a function of sequence and length.. | 49 |
| Figure 2.7 Mechanistic investigation of DNA on ITO NPs.. | 50 |
| Figure 2.8 DNA detection using DNA/ITO conjugates..... | 52 |

| | |
|--|----|
| Figure 3.1 Design and proof of concept for arsenate sensor using DNA/Fe ₃ O ₄ NPs.. | 59 |
| Figure 3.2 DNA adsorption behaviour by Fe ₃ O ₄ NPs.. | 62 |
| Figure 3.3 Desorption of the FAM-T ₁₅ from Fe ₃ O ₄ NPs by free phosphate or thymidine, demonstrating DNA adsorption occurs via the phosphate backbone. | 63 |
| Figure 3.4 Performance of FAM-C ₁₅ /Fe ₃ O ₄ conjugates as a sensor for arsenate and arsenite.. | 64 |
| Figure 3.5 Selectivity of sensor in arsenate detection..... | 65 |
| Figure 3.6 Improved sensitivity by pre-adsorbing arsenate..... | 67 |
| Figure 4.1 Schematics of the sensing strategy. | 73 |
| Figure 4.2 DNA adsorption and fluorescence quenching by various MONPs. | 76 |
| Figure 4.3 Fluorescence quenching efficiency of the FAM-24 mer DNA by ZnO NPs and Y ₂ O ₃ NPs.. | 77 |
| Figure 4.4 Phosphate-induced DNA release from various MONPs:.. | 79 |
| Figure 4.5 Effect of other oxyanions on DNA desorption..... | 80 |
| Figure 4.6 Optimization of sensor performance.. | 82 |
| Figure 4.7 Signal enhancement of FAM-labeled DNA adsorbed onto various MONPs. | 84 |
| Figure 4.8 The canonical score plot for fluorescence enhancement using three DNA/MONP (CeO ₂ , Fe ₃ O ₄ , and ZnO) sensors. | 85 |
| Figure 5.1 Fluorescent sensing H ₂ O ₂ by a DNA/nanoceria complex. | 93 |
| Figure 5.2 Effect of salt concentration on DNA recovery by H ₂ O ₂ | 95 |
| Figure 5.3 Effect of pH on DNA recovery by H ₂ O ₂ | 96 |
| Figure 5.4 Effect of DNA and length..... | 97 |
| Figure 5.5 Gel electrophoresis to check DNA integrity..... | 98 |

| | |
|--|-----|
| Figure 5.6 Potentiometric and conductometric titration. | 99 |
| Figure 5.7 Kinetics of pH change after mixing H ₂ O ₂ and nanoceria (1.5 mg/mL) in water or in 10 mM HEPES (pH 7.6) (left axis) and kinetics of H ₂ O ₂ decomposition with 3 μg/mL nanoceria (right axis). | 100 |
| Figure 5.8 A proposed mechanism of H ₂ O ₂ -induced DNA release by capping the nanoceria surface..... | 102 |
| Figure 5.9 Sensor performance in H ₂ O ₂ detection..... | 103 |
| Figure 5.10 Sensor performance for glucose detection..... | 105 |
| Figure 6.1 Characterization of Fe ₃ O ₄ NPs used in this work. | 114 |
| Figure 6.2 Proof of concept study of the effect of DNA on the TMB oxidization.. | 116 |
| Figure 6.3 Effects of DNA on the kinetics of TMB oxidation catalysed by DNA-modified Fe ₃ O ₄ NPs. | 118 |
| Figure 6.4 Effects of pH on the DNA-induced enhancement. | 120 |
| Figure 6.5 Kinetics of Alexa-DNA (50 nM) adsorption onto Fe ₃ O ₄ NPs (25 μg/mL) at pH 4 (acetate buffer, 10 mM).. | 121 |
| Figure 6.6 Gel image of DNA-Fe ₃ O ₄ treated with H ₂ O ₂ | 122 |
| Figure 6.7 Effect of electrostatic interaction on the DNA-induced enhancement.. | 123 |
| Figure 6.8 Effect of surface coating the peroxidase activity of Fe ₃ O ₄ NPs..... | 124 |
| Figure 6.9 Effect of DNA on the oxidase and peroxidase-like activity of nanoceria. | 125 |

List of Tables

| | |
|---|-----|
| Table 1.1 Metal oxide nanoparticles as enzyme-mimics | 35 |
| Table 2.1 The sequences and modification of DNA used in this work..... | 53 |
| Table 4.1 Information of metal oxides nanoparticles (MONPs) used in this work | 74 |
| Table 4.2 DNA sequences and concentrations for MONPs in the final sensor array. | 89 |
| Table 5.1 The sequences and modification of DNA used in this work..... | 106 |
| Table 6.1 ζ -potential of iron oxide NPs at various conditions | 114 |
| Table 6.2 The sequences and modification of DNA used in this work..... | 126 |

List of Abbreviations

| | |
|----------|--|
| A | adenine |
| ABTS | 2,2'-azino-bis(3-ethylbenzothiazoline-6-sulphonic acid |
| AFM | Atomic force microscopy |
| AuNPs | gold nanoparticles |
| bps | base pairs |
| C | cytosine |
| cDNA | complementary DNA |
| DA | dopamine |
| DAB | 3,3'-diaminobenzidine |
| DLS | dynamic light scattering |
| DNA | deoxyribonucleic acid |
| DNAzymes | catalytic DNA |
| dsDNA | double stranded DNA |
| FAM | 6-carboxyfluorescein |
| FBS | fetal bovine serum |
| G | guanine |
| GMP | guanosine monophosphate |
| GOx | glucose oxidase |
| GSH | glutathione |
| HEPES | 4-(2-hydroxyethyl) piperazine-1-ethanesulfonic acid |
| HRP | horseradish peroxidase |
| HR-TEM | high resolution transmission electron microscopy |
| ICP-MS | inductively coupled plasma mass spectrometry |
| ITO | indium tin oxide |

| | |
|-----------|--------------------------------------|
| ITO NPs | indium tin oxide nanoparticles |
| K_{cat} | rate constant |
| K_m | Michealis-Menten constant |
| LOD | detection o limit |
| MES | 2-(N-morpholino) ethanesulfonic acid |
| MONPs | metal oxide nanoparticles |
| OPD | o-phenylenediamine dihydrochloride |
| PAA | polyacrylic acid |
| PCR | polymerase chain reaction |
| PSS | polystyrene sulfonate |
| PZC | point of zero charge |
| RNA | ribonucleic acid |
| ROS | reactive oxygen species |
| sDNA | same DNA, no fluorophore |
| SOD | superoxide dismutase |
| ssDNA | single stranded DNA |
| T | thymine |
| TEM | transmission electron microscopy |
| TMB | 3,3',5,5'-tetramethylbenzidine |
| WHO | World Health Organization |

Chapter 1 Introduction

1.1 DNA as a Functional Molecule

1.1.1 The structure of DNA

Deoxyribonucleic acid (DNA) is the genetic information carrier of living organisms. Investigation into its biological functions has revolutionized human's insights into nature. In the past decades, DNA has also shown potential in chemistry, physics, material science, energy, and even computer science.^{1,2,3,4} The wide applications are attributable to the versatile functionalities of DNA, including molecular recognition, catalysis, constructing nanostructures, to name a few. From a chemical viewpoint, all of such functions are rooted from the unique structure of DNA.

1.1.1.1 Chemical components

DNA is a thread-like linear biopolymer and it has an extensive secondary structure. Two strands run in opposite directions (antiparallel, B-form) and twisted together to form a right-handed double helix (Figure 1.1A). Each strand is made up of four types of units called nucleotides (Figure 1.1B). A nucleotide is constructed from three components: a heterocyclic base or nucleobase, a pentose sugar, and a phosphate residue. The nucleobases for DNA are adenine (A), guanine (G), cytosine (C), and thymine (T) (Figure 1.1C). Nucleosides are the combination of a nucleobase and a monosaccharide (ribose in ribonucleic acid, RNA and 2-deoxyribose in DNA) (Figure 1.1D) Nucleotides are the phosphate esters of nucleosides, in which phosphate is typically joined to 5' position of the

sugar ring (Figure 1.1B). In DNA, nucleotides are linked via the phosphodiester bonds between the phosphate of one nucleotide and the 3' hydroxyl group of another one.

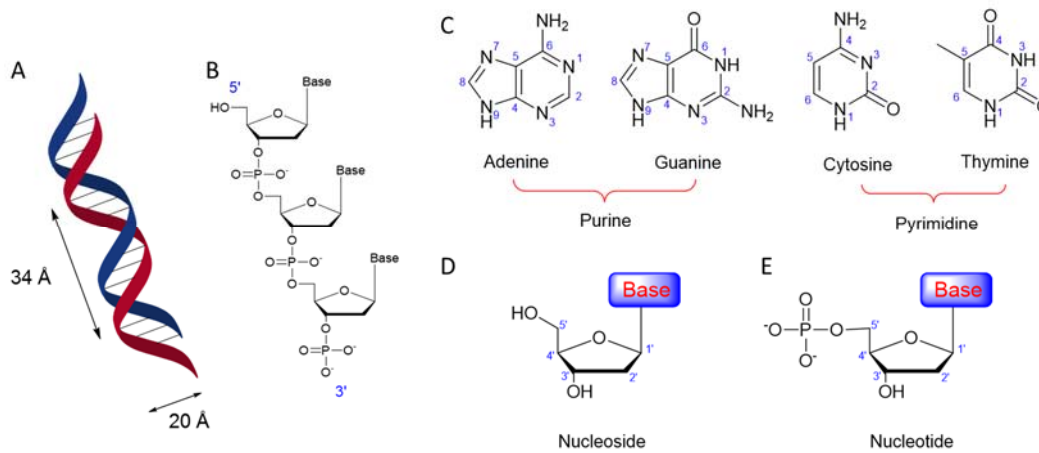


Figure 1.1 Chemical structures of DNA. (A) The double helix structure of double-stranded DNA. (B) A single-stranded DNA. (C) Four types of nucleobases in DNA. (D) Nucleosides composed of a nucleobase and a sugar. (E) Nucleotides composed of a phosphate, a nucleobase and a sugar.

The diameter of the most common B-DNA is 20 Å, and the vertical distance between adjacent DNA base pairs is 3.4 Å. Natural DNA typically contains thousands to millions of base pairs (bps) with a coiled or super-coiled structure in the biologically environment. However, short oligonucleotides can form persistent double helix up to 46-50 nm (i.e., 140-150 bps).⁵ Beyond that, DNA can no longer be treated as a rigid rod. My research is mainly focused on using short ssDNA (< 50-mer) as functional molecules in nanotechnology. Therefore, the following introduction will be mainly focused on short ssDNA or oligonucleotide, simply referred as DNA.

In the double helix structure, the sugar and phosphate backbone of the two DNA strands are exposed to the environment, whereas the nucleic bases are embedded. To hold

the two strands together, both hydrogen bonds and π - π stacking are involved. Hydrogen bonds are formed specifically between purine and pyrimidine bases. The A-T base pair possesses two hydrogen bonds, while G forms three hydrogen bonds with C (Figure 1.2A). Besides these canonical Watson-Crick base pairing, many other base pairings, for example Hoogsteen pairing, have also been identified.⁶ Stacking from adjacent DNA bases also makes contributions and even plays a dominant role in stabilizing the DNA duplex. Pi-stacking (π - π stacking) is the non-covalent attraction between aromatic rings with different modes (Figure 1.2B). In DNA structures, the bases are positioned face-to-face with offset orientation (Figure 1.2B, model ii).⁶

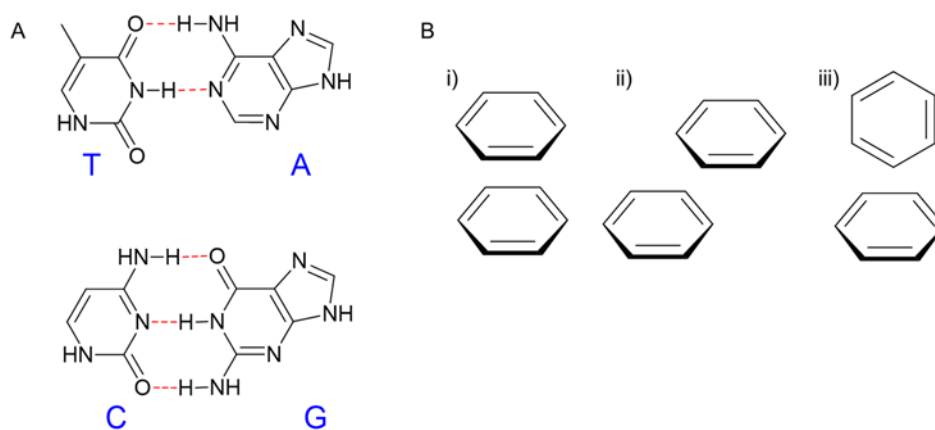


Figure 1.2 Interaction forces between DNA bases. (A) Canonical hydrogen bonds. (B) Typical π - π stacking modes: i) parallel face-centred, ii) parallel offset, and iii) perpendicular T-shaped.

1.1.1.2 Physicochemical properties of DNA

DNA is an anionic polymer in a physiological environment. The negative charge is mainly due to the phosphate backbone, which has a pK_a around 2.⁷ At the same time, the 2-deoxyribose are not charged. Protonation/deprotonation of DNA bases occur when the pH

is altered. For example, the N(7) of adenine can be half protonated when lowering the pH down to 3.5, resulting in a positive DNA base. A DNA strand rich in adenine (A), therefore, has a lower negative charge density at acidic environment. Such pH-dependent charge alternation is important in understanding the interaction between DNA and other biomolecules or materials.

With three distinct components, phosphate, sugar and bases, DNA provides multiple interaction modes with incoming substances.^{7,8} The negative charged phosphate backbone offers electrostatic interaction forces with positively charge molecules (e.g., proteins, metal ions). The nucleophilic phosphate residue can also bind to some hard Lewis acid via coordination bonds. The sugar ring in DNA lacks interaction sites with other molecules. DNA bases can form hydrogen bonds either as donor or as acceptors or both. The base ring can also achieve π - π stacking with aromatic molecules or materials rich in π electrons. The exocyclic keto group and base ring nitrogen can bind to certain metal ions by donating lone-pair electrons to form dative bonds.

1.1.1.3 DNA synthesis and modification

Long dsDNA can be isolated from cell nuclei. Modern molecular biology also provides methods (e.g., polymerase chain reaction, PCR) in synthesizing DNA. However, with these methods, only a small amount of long DNAs is obtained. For nanotechnology, short ssDNA is required. Thanks to chemical synthesis, solid-phase synthesis in particular, DNA with arbitrary sequence and length can now be readily prepared. Providers can deliver purchased DNA with high quality within days.

Furthermore, functional groups can be incorporated at specific positions of a DNA sequence during the chemical synthesis process. Typical functional groups include organic

fluorophores and linking groups. Fluorescence is a widely used technique in monitoring biomolecules with high sensitivity. However, DNA is intrinsically non-fluorescent. Organic fluorophores can be easily attached to DNA, making them tractable. Another important modification is the attaching of a linking group. For example, thiolated DNA now is routinely used in constructing DNA-modified gold nanoparticles (AuNPs), electrodes, and microarrays. Amino-modified DNA can be used to conjugate with molecules containing a carboxyl group. Biotin-modified DNA can be strongly attached to a target substance with a streptavidin based on the well-established biotin-streptavidin chemistry.⁹

1.1.2 Functional DNA

DNA had been considered to be chemically inert for a long time due to the stable double helix structures. Since the early 1990s, DNA has found versatile chemical functions in a diverse range of fields. Some typical functionalities are introduced to illustrate the use of DNA in molecular recognition and nanotechnology.

1.1.2.1 Base pairing

DNA can hybridize to its complementary strands based on the Watson-Crick base pairing, which forms the basis of many DNA detection technologies (e.g., DNA microarray). Aside from the Watson–Crick base pairing or canonical base pairing, non-canonical base pairing also exists in DNA, for example, G-quadruplexes and i-motif structures (Figure 1.3).¹⁰ G-quadruplexes are formed in guanine-rich nucleic acids. Four G bases composes a G-tetrapad via Hoogsteen hydrogen bonding (Figure 1.3A), and this square plane can be further stabilized by certain cations (e.g., K⁺). DNA rich in cytosine

can form quadruple-stranded structure (i.e., i-motif) under acidic conditions. In 1993, Gehring *et al.* discovered four strands of oligonucleotide (TCCCC) form the intermolecular i-motif.¹¹ The strands are held together by hydrogen bonding formed between cytosine and protonated cytosine (Figure 1.3B). Intramolecular i-motif can also be formed in C-rich DNA (Figure 1.3D). To form the i-motif, one of the cytosine bases in the base pairs requires to be protonated. Reversible folding and unfolding can be achieved by adjusting the solution pH.¹²

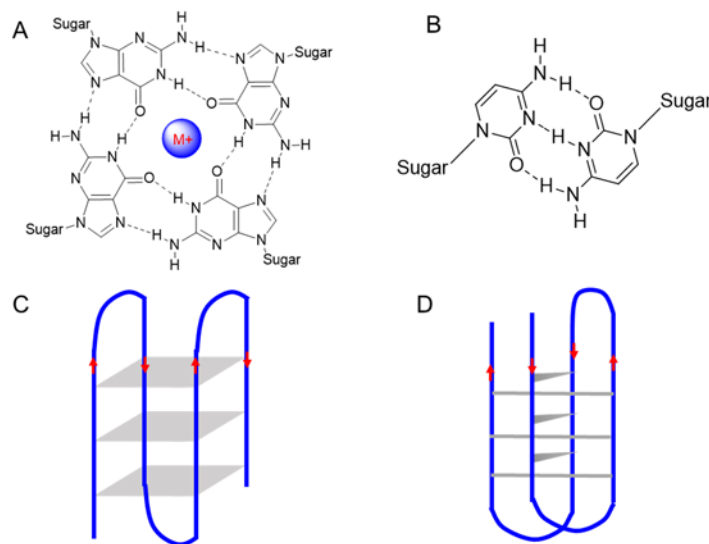


Figure 1.3 Typical structures formed by non-canonical base pairing. (A) A G-quadruplex plane composed by four G bases in the presence of metal ions. (B) Base pairing between two C with one protonated. (C) A schematic of G-quadruplex formed by G-rich DNA, (D) A schematic of i-motif structure formed by C-rich DNA.

1.1.2.2 DNA aptamers

Aptamers are single-stranded DNAs or RNAs that can bind to analytes beyond complementary sequences with high affinity and specificity. DNA aptamers can recognize various targets, including metal ion, small molecules, proteins, and even cells.^{13,14} In 1992, Bock and co-workers isolated the first DNA thrombin aptamer with a binding affinity (K_d)

in the range 25-200 nM thrombin.¹⁵ Structural investigation revealed that the ssDNA forms an intramolecular G-quadruplex (Figure 1.4A). The selection of a DNA aptamer for ATP was reported in 1995 by Huizenga and Szostak.¹⁶ This aptamer can also bind adenosine and AMP with a similar affinity. It was indicated two targets molecules (red dots in Figure 1.4 B) bind to one aptamer by forming a non-canonical G-A base pair.¹⁷ Over the last two decades a large number of DNA aptamers have been isolated and a few searchable aptamer databases were established.^{18,19,20}

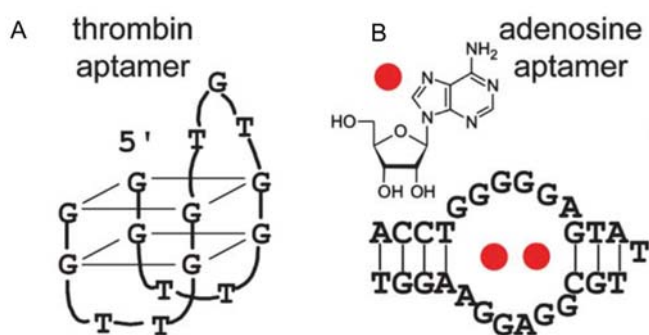


Figure 1.4 Examples of DNA aptamers. (A) A protein thrombin aptamer with a G-quadruplex structure. (B) A adenosine aptamer binds two targets with G-A base pair, Figure adapted with permission from ref (²¹). Copyright © Royal Society of Chemistry.

Aptamers are sometimes called chemical antibodies. Compared to real antibodies, aptamers exhibit similar even better binding affinity and specificity.⁴ At the same time, aptamers can be prepared in a more cost-effective way with large quantities using chemical synthesis. In addition, aptamers, especially DNA aptamers, are more thermal stable. Upon heating, antibodies may lose their secondary structures and hence functionality. But DNA can maintain its functionality even after several cycles of heating and cooling.⁴

1.1.2.3 DNAzymes

DNA can also function as enzymes with catalytic functions.⁴ In the early 1980s, Cech²² and Altman²³ discovered that natural RNA (ribozymes) can act as enzymes, catalyzing a lot of chemical reactions. More than a decade later, catalytic DNA (DNAzymes) was found by *in vitro* selection.²⁴ A diverse range of reactions, including RNA cleavage, DNA cleavage, RNA ligation, DNA ligation, DNA phosphorylation, and amide hydrolysis can now be catalyzed by DNAzymes.²⁵ These discoveries have revolutionized the long-lasting concept of enzymes.

1.1.2.4 DNA nanostructures

The simple base pairing principle can not only be used in cDNA detection, but also in constructing DNA-based nanostructures. In early 1980s, Seeman and co-workers first reported the self-assembly of four ssDNAs into a four-way junction.^{26,27} The branched DNA junctions further assembled into 2-D lattice via the sticky ends (Figure 1.5A). In 2009, the Seeman group successfully obtained the 3-D DNA crystals using well designed connectors with proper sticky ends.²⁸ Another interesting DNA nanostructure is DNA origami. In 2006, Rothemund reported that he was able to assemble a 7-kilobase ssDNA with over 200 short ssDNAs into various 2-D shapes (Figure 1.5C).²⁹ After this seminal work, several groups reported the assembly of DNA origami with 3-D structures.^{30,31,32}

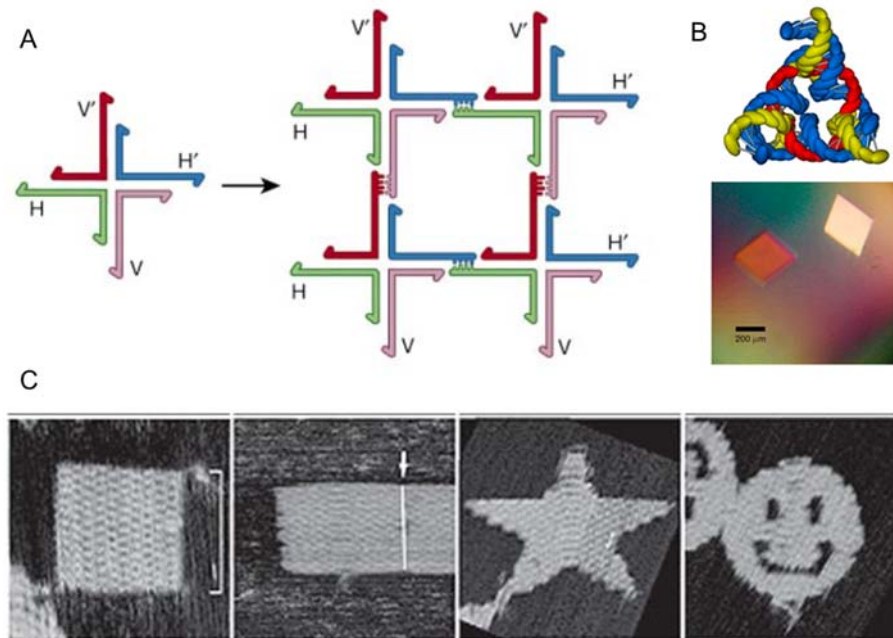


Figure 1.5 DNA as building blocks to form nanostructures. (A) Four ssDNA assembled into a four-way junction and further into 2-D lattice.³³ (B) 3-D DNA crystals formed by DNA with sticky-ends (top, the motif structure; bottom, the optical image of the crystal).²⁸ (C) Atomic force microscopy (AFM) images of DNA origami nanostructures with different shapes (from left to right): square, rectangle, star, and smiley face.²⁹ Figure adapted with permission from: (A) ref (³³) Copyright © Nature Publishing Group; (B) ref (²⁸) Copyright © Nature Publishing Group; and (C) ref (²⁹) Copyright © Nature Publishing Group.

1.2 DNA in Bionanotechnology

The last few decades have witnessed the rapid development of nanotechnology. Nanomaterials generally refer to materials whose scales, at least one dimension, are between 1-100 nm. The nanoscale materials exhibit dramatic different electronic, mechanical, and optical properties compared to their bulk counterparts. One of the major

features of nanomaterials is the high surface-to-volume ratios, which allows the further modification with functional molecules. The convergence of nanotechnology and biology has resulted in the development of bionanotechnology. These “value-added” bio-nano conjugates combine the recognition property of biomaterials and the unique catalytic, electronic and optical features of nanomaterials and find promising values in tissue engineering, drug and gene delivery, biosensing and imaging, diagnostics, and cancer therapy.^{9,34}

DNA has been extensively coupled to nanomaterials in biological and medical applications.^{4,10,35,36,37} As mentioned above, DNA can hybridize with its complementary strands. DNA aptamers can recognize versatile targets with high sensitivity and selectivity, such as metal ions, cancer biomarkers, proteins, and even cells. DNAzymes are able to catalyze chemical reactions in the presence of cofactors. On the other hand, the nanomaterials possess optical, magnetic, and mechanical properties. DNA-modified nanomaterials combine the functions of each component. DNA-functionalized AuNPs is perhaps the most mature example in bionanotechnology. Here, using DNA/AuNPs as an example, I will introduce the conjugation strategies, properties, and some typical applications in biosensing.

1.2.1 Interfacing AuNPs with thiolated DNA

1.2.1.1 Modifying AuNPs with thiolated DNA

In 1996, the Mirkin group³⁸ and the Alivisatos group³⁹ first reported the coupling of DNA with AuNPs and controlled assembly. To prepare the conjugates, thiolated DNA was used in both works since thiol forms a strong dative bond with gold.⁹ However, the

commonly used AuNPs have negatively charged citrate ions on the surface. DNA is also negatively charged because of its phosphate backbone. The conjugation of DNA with AuNPs is, as a result, inhibited by electrostatic repulsion. While adding NaCl can inhibit this charge repulsion, it may also cause irreversible aggregation of AuNPs. To solve this problem, Mirkin and coworkers proposed a salt-aging strategy to obtain DNA/AuNPs with retained colloidal stability.⁴⁰ In the method (Figure 1.6A), NaCl is gradually added to facilitate DNA attaching and to avoid particle aggregation. Furthermore, AuNPs with a small amount of DNA strands can withstand the addition of more NaCl. Finally, AuNPs with a high DNA density are obtained. Approximately 180 strands of thiolated DNA can be attached on a 20 nm AuNP when the concentration of NaCl is close to 1 M.⁴⁰ Based on the calculation of DNA footprint on AuNPs surface, a standing-up conformation of DNA strands was proposed.⁴¹ The high density and resulted standing-up conformation of DNA is important in achieving the collective effect of DNA-functionalized AuNPs in biosensing, assembly, and cellular uptake.

While the salt-aging method has been generally accepted in preparing DNA/AuNPs, the process is quite time-consuming (~ 2 days). Several alternative methods were then raised to shorten the preparation process. Protection agents (e.g., surfactants) were used to replace citrate ions on AuNPs surface.⁴² In this way, NaCl can be added quickly to the DNA/AuNPs mixture without aggregating AuNPs. However, these methods still need a long incubation time, and remaining capping agents can be potentially toxic in a biological environment. Zhang and co-workers reported a facile method to prepare reliable DNA/AuNPs within 3 min.⁴³ After mixing DNA with AuNPs, they simply adjusted the solution pH to 3 using a citrate buffer and achieved instantaneous attachment of thiolated

DNA to AuNPs. The mechanism was proposed to be a synergistic effect between pH and salt. At lower pH, both DNA and citrate-capped AuNPs can be partially protonated. The charge repulsion is then significantly reduced and the strong bonding between gold and thiol takes place. This convenient method has also been successfully applied in functionalizing gold nanorods⁴⁴ and silver nanoparticles⁴⁵ with thiolated DNA.

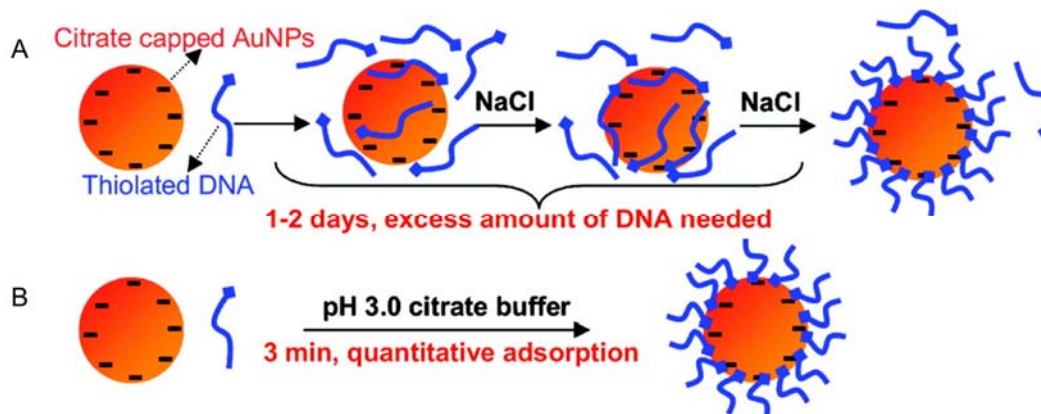


Figure 1.6 Schematics of conjugating thiolated DNA with AuNPs. (A) The salt-aging method. (B) The low pH method. Figure adapted with permission from ref (⁴³). Copyright © American Chemical Society.

1.2.1.2 Features of AuNPs with thiolated DNA

The DNA/AuNPs conjugates combine the properties of each component. Using thiolated DNA, a high DNA density on AuNPs surface can easily be achieved. With this DNA layer, the conjugates exhibit some improved and even distinct properties.

Improved colloidal stability. Due to the large surface-to-volume ratio and high free energy, colloidal nanoparticles tend to aggregate. The unwanted particle aggregation should be avoided since it may dramatically alter the physiochemical properties of nanomaterials. DNA is a negatively charged biopolymer. Once attaching DNA strands onto

the nanoparticles surface, the stability of colloidal nanoparticles can be improved via two stabilization mechanisms: electrostatic repulsion and steric effect. For example, the commonly used AuNPs are capped and stabilized by the weakly adsorbed citrate ions. Simply adding NaCl results in irreversible particle aggregation indicated by the color change and precipitation. However, with a DNA modification layer, AuNPs maintain the colloidal stability.^{40,43,46,47} This improved stability highlights the importance of the negative DNA layer in withstanding the increased ionic strength. Furthermore, even aggregated by adding a higher concentration of NaCl, the AuNPs precipitate can well re-disperse in water without aggregation. The re-dispersion of AuNPs precipitates suggests that the DNA layer also provides steric effect and prevents AuNPs interacting with each other.

The conjugation of DNA with nanomaterials not just improves the stability of nanomaterials, but also inhibits the degradation of DNA by enzymes (e.g., DNase I). Compared to the free DNA in solution, DNA attached on AuNPs showed a slower digestion.⁴⁸ This protection effect is particularly important in gene delivery, which requires a long pathway before arriving at the targeting sites.

Enhancing molecular recognition. In homogenous solution, DNA molecules are uniformly dispersed. However, on the surface of nanomaterials, a high local DNA density is achieved. It has been reported that this high density DNA can function cooperatively and fundamentally alter the recognition process, also known as synergism. DNA immobilized on the surface of AuNPs also showed improved binding affinity towards its cDNA compared to the molecular counterpart.⁴⁹ In the seminal work, Mirkin and co-workers proved that the melting of spherical nucleic acid (DNA-modified spherical AuNPs)

occurred in a much narrower temperature window. The sensing platform was designed by modifying 13-nm AuNPs with two distinct probe ssDNAs (Figure 1.7A, blue and red strands). The linking DNA was designed to have two blocks, each of which was complementary to the probe DNA on AuNPs surface. In the absence of DNA target, the AuNPs were well separated, showing red color in solution. Once introducing DNA target, AuNPs aggregates were formed, showing blue color. If the temperature was increased, the DNA-AuNPs aggregates can disperse in solution again, resulting in the recovery of red color. This melting behavior was also monitored by the variation of absorbance at 260 nm (Figure 1.7C). The melting curves were much sharper compared to that of conventional fluorophore-labeled DNA.

A detailed study of the melting behavior of DNA/AuNPs aggregates was carried out by the Mirkin group.⁵⁰ Several parameters, including salt concentration, DNA surface density, length of linker DNA, and particle size, may affect the melting curves. It was observed that particles size significantly affect the sharpness of melting profiles. A cooperative melting model was provided to explain the sharp melting profiles. The high density of DNA probes on AuNPs offer multiple links between nanoparticles. Also, the high local salt concentration of DNA/AuNPs conjugates determines the melting temperature.

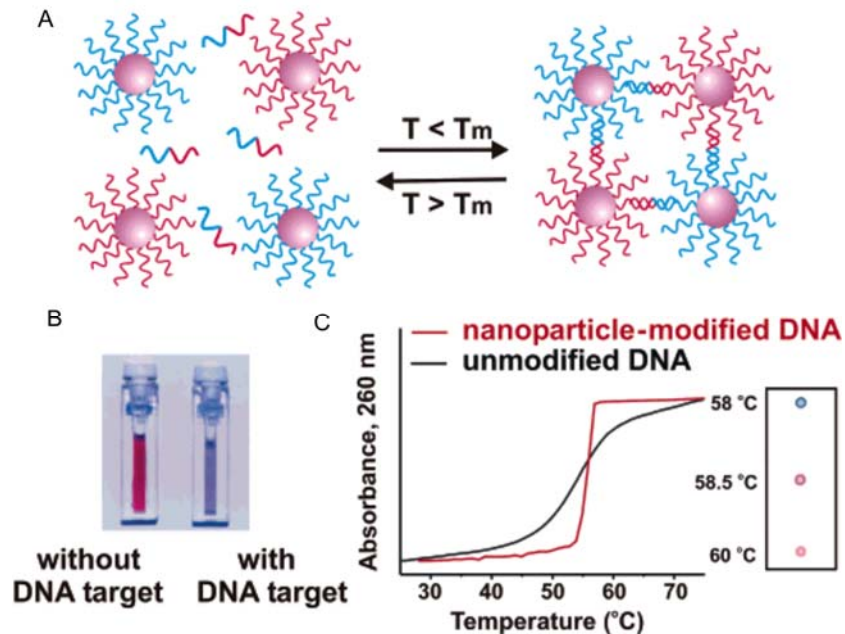


Figure 1.7 Cooperative effect in the DNA/AuNPs assembly/melting process. (A) Schematics of the modification of AuNPs with two probe DNA, blue and red. The linker DNA has two parts, each one complementary to the probe DNA. (B) Color change of DNA/AuNPs in the absence and presence of DNA target. (C) The melting curves of DNA/AuNPs and DNA. The right panel shows the color change spotted in a silica support. Figure adapted with permission from ref (⁵¹). Copyright © American Chemical Society.

Facilitating cellular uptake. The condensation on nanomaterials surface can fundamentally alter the way DNA interacts with cells. Gene therapy needs the successful delivery of nucleic acids into the specific sites. Since both nucleic acids and cell membranes are negatively charged, the crossing of nucleic acid is inhibited. To facilitate the delivery, transfection agents are typically required. Mirkin and co-workers reported that DNA-modified AuNPs, even with a negative surface charge, can enter cells with high efficiency.^{48,52} Further studies showed that the dense DNA layer is important for the

enhanced cellular uptake.^{53,54,55} AuNPs without DNA layer or with other modification did not enter cells with equally high efficiency. Furthermore, highly dense DNA on other nanoparticles⁵⁶ or even without core materials⁵⁷ still exhibit high transfection efficiency.

1.2.2 Interfacing AuNPs with non-thiolated DNA

1.2.2.1 Modifying AuNPs with non-thiolated DNA

Non-thiolated DNA has also shown promising values in functionalizing AuNPs. Compared to thiolated DNA, non-thiolated DNA is more cost effective. The major attraction forces between AuNPs and non-thiolated DNA arise from the bases-Au interaction. Coordination bonds can be formed between DNA bases with soft Lewis acid gold (Figure 1.8). The DNA bases adsorption by gold measured by temperature-programmed desorption-infrared reflection absorption spectroscopy (TPD-IRAS) and temperature-programmed desorption-mass spectroscopy (TPD-MS)^{58,59} indicates that the adsorption energy is over 100 kJ/mol. G binds to gold the most strongly followed by A, C, and T.

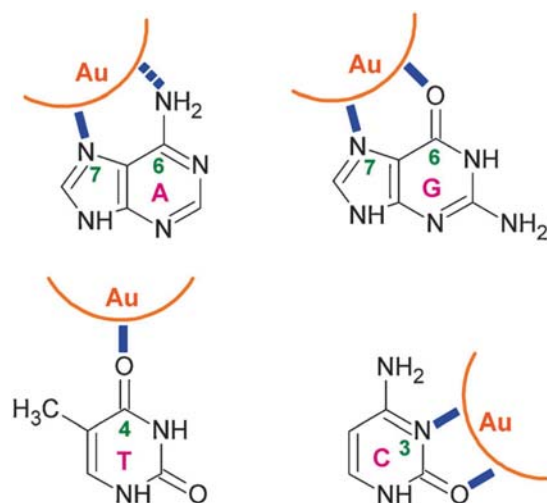


Figure 1.8 Interaction between DNA bases and AuNPs. The blue lines indicate interaction sites (the dashed lines suggest a possible weak interaction). Figure adapted with permission from ref (7). Copyright © Royal Society of Chemistry.

The adsorption of non-thiolated DNA onto AuNPs was also inhibited by electrostatic repulsion. To screen the charge repulsion, salt (e.g., NaCl) is often added to increase the ionic strength.^{60,61,62,63} The adsorption kinetics and capacity of non-thiolated DNA is dependent on the salt concentration.⁶⁰ At high salt concentration, DNA compacts more tightly and occupies less space, resulting in more DNA binding to the gold surface. Furthermore, salts also affect the DNA adsorption process beyond adjusting ionic strength. Monovalent cations (Li^+ , Na^+ , K^+ , Rb^+ , Cs^+) exhibit increasing ability in destabilizing AuNPs and promoting the initial DNA adsorption as the ionic radius increases.⁶⁴

The adsorption of DNA onto AuNPs strongly depends on the DNA sequence. DNAs rich in A or C bind are more easily to be adsorbed than those rich in T. The sequences determine the conformation and capacity of DNA on AuNPs surface. While more than 120 strands of poly A₁₅ adsorb on each 13 nm AuNP, only ca. 20 strands of poly

T₁₅ on each particle. This large difference can be explained by different affinities between DNA bases and gold surface. It may also indicate that poly A₁₅ adapts a standing-up conformation, since the capacity is close of thiolated DNA. This model was further confirmed the high adsorption capacities of DNA with terminal A or C.⁶¹

1.2.2.2 Features of AuNPs with non-thiolated DNA

AuNPs modified with non-thiolated DNA have also found interesting properties and applications in biosensing. Similar to thiolated DNA, non-thiolated DNA can also protect AuNPs from salt-induced aggregation.⁴⁶ However, dsDNA with embedded bases has a much lower affinity with AuNPs. Based on this discrimination ability of AuNPs, Li and Rothberg developed a DNA biosensor (Figure 1.9). This colorimetric sensor can detect target DNA with high sensitivity (< 100 femtomoles) and high selectivity (single base mismatch) in 5 min.

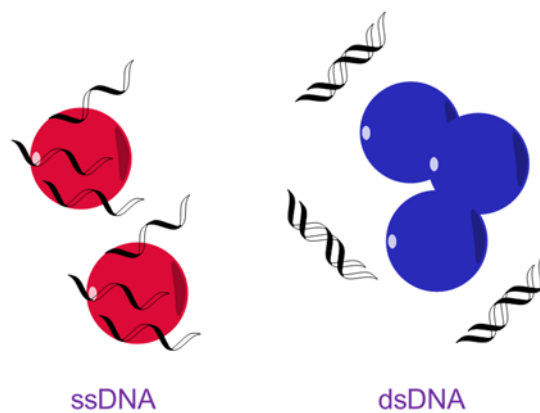


Figure 1.9 Schematics of DNA detection using AuNPs. AuNPs can adsorb ssDNA but not dsDNA. AuNPs with ssDNA are still red even after adding NaCl. DNA duplex is formed in the presence of cDNA, and further adding NaCl results in a blue color.

Non-thiolated DNA strands adsorb onto AuNPs mainly through bases and those rich in A bind more strongly. It is possible then to design a poly-A block as an anchoring group. Zhang and co-workers were able to control the DNA loading density and polarity on AuNPs.⁶¹ Based on this strategy, colorimetric detection of DNA⁶³ and surface-enhanced resonance Raman scattering detection of Hg²⁺⁶⁵ have been achieved.

1.3 Metal Oxide Nanomaterials

Metal oxides nanomaterials encompass a large number of important materials, for instance, iron oxide, cerium oxide, zinc oxide, tin oxide, zirconium oxide, and titanium oxide. These nanosized metal oxides exhibit interesting optical, catalytic, and magnetic properties and provide surface modification sites for further biomolecules immobilization. Protein enzymes and functional DNA, for example, have been combined with various metal oxides to construct bioelectronics sensors.⁶⁶ In this section, three important properties of metal oxides will be introduced, including DNA immobilization, anions adsorption (arsenic as an example), and enzyme-mimic activities.

1.3.1 Metal oxide-solution interface

Once dispersed in aqueous solution, the surface of metal oxides become charged. The metal ions on surface possess a lower coordination number compared to that in the bulk. As a result, chemisorption of water occurs (Figure 1.10A). The surface could be positive, negative or neutral depending on the property of the oxide, and also solution pH.

When dispersed in buffer solutions with counterions, similar to other colloidal systems, metal oxides exhibit an electric double-layer structure (Figure 1.10B).

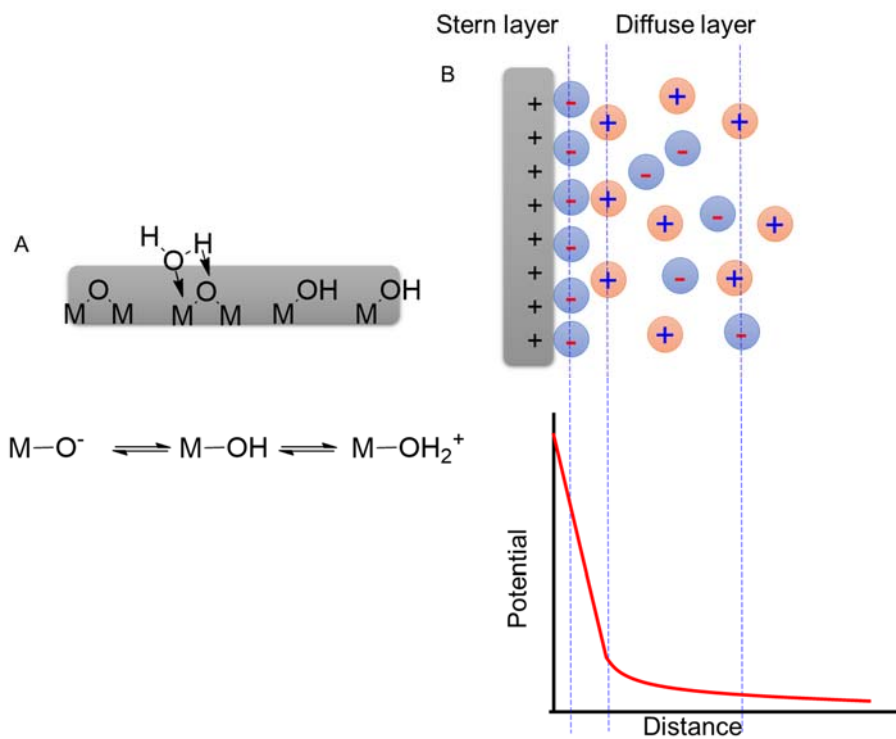


Figure 1.10 Surface properties of metal oxides in aqueous solutions.

1.3.2 Interfacing metal oxides with DNA

Over the last decades, DNA-functionalized metal oxide nanoparticles (MONPs) have been explored in biosensing, drug delivery, cancer diagnostics and therapy. DNA can be attached onto metal oxide nanoparticles either indirectly via a linker or a coating layer or directly by adsorption.

1.3.2.1 Attaching DNA on MONPs “indirectly”

With a modification layer, MONPs show improved stability as well as additional functional groups. DNA can then attached by electrostatic interaction or covalent bonds.

For example, Scherer *et al.* reported that gene delivery can be achieved using a polyethyleneimine (PEI) encapsulated Fe₃O₄ NPs.⁶⁷ DNA was simply adsorbed on the positive charged PEI surface via electrostatic attraction. Another common strategy is using the silane chemistry by forming silicon-oxygen bond with the oxides surface. Typically, MONPs are treated with bifunctional organosilanes to introduce amine or thiol groups. Further attachment of DNA can be achieved by physisorption⁶⁸ or forming covalent bonds.⁹

A thick coating layer may undermine the intrinsic properties of the nanomaterials.⁶⁹ In this regard, small molecules as linkers are preferred. Mirkin and co-workers developed a DNA/Fe₃O₄ conjugate with a high DNA density (up to 70 strands per 10 nm particle) via click chemistry.⁵⁶ This composite exhibited characteristic features of spherical nucleic acids, such as cooperative melting and high cellular uptake.⁵² The electrophilic surface of many metal oxides (e.g., iron oxide) can bind nucleophilic molecules through the metal's empty orbitals.⁹ In this respect, cross linkers with functional groups, including phosphate, sulfate, carbonate, and hydroxyl groups can be used for DNA linking. Paunesku *et al.* prepared DNA/TiO₂ nanocomposites using dopamine as the linker.⁷⁰ Dopamine can bind strongly to metal oxides⁷¹ and the remaining primary amine is available for DNA attachment.^{70,72} The obtained composite exhibited multiple activities, including photocatalytic activity, molecular recognition ability, and light-responsive DNA endonuclease activity.⁷⁰

1.3.2.2 Adsorbing DNA on MONPs “directly”

Pristine metal oxides have also been used to interface with non-modified DNA. The phosphate backbone of DNA can bind to the metal oxide surface via electrostatic interaction and/or coordination bonds. Compared to the indirect strategy, interfacing DNA

with oxides directly has shown several unique features and found applications in biosensing, gene delivery, and photocatalysis.

By directly interfacing DNA with metal oxides, the oxidation of bases, hybridization with cDNA, and forming complex with targets can be detected. Electrochemical detection of nucleic acids relied on the attaching of DNA on the electrodes. Thorp and co-workers reported that long strands of DNA (over 1000 bps) can be directly adsorbed on the indium tin oxide (ITO) electrode without cross linkers or surface coating layers.^{73,74,75} The adsorbed DNA can resist repeated washing and heating operations. Electrocatalytic oxidation of guanine by $\text{Ru}(\text{bpy})_3^{3+}$ (bpy = 2,2'-bipyridine) can then be detected with high sensitivity. The binding mode was proposed to be metal-phosphate interaction. Metal oxides (e.g., ZrO_2) can also be used to as a linker to immobilize DNA on glassy carbon electrode, which cannot adsorb DNA directly.⁷⁶ If the probe DNA was first adsorbed on the electrode, cDNA-induced hybridization can be detected. Using this strategy, Malhotra and co-workers^{66,77,78} have developed electrochemical sensors for bacteria.

Fluorescent biosensors based on functional DNA and pristine metal oxides have also been developed. Several metal oxides can adsorb fluorescently labeled and quench the fluorescence. Adding cDNA or target analytes then induces the probe desorption and fluorescence recovery. Alternatively, pre-formed dsDNA or aptamer-target complexes have lower affinities to the metal oxides than ssDNA. Zhang and co-workers evaluated the differential adsorption of ssDNA and dsDNA on TiO_2 , and found that the latter can be adsorbed less efficiently.⁷⁹ Control experiments showed non-target DNA did not induce significant inhibition, suggesting the specificity of TiO_2 in DNA detection. Using a similar

strategy, Song and co-workers developed a sensitive DNA sensor (LOD below nM) based on the pristine α -Fe₂O₃ NPs.⁸⁰ DNA labeled with various organic dyes can be effectively adsorbed and quenched by α -Fe₂O₃ NPs. Liu and co-workers developed a fluorescence turn-on biosensor for thrombin using the thrombin aptamer and Fe₃O₄ NPs.⁸¹ The LOD was as low as 0.5 nM. Some 2-D layered metal oxide nanomaterials also show capability in discriminating ssDNA and dsDNA and have been utilized as biosensors and gene delivery vehicles. Zou and co-workers reported that MnO₂ nanosheets can effectively adsorb ssDNA but not dsDNA. The fluorescence quenching ability of MnO₂ made it possible to design DNA-based biosensor for cDNA and adenosine.⁸²

Another feature of directly interfacing DNA with metal oxides is that the surface activities of the nanomaterials can be modulated. Ibuki and co-workers evaluated the role of DNA adsorption on the removal and degradation of organic dyes by TiO₂.⁸³ They found that DNA-modified TiO₂ can adsorb several organic dyes with significant improved efficiency. While only 5.8% of crystal violet, for example, was removed by pristine TiO₂, 96.8% was removed by DNA/TiO₂. In addition, the photocatalytic activity of TiO₂ in degrading the dyes was also enhanced. While it seems not a cost-effective way of using DNA in removing organic dyes, this study provided interesting insights into surface chemistry of DNA-modified metal oxides.

The surface redox property of nanomaterials can also be inhibited by DNA adsorption. Pautler and co-workers reported that the oxidase-like behavior of nanoceria was inhibited by DNA adsorption.⁸⁴ The presence of DNA blocked the direct interaction between the substrate and the nanoceria surface. As a result, the substrate oxidation was slowed down.

Metal oxides may dissociate in a reducing environment. Tan and co-workers reported a DNAzyme/MnO₂ nanocomposite for gene silencing.⁸⁵ Several roles of the MnO₂ nanosheets were highlighted. First, MnO₂ can adsorb DNAzyme directly and act as a fluorescence quencher. Second, MnO₂ protected DNA from enzymatic digestion. Third, MnO₂ nanosheets can be reduced to Mn²⁺ after interfacing with intracellular glutathione (GSH). The free Mn²⁺ further activated the released DNAzyme.

1.3.3 Interfacing metal oxides with arsenic

MONPs have been widely used in water treatment due to the excellent adsorption and removal capability.^{86,87,88} They can efficiently remove a diverse range of contaminants, including heavy metal ions, oxyanion, and organic molecules. Many oxyanions (e.g., phosphate, arsenate, chromate, silicate) are harmful when the concentrations are higher than the permissible limit. Metal oxides are extremely efficient in removing these anions via forming surface complexes. For example, iron oxide,⁸⁶ aluminum oxide,⁸⁶ titanium oxide,⁸⁹ zirconium oxide,⁹⁰ nickel oxide,⁹¹ have been used to remove arsenic from water. Iron oxide is particularly interesting because of the low cost, biocompatibility, and magnetic properties. Here, using arsenic adsorption as an example, the importance of materials as well as interaction mechanisms will be introduced.

1.3.3.1 Arsenic contamination

Arsenic (As) is a ubiquitous element in nature. It has been found in the earth crust, soil, natural water, and living organism. Humans have also used arsenic in medicine, agriculture, livestock, electronics, and metallurgy for a long history.⁹² Both organic and inorganic species of arsenic are extremely toxic; long-term exposure to even low

concentrations of arsenic results in many adverse health effects, damaging the skin, heart, stomach, and nervous system.^{92,93,94,95} The wide distribution of arsenic poses great threats to human health. Drinking water in many countries (e.g., Argentina, Bangladesh, China, India, Mexico, and Myanmar) are contaminated by arsenic.⁹⁶ Given the chronic effects of arsenic in drinking water, many organizations and governments have reduced the recommended value of arsenic. The guideline value for arsenic was initially set to be 50 µg/L (0.67 µM). In 2001 the World Health Organization (WHO) adjusted it to 10 µg/L (0.13 µM). The US Environmental Protection Agency (US-EPA) has also reduced the limit from 50 µg/L to 10 µg/L in 2001. However, many developing countries still use the 0.67 µM limit since their water arsenic level is too high but they cannot afford the resources to purify water to the lower limit. The most common arsenic species in water include arsenate (As(V), AsO₄³⁻) and arsenite (As(III), AsO₃³⁻).⁹⁷ Under oxidizing conditions, arsenate is the dominating form and its protonation state is a strong function of pH. At neutral pH, H₂AsO₄⁻ and HAsO₄²⁻ co-exist.⁹⁸

1.3.3.2 Adsorption and removal of arsenic by iron oxide

Iron oxides/hydroxides have been used to remove As(V) and As(III) via adsorption for a long time. Early works were focused on studying the effects of arsenic concentration, ionic strength, pH on the adsorption and removal by different iron oxides/hydroxides. Pierce and co-workers investigated the adsorption of arsenic on amorphous iron hydroxide. The adsorption was found to obey the Langmuir model by examining the adsorption isotherms.^{99,100} Raven and co-workers¹⁰¹ tested the adsorption of arsenic on ferrihydrite under different pH. The adsorption of As(V) was more favored at low pH in the range of

4-9. With increasing pH, As(III) adsorption was enhanced with an adsorption maximum at ca. pH 9.0.

The size of iron oxide/hydroxide used in the early works was not well controlled, although nanosized particles may exist. Nanoscale metal oxides are potentially more efficient in adsorbing arsenic with large surface-to-volume ratios and more binding sites. Mayo and co-workers evaluated the effect of size of Fe₃O₄ NPs on the adsorption of arsenic.¹⁰² When the particle size was decreased from 300 nm to 12 nm, a 200 times enhancement in arsenic adsorption was achieved. The authors suggested both increased surface area and binding sites contributed to the improvement. Hristovski and co-workers examined 16 commercial metal oxide nanoparticles in arsenic removal. Fe₂O₃ NPs and other three oxides exhibited the highest efficiency.⁹¹

While nanoparticles are more effective in adsorption, aggregation may occur due to the unmodified surface. To avoid the aggregation, iron oxide nanoparticles composites have been developed. One common strategy is to anchor nanoparticles in supports, for example, sand,¹⁰³ bentonite,¹⁰⁴ zeolite,¹⁰⁵ and silica.¹⁰⁶ Yang and co-workers encapsulated γ -Fe₂O₃ (ca. 6 nm) in macroporous silica.¹⁰⁶ By anchoring the nanoparticles in the silica matrix, aggregation can be avoided during the arsenic adsorption process. The composite can efficiently adsorb both As(V) and As(III), reducing the concentration from 100 μ g/L to 2 μ g/L.

1.3.3.3 Interaction mechanism

The interaction mechanism between arsenic and iron oxide has also been investigated using several spectroscopic methods. Anions could bind the particle surface by forming outer-sphere complexes or inner-sphere complexes (Figure 1.10A). In the

outer-sphere complexes, anions adsorb on the hydration shell of the particles via electrostatic interaction. In the inner-sphere complexes, anions bind specifically on the particle surface by coordination bonds. Both arsenate and arsenite can form inner-sphere complexes with various iron oxides based on extended X-ray absorption fine structure spectroscopy measurement.^{107,108,109,110} Goldberg and co-workers examined the interaction mechanism of As(V) and As(III) with amorphous iron oxide using *in situ* Raman and Fourier transform infrared (FTIR).¹⁰⁸ In their model, As(V) forms inner-sphere surface complexes, whereas As(III) forms both inner- and outer-sphere complexes with iron oxide.

More specifically, three types of binding modes between arsenate and iron oxides have been proposed (Figure 1.10B). The bidentate binuclear mode appears to be the dominant complex.^{107,108,109,110,111,112} Other two modes have also been observed. Fendorf and co-workers claimed that the binding mode is dependent on the surface coverage of arsenate.¹⁰⁹ When the coverage is low, arsenate mainly binds to the surface by forming monodentate complex. However, when the coverage is high, the bidentate binuclear complex dominates. Both complexes exist at intermediate coverage. As(III) also mainly forms bidentate binuclear complex with the oxide surface.¹⁰⁷

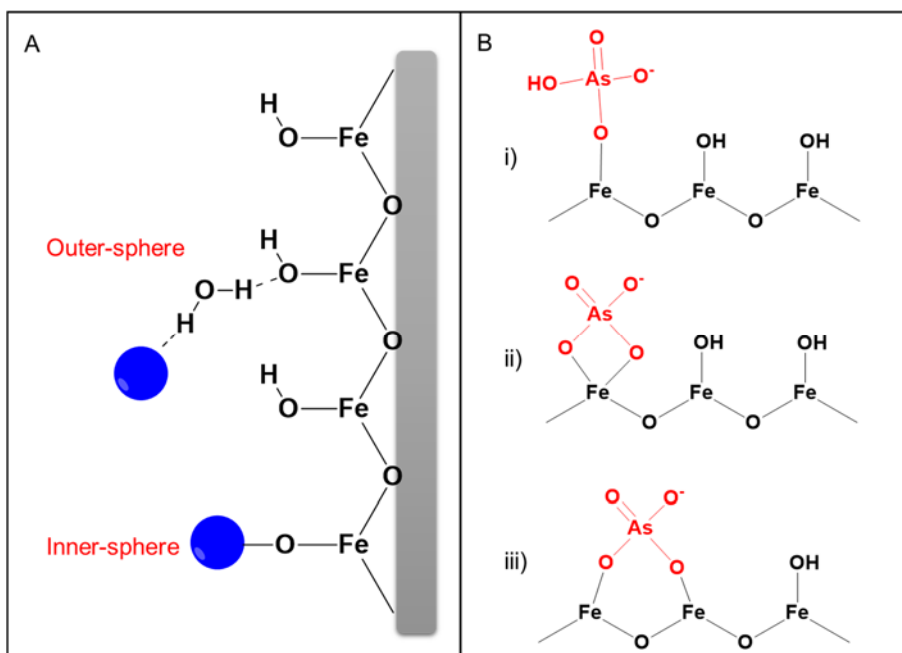


Figure 1.11 Schematics of interaction mechanisms of anion with iron oxides. (A) Outer-sphere and inner-sphere complexes. (B) Different binding modes between arsenate and iron oxides: i) monodentate mononuclear, ii) bidentate mononuclear, and iii) bidentate binuclear.

Since both As(V) and As(III) form stable complexes with iron oxides, the adsorption of both species may be competitive. Jain and coworkers revealed that As(V) bound more strongly to ferrihydrite than As(III).¹¹³ Qi and Pichler also evaluated the co-adsorption of As(V) and As(III) onto ferrihydrite as a function of pH.¹¹⁴ At acidic conditions (pH 4), the adsorption of As(V) was favoured, whereas at pH above 6, the adsorption of As(III) was preferred. Other common anions existing in environment may also affect the adsorption of arsenic. Frau and co-workers evaluated the influence of four major anions, phosphate, carbonate, sulfate, and chloride, on the arsenate adsorption by

ferrihydrate.¹¹⁵ The kinetic studies showed anions have a competitive role in arsenate adsorption by the following order: phosphate>carbonate>sulfate>chloride. While other anions have a moderate effect, phosphate can strongly affect arsenate adsorption, since it shares a similar chemical structure with arsenate.

Two models have been proposed to explain the experimental data regarding the competitive adsorption of phosphate and arsenate. In the first model, phosphate and arsenate share the binding sites on the oxides surface. Within this model, phosphate inhibition of arsenate adsorption or arsenate inhibition of phosphate adsorption were observed on several iron oxides.^{116,117,118} The binding affinity of arsenate with iron oxide was slightly stronger than that of phosphate.¹¹⁹ In the second model, the particle surface is not homogeneous. While arsenate binds only to one type of site, phosphate binds to two types of sites on the particle surface. This model was proposed by Zeng and co-workers.¹²⁰ They found that more phosphate can be adsorbed by ferrihydrate than arsenate in single-component experiments. In addition, the presence of phosphate did not significantly affect the arsenate adsorption as expected. The exact interaction mechanisms between anions and iron oxides (and other oxides) still need more investigations.¹¹⁰

1.3.4 Metal oxides with enzyme-like activities

1.3.4.1 Introduction to nanozymes

Nanomaterials as enzyme mimics (nanozymes) have received considerable attention recently.^{121,122,123} These nanozymes have found diverse applications in biosensing, cancer diagnostics and therapy, stem cell growth, and neuroprotection. Until now, a wide range of nanomaterials, including gold nanoparticles,^{124,125} metal oxides,^{126,127,128,129} and

carbon-based nanomaterials,^{130,131} have been reported to possess oxidase, peroxidase, catalase, and superoxide dismutase like activities.

The first series of nanomaterials reported with enzyme-like activities are fullerene and its derivatives. In 1990s, soluble fullerene derivatives were reported to cleave DNA,¹³² and scavenge free radicals.^{133,134} More recently, other carbon-based nanomaterials, for example, carbon nanotube,^{135,136} graphene oxide,^{130,137,138,139,140} and carbon dots^{140,141} have also been reported to exhibit peroxidase-like activity. The terminology “nanozyme” was not coined until 2004 by Scrimin and co-workers to describe the ribonuclease-like, esterase-like activity of functionalized AuNPs.^{142,143,144,145,146} However, the catalytic activity of modified AuNPs was actually from the surface monolayer rather than the particle core. In 2004, Rossi and co-workers¹²⁴ reported that the “naked” gold nanoparticles without a surface coating layer exhibited glucose oxidase (GOx) like activity. Nanozyme was then widely accepted to represent nanomaterials with intrinsic enzyme-like activities.

Compared to natural enzymes, nanozymes have several advantages. First, nanozymes are much more stable compared to natural protein enzymes. Heating protein enzymes may result in the loss of their secondary structures and hence the catalytic functionality. However, nanomaterials can maintain the high activity even after thermal treatment.^{121,122,123} Second, the preparation of nanozymes is more efficient and cost-effective. While the preparation of natural enzymes is very complex, the synthesis of nanozymes can be easily achieved with low cost and large quantities. Third, the surface of nanozymes can be further modified with functional biomolecules using different conjugating chemistry. Lastly, the intrinsic optical, magnetic properties of nanomaterials can be further incorporated with the enzyme-like activity.

1.3.4.2 Metal oxide with oxidase-like activity

Oxidase catalyses the oxidization reaction of the substrate using dissolved oxygen rather than H_2O_2 as the oxidizing agent. Currently, few metal oxide nanoparticles have been reported with oxidase-like activity. In 2009, Asati *et al.* first demonstrated that cerium oxide nanoparticles (nanoceria) exhibited oxidase-like activity.¹²⁷ Chromogenic substrates were used to evaluate the activity (Figure 1.11A). Higher activity was found to be at lower pH (pH 4) using smaller size (~5 nm) with a thin coating layer. Aside from nanoceria, MnO_2 nanowire,¹⁴⁷ Mn_3O_4 NPs,¹⁴⁸ $CoFe_2O_4$ NPs,¹⁴⁹ MoO_3 NPs¹²⁹ have also been identified as oxidase-mimics.

MONPs with oxidase-like activities can be used to construct immunoassays. Asati and co-workers modified nanoceria with folic acid, which could specifically recognize tumor cells (Figure 1.11B).¹²⁷ After binding to the target cells, nanoceria can induce 3,3',5,5'-tetramethylbenzidine (TMB) oxidation, producing a blue color. Using this strategy, lung cancer cells were successfully detected. Control experiment was performed with H9c2 cardiac myocytes, in which TMB oxidation was not observed.

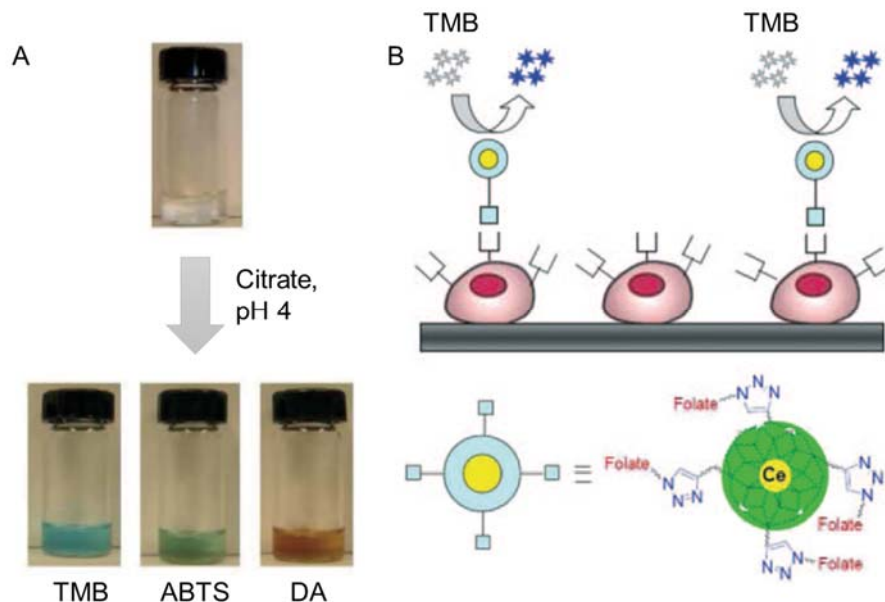


Figure 1.12 Nanoceria with oxidase-like activity. (A) The oxidation of different substrates, TMB, 2,2'-azino-bis(3-ethylbenzothiazoline-6-sulphonic acid (ABTS), and dopamine (DA) catalysed by nanoceria. (B) A schematic of using nanoceria in constructing immunoassays. Figure adapted with permission from ref (¹²⁷). Copyright © John Wiley and Sons.

1.3.4.3 Metal oxides with peroxidase-like activity

Peroxidase catalyzes the substrate oxidation in the presence of H_2O_2 . In 2007, Yan and co-workers discovered that magnetic Fe_3O_4 NPs exhibit peroxidase-like activity.¹²⁶ Fe_3O_4 NPs can catalyze the oxidization of TMB, 3,3'-diaminobenzidine (DAB), and o-phenylenediamine dihydrochloride (OPD) by H_2O_2 . The authors evaluated Fe_3O_4 with different sizes (30, 50, and 300 nm) and found that smaller particles have higher activity. Comparison of Fe_3O_4 with natural enzyme horseradish peroxidase (HRP) was carried out. Similar to HRP, the nanozyme activity is dependent on reaction pH and temperature.

However, the nanozyme can retain the activity after incubation at a wide range of pH and temperature. Enzyme constants were obtained based on steady-state kinetics assays. The Michealis-Menten constant (K_m) indicates the binding affinity of the substrate to the enzyme. While H_2O_2 has higher affinity to HRP than that to Fe_3O_4 , the other substrate TMB binds to Fe_3O_4 more strongly than HRP. Rate constant (K_{cat}) indicates the catalytic rate of enzymes. The nanozyme shows a 40-time higher rate constant, which is attributed the multiple catalytic sites of nanoparticles. This seminal work by Yan and co-workers stimulated many groups to investigate the enzyme-like activity of nanomaterials. Some typical examples of metal oxide nanoparticles with peroxidase-like activity are listed in Table 1.1.

A straightforward application of nanozymes with peroxidase-like activity is to detect H_2O_2 based on the color change of the co-substrate (e.g., ABTS, TMB).¹⁵⁰ Using this colorimetric method, H_2O_2 around 1 μM can be detected. Jiang and co-workers improved the detection sensitivity ($LOD < 10$ nM) using a fluorescent dye, Rhodamine B.¹⁵¹ The oxidation of Rhodamine B by H_2O_2 catalyzed Fe_3O_4 NPs induced the fluorescence quenching. When glucose oxidase (GOx) is combined with nanozymes, selective and sensitive detection of glucose can be achieved. GOx catalyzes the glucose oxidation by oxygen with H_2O_2 as the product. By detecting generated H_2O_2 using ABTS/ Fe_3O_4 , Wei and Wang developed a colorimetric sensor for glucose as low as 30 μM .¹⁵⁰ Applications of metal oxide nanozymes in immunoassays,¹²⁶ bacteria detection,¹⁵² and biofilm elimination^{153,154} have also been developed.

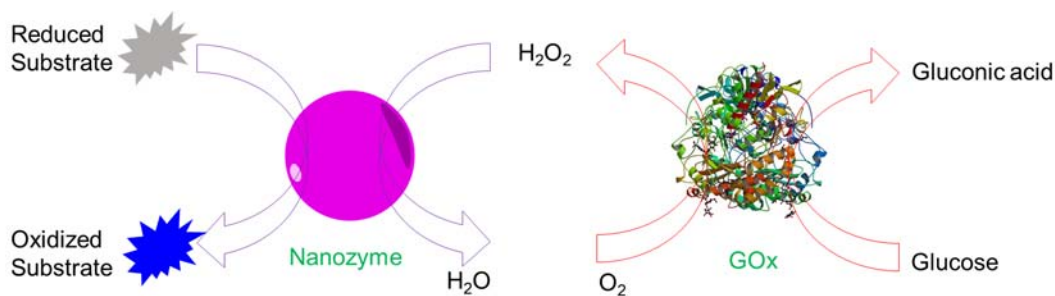


Figure 1.13 Schematics of sensing H_2O_2 and glucose using nanozymes with peroxidase-like activity and GOx.

1.3.4.4 Metal oxides with catalase- and/or SOD-like activity

Reactive oxygen species (ROS) and free radicals are the by-products in a wide range of physiological reactions. Excess ROS can induce oxidative damage to biomolecules.¹⁵⁵ Nature has developed several enzymes (e.g., catalase and superoxide dismutase, SOD) to diminish ROS and other free radicals. The enzyme SOD catalyzes the dismutation of superoxide anions ($\text{O}_2^{\cdot-}$) into H_2O_2 and O_2 . The enzyme catalase catalyzes the decomposition of H_2O_2 into O_2 and H_2O . In 2007, Self and co-workers reported that nanoceria acts as SOD based on a competitive assay.¹⁵⁶ The enzyme activity is comparable to natural enzymes. In a later work, the same group reported that nanoceria also mimics catalase in diminishing H_2O_2 .¹⁵⁷ It is interesting to note the activity is strongly dependent on the ratio of $\text{Ce}^{3+}/\text{Ce}^{4+}$. At a low $\text{Ce}^{3+}/\text{Ce}^{4+}$ ratio, the catalase activity dominated; at a high $\text{Ce}^{3+}/\text{Ce}^{4+}$ ratio, the SOD activity prevailed. While some models were proposed to elucidate the mechanisms, experimental evidences are still in lack.^{122,123}

With catalase and SOD activities, nanoceria has been used to protect cells from oxidative stress. Radiation therapy is widely used in treating cancer. While the technique is efficient in killing cancer cells, it also generates free radicals, which cause damage to

normal cells. Seal and co-workers reported that nanocerium could protect normal cells against radiation but not cancer cells.¹⁵⁸

Aside from nanocerium, iron oxide^{159,160} and cobalt oxide^{128,161,162} have also been reported to have catalase-like activity. Gu and co-workers found that both Fe₃O₄ and γ -Fe₂O₃ exhibited the capability in decomposing H₂O₂ at neutral conditions (pH 7.4).¹⁵⁹ The authors suggested that iron oxide nanoparticles could be potentially used in protecting cells from H₂O₂-induced damage. In a recent study, Fan and co-workers demonstrated the catalase-like activity of iron oxide nanoparticles *in vivo*.¹⁶⁰ Some other applications of catalase-like nanozymes are summarized in Table 1.1.

Table 1.1 Metal oxide nanoparticles as enzyme-mimics

| Activity | Material | Application | References |
|------------|--|---|------------|
| Oxidase | CeO ₂ | Immunoassay for cancer cell detection | 127 |
| | CoFe ₂ O ₄ | Sulfite detection in white wines | 149 |
| | MnO ₂ | Immunoassay for bacteria detection | 147 |
| | Mn ₃ O ₄ | Phenol detection | 148 |
| | MoO ₃ | Recovery of sulphite oxidase activity | 129 |
| Peroxidase | Fe ₃ O ₄ | Immunoassays | 126 |
| | | H ₂ O ₂ and glucose detection | 150 |
| | | Pesticide and nerve agent detection | 163 |
| | | Strip for Ebola detection | 152 |
| | | Biofilm elimination | 153 |
| | α -Fe ₂ O ₃ | NA | 164 |

| | | | | |
|----------|--------------------------------|--|-----|-----|
| | $\gamma\text{-Fe}_2\text{O}_3$ | Enhance H_2O_2 -induced cell damage | 159 | |
| | Co_3O_4 | NA | 165 | |
| | | Immunohistochemical assay for vascular endothelial growth factor detection | 128 | |
| | V_2O_5 | Prevent biofilm formation | 154 | |
| | CuO | H_2O_2 and glucose detection | 166 | |
| | CoFe_2O_4 | H_2O_2 and glucose detection | 167 | |
| Catalase | CeO_2 | Antioxidants | 168 | |
| | | Anti-inflammatory property | 169 | |
| | | Radical scavenger | 170 | |
| | | Promote stem cell growth | 171 | |
| | | Anti-apoptotic activity | 172 | |
| | | H_2O_2 and glucose detection | 173 | |
| | | Drug delivery | 174 | |
| | | Degradation of Nerve Agents | 175 | |
| | Fe_3O_4 | Diminishing cytotoxicity ($\gamma\text{-Fe}_2\text{O}_3$) | 159 | |
| | | Antioxidant | 160 | |
| | Co_3O_4 | NA | 165 | |
| | | H_2O_2 detection | 161 | |
| | SOD | CeO_2 | NA | 156 |

1.4 Research Goals and Thesis Outline

Previous studies have shown that DNA is a versatile biomolecule in interfacing with inorganic nanomaterials. However, the majority of previous work has focused on coupling DNA with nanomaterials indirectly. While the colloidal stability of nanomaterials is improved, one should realize that the surface activity of many materials is actually sacrificed. For example, many unique functions of pristine metal oxide nanoparticles are relied on the direct interaction of reactive surface sites with substrates. Therefore, the primary focus of this thesis is to interface DNA with pristine MONPs directly to highlight the surface properties of materials. MONPs studied in this thesis include ITO, Fe₃O₄, CeO₂, Al₂O₃, CoO, Co₃O₄, Cr₂O₃, Fe₂O₃, In₂O₃, Mn₂O₃, NiO, SiO₂, SnO₂, anatase-TiO₂ (a-TiO₂), rutile-TiO₂ (r-TiO₂), WO₃, Y₂O₃, ZnO, and ZrO₂. The major goals of this thesis are to understand the surface chemistry in DNA adsorption process, and in DNA desorption in the presence of interference analytes, such as cDNA, oxyanions, and H₂O₂. Based on the fundamental understandings, I also propose the design of functional sensors for environmental and/or biological targets. The thesis consists of seven chapters with a common focus of studying DNA adsorption and desorption from MONPs surface.

Chapter 2 describe the adsorption of fluorescently labeled ssDNA by ITO NPs. The adsorption behavior as a function of pH, salt concentration, DNA sequence and length, materials composition are systematically studied. In addition, the interaction mechanism are investigated via displacements assays. Lastly, cDNA-induced DNA recovery is evaluated for further biosensor design. While electrochemical and photochemical biosensors based on ITO for DNA detection have been developed, such a fundamental study is lacking.

Chapter 3 describes the interaction between DNA and Fe₃O₄ NPs using a same methodology outlined in chapter 2. More importantly, desorption of DNA as a function of anions are evaluated. A sensitive arsenate sensor bases on displacement reaction is constructed. With this sensor design, DNA probe can be creatively used to detect anions.

Chapter 4 describes the interaction between DNA and 19 MONPs listed above. The behaviors of DNA adsorption, fluorescence quenching, and DNA desorption upon adding anions are investigated step-by-step. Finally, three oxides CeO₂, Fe₃O₄, and ZnO are screened to construct a sensor array to discriminate similar anions: arsenate, arsenite, and phosphate. As a proof of concept, the sensor array further improves the displacement sensor in chapter 3 in terms of discriminating multiple similar analytes.

Chapter 5 describes a DNA release behavior from nanoceria surface in the presence of H₂O₂, a biologically important ROS. DNA desorption as a function of pH, salt concentration, DNA sequence and length are systematically evaluated. Gel electrophoresis, surface functional titration, and surface charge measurement are carried out to investigate the reaction mechanism. Finally, DNA/nanoceria as a H₂O₂ and glucose sensor is tested in terms of sensitivity, selectivity, and response time. Such a DNA/nanoceria sensor represents a new way to detect ROS.

Chapter 6 describes the using of DNA in modulating the peroxidase activity of iron oxide nanoparticles. The effect of DNA length, sequence, surface coatings are systematically studied. Mechanistic investigation is performed by carrying out gel electrophoresis, surface charge measurement, and altering reaction substrate. While functional sensors have been based on the peroxidase activity of Fe₃O₄ for DNA detection, such a fundamental study is lacking.

Chapter 7 describes the conclusion in each chapter of this thesis, contribution of this research, and recommendations for future studies.

Chapter 2 DNA Adsorption by Indium Tin Oxide (ITO)

Nanoparticles

The results presented in this chapter have been published as:

Biwu Liu and Juewen Liu, DNA Adsorption by Indium Tin Oxide (ITO) Nanoparticles.

Langmuir, 31, 371–377, 2015.

2.1 Introduction

DNA-functionalized nanomaterials have attracted extensive research interests. These hybrid materials combine the molecular recognition and programmable property of DNA with the physical properties of inorganic nanoparticles, showing promising applications in many fields including biosensing,^{4,51,176,177,178} drug delivery,¹⁷⁹ materials science,^{180,181} and nanotechnology.^{182,183,184,185} Over the past two decades, many nanomaterials, such as metallic nanoparticles,³⁸ semiconductor quantum dots,¹⁸⁶ and nanoscale carbon materials (e.g., carbon nanotubes and graphene oxide),¹⁸⁷ have been modified with DNA. Each type of material has its own interaction force for DNA adsorption.

A key step in constructing such materials is the attachment of DNA to the particle surface. Depending on the surface chemistry, several conjugation methods have been developed, including covalent bonding, metal coordination, and physisorption.⁹ While covalent attachment provides a strong linkage with DNA, physisorption is attractive due to its simplicity, cost-effectiveness and reversible binding. For examples, DNA is readily adsorbed onto the graphene oxide surface via π - π stacking, and the complementary DNA (cDNA) induces DNA desorption by forming a duplex.^{187,188} For gold nanoparticles

(AuNPs), while thiolated DNA is the main reagent for attachment, non-thiolated DNA has recently emerged as an alternative.^{63,189}

Indium-doped tin oxide (ITO) is a very important material because it is both transparent and conductive.¹⁹⁰ ITO electrodes are used in electrical¹⁹¹ and photoelectrochemical¹⁹² biosensors for DNA as well as other targets. For example, Gao *et al.* developed a photoelectrochemical DNA sensor by conjugating an aldehyde-modified capture DNA onto a silanized ITO electrode.¹⁹³ The cDNA hybridization was followed by tagging a photoactive intercalator and the increased photocurrent. In other applications, direct DNA/ITO interaction was utilized for the detection of cDNA,⁷³ DNA methylation,¹⁹⁴ and pathogen.¹⁹⁵ At the same time, nanoscale ITO particles are particularly interesting in making electrodes.¹⁹⁶ Some DNA-ITO nanoparticle (NP) conjugates have been made into conductive networks for DNA detection.¹⁹⁷

In spite of these analytical applications, little is known about the fundamental interactions between DNA and ITO. In this chapter, we study the adsorption of DNA oligomers on ITO NPs as a function of pH, salt concentration, and DNA sequence. By changing the oxide composition and displacement experiments, we also proposed the adsorption mechanism. Finally, ITO was used to achieve DNA induced DNA desorption.

2.2 Results and Discussion

2.2.1 Characterization of nanoparticles

To have a complete understanding, in addition to ITO, we also studied In₂O₃ and SnO₂, which are the basic ingredient of ITO. Instead of studying bulk planar surfaces, we chose to use their NPs to achieve a large surface area and high adsorption capacity. In

addition, NP interaction with DNA can be conveniently followed by optical spectroscopy in the solution phase. From TEM images (Figure 2.1), the diameters of three NPs are around 50 nm with a wide distribution. All these NPs appear aggregated, which is also reflected from their hydrodynamic sizes (e.g., > 200 nm) by dynamic light scattering (DLS, Figure 2.2A). Aggregation is attributed to the lack of strong capping ligands and weak surface charge (*vide infra*). We are interested in studying DNA interaction with the native oxide surface, and intentionally avoided adding strong ligands.

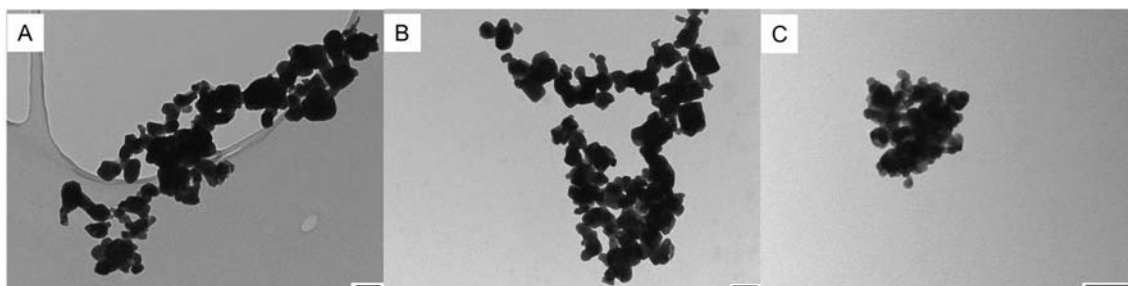


Figure 2.1 TEM micrographs of NPs used in this work. (A) ITO NPs, (B) In_2O_3 NPs, (C) SnO_2 NPs. The scale bar is 100 nm.

Since DNA is highly negatively charged, the surface charge of the oxides is likely to be important for determining the interaction force. We next measured the ζ -potential of the NPs as a function of pH (Figure 2.2B). All the three NPs are positively charged at low pH and negatively charged at high pH. The point of zero charge (PZC) is however different for each oxide. The ITO NPs are negatively charged when pH is higher than 7 and its PZC is between pH 6 and 7. Interestingly, the PZC of SnO_2 is close to 4 and In_2O_3 is between 7 and 8. This suggests that the surface charge of ITO might be controlled by either tuning pH or by changing the Sn/In ratio. Most oxides are capped by hydroxide groups in water,

and their surface charge normally comes from the (de)protonation of these surface hydroxyl groups.

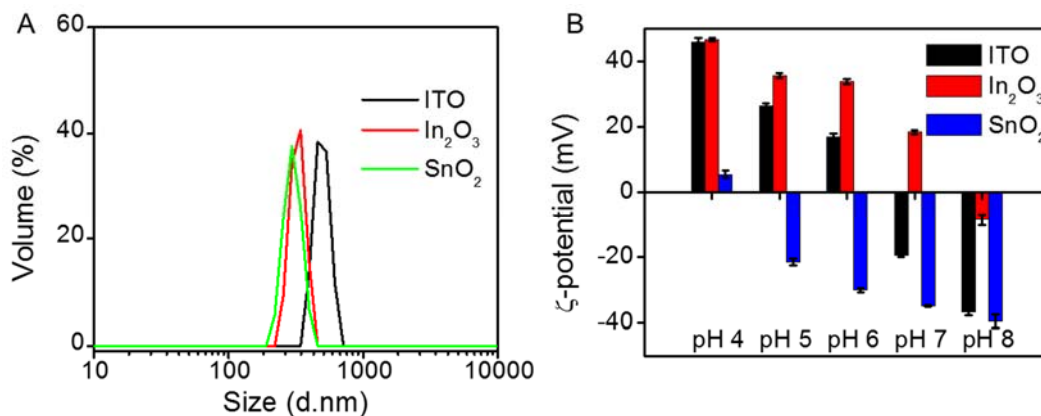


Figure 2.2 Dynamic light scattering measurement of three NPs. (A) Hydrodynamic sizes of three NPs. (B) ζ -potential of three NPs as a function of pH (4, 5, 6, 7, 8). The NPs were dispersed in designed buffers (10 mM).

2.2.3 Effect of pH

After understanding surface charge of NPs, we tested the effect of pH for DNA adsorption. We employed an Alexa Fluoro 488 (AF) labeled 12-mer DNA (Alexa-DNA1, sequence in Table 2.1) and this fluorophore maintains its fluorescence intensity even at acidic conditions. At pH 4, all the three NPs quenched the fluorescence (Figure 2.3A). This indicates two important facts. First, DNA can be adsorbed by all these NPs at pH 4. Second, these NPs can quench adsorbed fluorophores, which provides a convenient method for subsequent studies. This is consistent with that all the NPs are positively charged at pH 4. At pH 7, almost no quenching was observed for SnO₂, and ITO showed moderate quenching. Full quenching was achieved only with In₂O₃. This trend also agrees with the

surface charging of the NPs at pH 7. This simple experiment established that AF-labeled DNA is a useful probe for studying DNA adsorption.

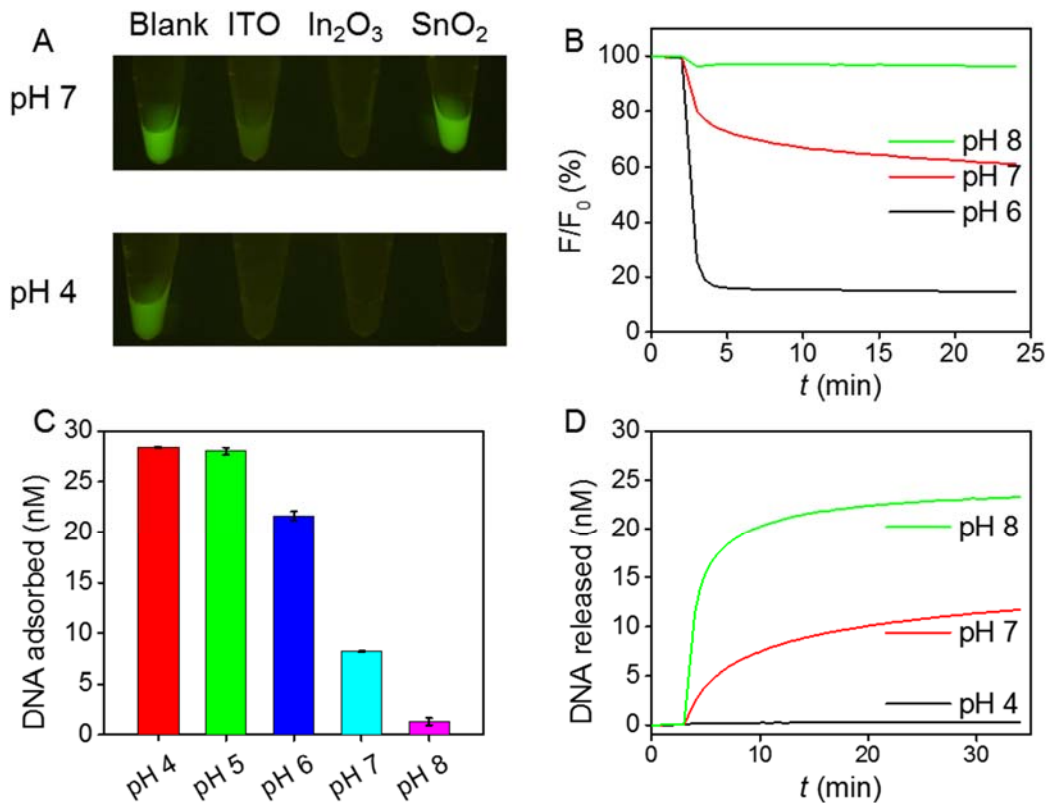


Figure 2.3 Effect of pH on DNA adsorption by ITO NPs. (A) Photographs showing fluorescence quenching of Alexa-DNA1 (100 nM) by the three oxide NPs (500 $\mu\text{g/mL}$) at pH 7 and pH 4. The blank groups are the free DNA without any oxides. The photographs were taken under a Blue-Light Transilluminator. Effect of pH on the (B) adsorption kinetics, (C) loading capacity, and (D) desorption kinetics of Alexa-DNA1 on ITO. The buffer concentration is 10 mM in the absence of additional salt.

For a quantitatively study, we measured the kinetics of DNA adsorption (Figure 2.3B). At pH 8, almost no DNA was adsorbed onto ITO NPs as indicated by stable fluorescence signals. However, a dramatic fluorescence decrease was observed at pH 6 attributable to

the change of surface charge of ITO NPs from negative to positive. The rate of adsorption is quite fast, approaching equilibrium in ~ 1 min at pH 6, while slower adsorption occurred at pH 7. The effect of pH was also studied by measuring the DNA loading capacity at various pHs (Figure 2.3C). Using a higher concentration of DNA (30 nM) and after 2 h incubation, over 95% DNA adsorption was achieved at low pH, while less than 5% DNA was adsorbed at pH 8.

Next we studied the reversibility of DNA adsorption. When the pH of the prepared DNA/ITO conjugates was adjusted back to neutral or basic, a fast fluorescence increase was observed (Figure 2.3D), suggesting DNA desorption. Combined with the ζ -potential measurement in Figure 2.2B, we conclude that electrostatic interaction plays a critical role in DNA adsorption.

2.2.3 Effect of ionic strength

Since most DNA assays are performed at neutral or physiological pH, next we studied DNA adsorption at pH 7.6. At this pH, both DNA and ITO NPs are negatively charged, and adding salt might be useful for screening charge repulsion. Figure 2.4A shows the adsorption kinetics as a function of NaCl concentration. In the absence of NaCl, there is a fast initial fluorescence drop followed by a slow decrease. The addition of NaCl indeed increased the adsorption rate. However, salt concentration did not appear to very important, where similar adsorption was achieved with 30 mM and 300 mM NaCl. The effect of NaCl on DNA loading capacity is also similar (Figure 2.4B). With over 30 mM salt, the capacity reached saturation. This study suggests that the electrostatic repulsion is quite weak between DNA and ITO at pH 7.6 and it can be effectively screened with just 30 mM NaCl.

From the DNA loading capacity data, we reason that the electrostatic repulsion among DNA is also weak on ITO. For example, adsorption of thiolated DNA by AuNPs is strongly influenced by NaCl concentration and the highest adsorption capacity was achieved at 700 mM NaCl.⁴⁰ Such high salt is mainly used to screen the repulsion among the dense DNA layer that are in an upright conformation. For ITO, the DNA capacity at neutral pH is much lower (vide infra) and salt only needs to screen the DNA/ITO repulsion.

The effect of NaCl was further highlighted by studying the desorption kinetics of DNA from ITO NPs at pH 4 (Figure 2.4C). As discussed above, at pH 4, ITO NPs are positively charged, and adsorb DNA through electrostatic interactions. This interaction can be weakened by increasing the NaCl concentration. From 0 to 300 mM NaCl, a gradual increase in DNA desorption occurred. It is also interesting to note that only less than 10% DNA desorbed even with 300 mM NaCl, suggesting the strong interaction of DNA with ITO NPs at low pH.

Next, we compared the adsorption kinetics of FAM-labeled DNA₂ by the three NPs (Figure 2.4D). While it is difficult to compare nanoparticles with different sizes, we herein chose to use the same mass concentrations of three materials. The surface area is in much excess if DNA can be efficiently adsorbed compared to AuNPs with the similar size. As expected, In₂O₃ is the most effective in DNA adsorption, while SnO₂ is the slowest, leaving ITO in between. This again agrees with the surface charging property. SnO₂ is highly negatively charged at pH 7.6 and the added NaCl was insufficient to screen the repulsion.

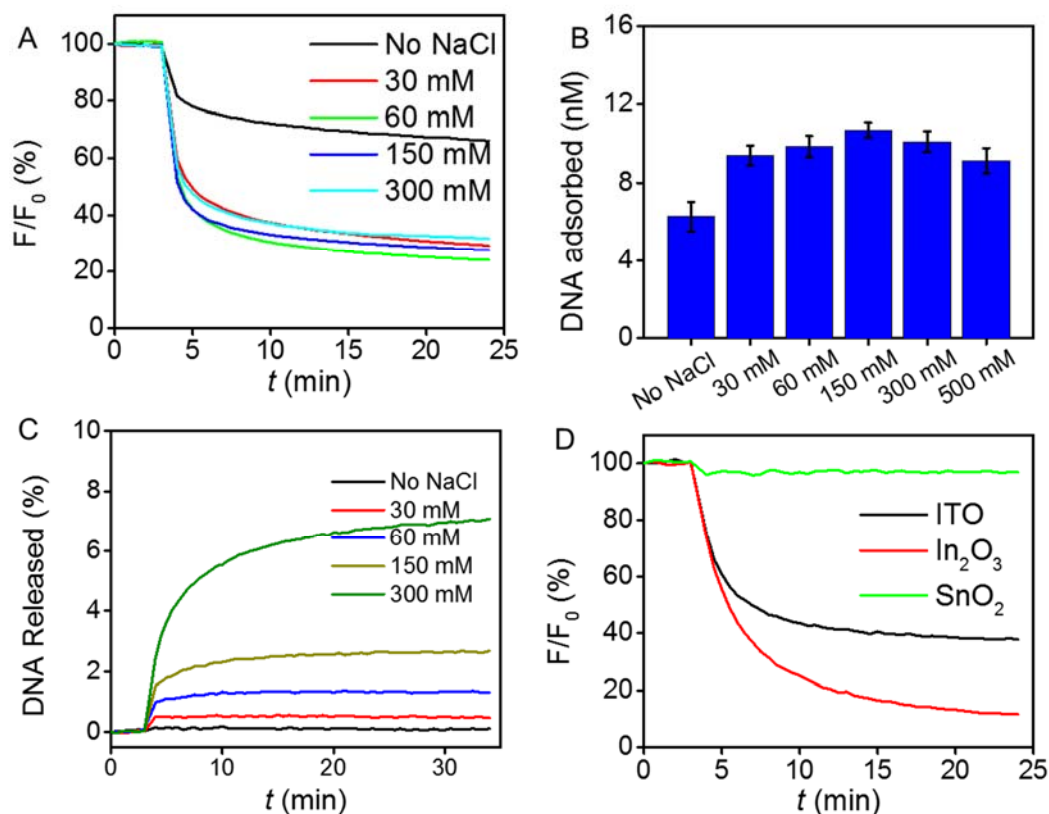


Figure 2.4 Effect of ionic strength on DNA adsorption and desorption by ITO NPs. (A) Adsorption kinetics and (B) loading capacity of FAM-DNA2 on ITO NPs as a function of NaCl concentration (10 mM HEPES, pH 7.6). (C) Desorption kinetics of Alexa-DNA1 on ITO NPs at pH 4 at various concentrations of NaCl. (D) The DNA adsorption kinetics onto various oxides.

To further understand the mechanism of adsorption, the adsorption isotherm by ITO NPs was measured (Figure 2.5). It exhibits a typical Langmuir type of adsorption behavior, indicating monolayer and reversible adsorption. The highest DNA loading coverage is ca. 12 nM for a 24-mer DNA (FAM-DNA2) onto 50 $\mu\text{g/mL}$ ITO NPs. Assume the NPs are 50 nm in diameter and 50 $\mu\text{g/mL}$ of ITO NPs is ca. 0.178 nM. Therefore each ITO NP adsorbs

68 molecules of 24-mer DNA. Compared thiolated DNA onto 50 nm AuNPs (640 ± 80 DNAs per particles),⁴¹ this coverage is much lower. This suggests that the DNA wraps around ITO instead of adopting an upright conformation as in the case of AuNPs.

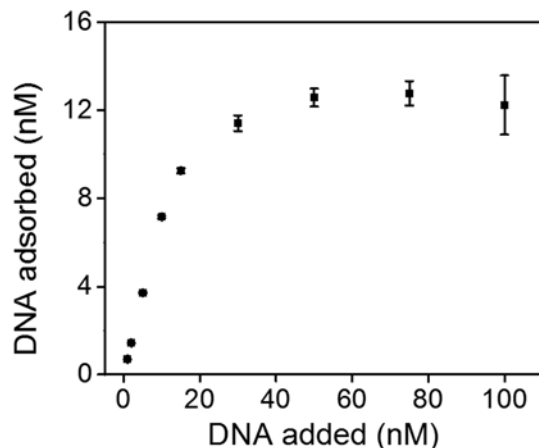


Figure 2.5 DNA (FAM-DNA2) adsorption isotherm by ITO NPs.

2.2.5 Effect of DNA length and sequence

One advantage of DNA-based assays is that the length and sequence of DNA can be readily controlled, which may provide further mechanistic insights. The loading of FAM labeled homo 15-mer DNA at pH 7.6 (NaCl 150 mM) and at pH 4 was performed (Figure 2.6A). The loading capacities of all DNA at pH 4.0 are 50-100 folds of those at pH 7.6, highlighting the importance of surface charge of the oxides. Since poly-A and poly-C DNA can be partially protonated at pH 4, they showed higher capacity than the poly-G and poly-T DNA.

Next, we studied the effect of DNA length (Figure 2.6B). At pH 4, the A₁₅ DNA adsorbed the most. Although its loading is only ~20% more than that for A₅, its number of adenine nucleotide is ~300% more. We reason that the 5-mer DNA is too short and it has

very weak affinity. On the other hand, the 30-mer DNA is too long and it occupies more footprints on the particle surface. The capacity of the 30-mer DNA is roughly 50% of the 15-mer and therefore, they adsorb a similar number of nucleotides. At pH 7.6, all the DNAs were adsorbed with a very low capacity, and this is again attributed to the strong charge repulsion with the ITO surface.

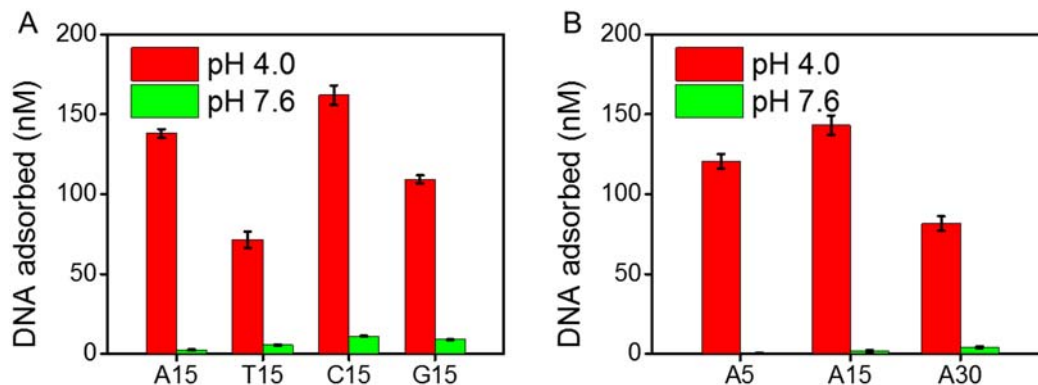


Figure 2.6 DNA adsorption as a function of sequence and length. The effect of DNA (A) sequence and (B) length on loading capacity onto ITO NPs at pH 4.0 and 7.6. The initial concentration of DNA added at pH 7.6 and 4.0 are 30 nM and 200 nM, respectively.

2.2.6 Mechanistic investigation

A DNA has two main components that could be responsible for adsorption: phosphate and the nucleobases. To understand the adsorption mechanism, a series of displacement experiments were carried out. The DNA/ITO conjugates were exposed to nucleosides and several anions. No significant DNA desorption was observed in the presence of the nucleosides at pH 7.6, suggesting the lack of strong interaction between the bases and ITO (Figure 2.7A). We also tested the effect of various common anions (Figure 2.7B). Citrate and phosphate displaced adsorbed DNA quickly while the other anions had

no effect. Therefore, it is likely that the phosphate on DNA backbone is responsible for DNA adsorption. The interaction was further confirmed by measuring the ζ -potential of ITO NPs in the presence of phosphate. At pH 4, phosphate can displace the surface hydroxyl groups by forming inner-sphere complexes with the low-coordinated In and/or Sn on ITO NPs surface. Such displacement alters the surface charge from positive to negative (Figure 2.7C). Taken together, the phosphate backbone of DNA electrostatically adsorb onto ITO.

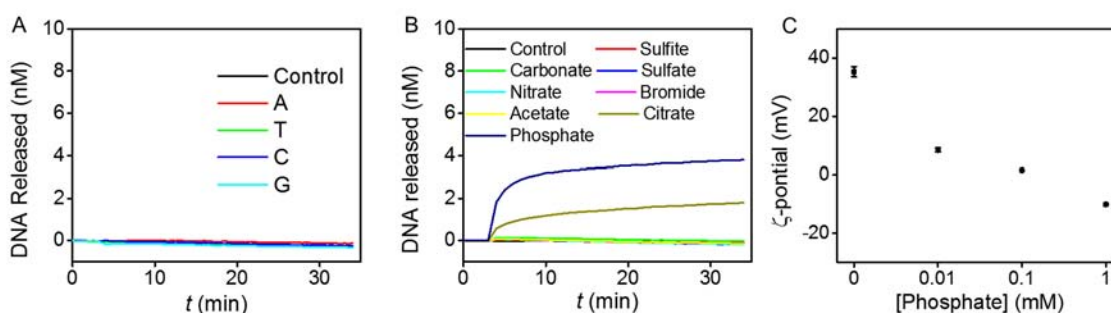


Figure 2.7 Mechanistic investigation of DNA on ITO NPs. Displacement of DNA by (A) 1 mM nucleosides and (B) 1 mM various anions. (C) ζ -potential of ITO NPs as a function of phosphate concentration. The NPs were dispersed in acetate buffer (pH 4, 20 mM).

2.2.7 DNA-induced desorption

After understanding DNA adsorption, we next studied cDNA induced desorption. The FAM-labeled probe DNA was first adsorbed onto ITO. Addition of cDNA induced a concentration-dependent fluorescence recovery (Figure 2.8A). As low as 0.7 nM cDNA can be detected based on signal greater than 3 times of background variation (inset). This performance is comparable to that reported with GO for a similar detection scheme.^{187,198} It is interesting to note that at high cDNA concentration (e.g., 60 nM); the released FAM-

DNA2 was only 66% of the adsorbed. The remaining probe were still adsorbed. This suggests that the surface of ITO might be heterogeneous and the places with more indium component might adsorb DNA more stably and cannot be released by the cDNA.

To test the specificity of this cDNA induced probe release, we also added a DNA with the same sequence as the probe DNA but non-labeled (named sDNA, Figure 2.8B). In this case, the released probe DNA was negligible, suggesting that formation of duplex is a driving force for DNA desorption. Since duplex DNA still maintains negatively charged property, it suggests that rigid duplex binding to ITO surface is less favorable compared to the flexible single-stranded DNA (Figure 2.8E, i). To compare ITO with its components, we adsorbed FAM-labeled DNA onto In_2O_3 . SnO_2 was not included since it does not adsorb DNA at pH 7.6. Then cDNA was added. It is interesting to note that In_2O_3 exhibits a low response in the presence of cDNA (Figure 2.8D), which might be related to its positive surface charge and can further adsorption the cDNA. It is likely that SnO_2 has a modulation effect to weaken adsorption capability. Our ITO NPs contain 10% SnO_2 and 90% In_2O_3 , meaning that a small doping can significantly adjust the adsorption affinity (Figure 2.8 E, ii).

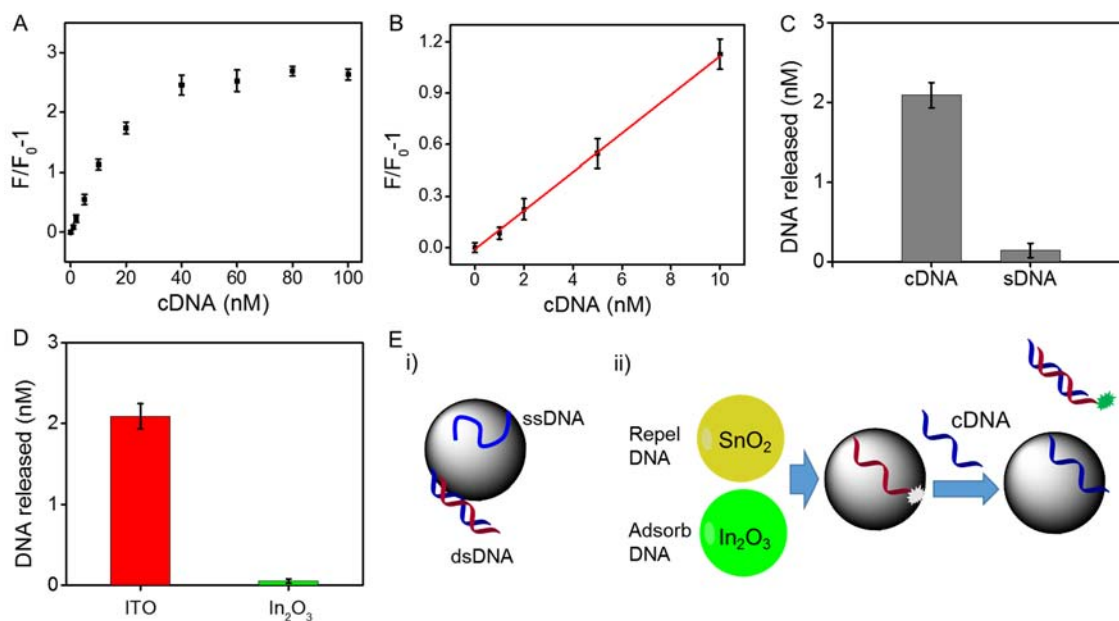


Figure 2.8 DNA detection using DNA/ITO conjugates. (A) Fluorescence recovery as a function of cDNA concentration. (B) Fitting the linear part of (A). (C) Comparison of cDNA and sDNA (same DNA, no fluorophore) induced probe DNA release. (D) Comparison of ITO and In_2O_3 in cDNA-induced DNA recovery. (E) Proposed models in cDNA-induced DNA recovery from ITO NPs.

2.3 Materials and Methods

2.3.1 Chemicals

All of the DNA samples were purchased from Eurofins Scientific (Huntsville AL). Their sequences and modifications are shown in Table 1. The indium oxide NPs (In_2O_3 , 20-70 nm, stock # US3250), tin dioxide NPs (SnO_2 , 18 nm, stock # US3470) and indium tin oxide NPs (In_2O_3 : SnO_2 = 90: 10, 20-70 nm, stock # US3855) were purchased from US Research Nanomaterials, Inc. (Houston, TX). Sodium acetate, sodium citrate, sodium phosphate, sodium chloride, 4-(2-hydroxyethyl) piperazine-1-ethanesulfonic acid

(HEPES), 2-(N-morpholino) ethanesulfonic acid (MES) and nucleosides were from Mandel Scientific (Guelph, ON, Canada). Milli-Q water was used for all of the experiments.

Table 2.1 The sequences and modification of DNA used in this work

| DNA names | Sequences (from 5' to 3') and modifications |
|---------------------------|--|
| Alexa-DNA1 | TCA CAG ATG CGT-Alexa Fluoro 488 |
| FAM-DNA2 | FAM-ACG CAT CTG TGA AGA GAA CCT GGG |
| sDNA | ACG CAT CTG TGA AGA GAA CCT GGG |
| cDNA | CCC AGG TTC TCT TCA CAG ATG CGT |
| FAM-A₅ | FAM-AAA AA |
| FAM-A₁₅ | FAM-AAA AAA AAA AAA AAA |
| FAM-T₁₅ | FAM-TTT TTT TTT TTT TTT |
| FAM-C₁₅ | FAM-CCC CCC CCC CCC CCC |
| FAM-G₁₅ | FAM-GGG GGG GGG GGG GGG |
| FAM-A₃₀ | FAM-AAA AAA AAA AAA AAA AAA AAA AAA AAA AAA |

2.3.2 Transmission electron microscopy and dynamic light scattering measurements

Transmission electron microscopy (TEM) images of the three metal oxide NPs were acquired using a Philips CM10 transmission electron microscope. Samples were prepared by dropping oxides dispersion into a copper grid, and put in a fume hood at room temperature overnight. The ζ -potential of oxide dispersions was measured by dynamic light scattering (DLS) using Malvern Nanosizer ZS90. To measure the ζ -potential of NPs at different pH, the oxides were dispersed in designed pH buffers (10 mM, acetate buffer for pH 4 and 5, MES for pH 6, and HEPES for pH 7 and 8). The hydrodynamic size of metal

oxides dispersed in HEPES (pH 7.6, 10 mM) was also measured by the same instrument. The temperature was maintained at 25 °C during measurement. The final concentration of oxide NPs was 50 µg/mL.

2.3.3 DNA adsorption and desorption kinetics

To study the effect of pH on adsorption kinetics, Alexa-DNA1 (10 nM) was dissolved into buffers at different pH (10 mM). The initial fluorescence of free DNA (F_0) was monitored for 3 min (excitation at 485 nm, emission at 535 nm) using a microplate reader (Infinite F200Pro, Tecan). After a quick addition of ITO NP dispersion (final concentration 50 µg/mL), the fluorescence was monitored for another 20 min. The fluorescence intensity (F) was then normalized based on F_0 . The DNA adsorption kinetics as a function of NaCl concentration (FAM-DNA2 10 nM, ITO 50 µg/mL) was performed in a similar way. Adsorption kinetics of FAM-DNA2 (10 nM) onto three oxides (ITO, In_2O_3 , and SnO_2) was carried out in HEPES buffer (pH 7.6, NaCl 150 mM) using the same mass concentration of materials (50 µg/mL).

To study desorption of DNA from ITO NP surface, the DNA-ITO conjugates were prepared as described above at designed conditions. To test the effect of pH on DNA desorption, for example, the DNA-ITO conjugates were prepared by incubating Alexa-DNA1 (300 nM) with ITO NPs (500 µg/mL) at pH 4 for 1 h. After diluting the conjugated with Mill-Q water 10 times and monitoring the background fluorescence for 3 min, the pH was adjusted by adding 20 mM pH 7 or pH 8 HEPES buffer. The fluorescence was monitored for another 30 min.

To study the displacement of adsorbed DNA by nucleosides or inorganic anions, FAM-DNA2 (10 nM) was adsorbed onto ITO NPs at pH 7.6 (HEPES 10 mM, NaCl 150 mM). Nucleosides or anions (1 mM) were introduced to induce DNA desorption. The released DNA was calculated based on the free DNA in the same buffer conditions.

2.3.4 DNA loading capacity

The DNA loading capacity was measured based on the fluorescence decrease upon adding ITO or other oxides under various designed conditions. To test the effect of NaCl on DNA loading capacity at pH 7.6, for example, FAM-DNA2 (30 nM) was incubated with ITO (50 µg/mL) at varying concentrations of NaCl. After 2 h incubation, the fluorescence was measured to calculate adsorbed DNA. The pH dependent loading capacity was determined in a similar way by adsorbing Alexa-DNA1 (30 nM) onto ITO (50 µg/mL) at designed buffer conditions in the absence of additional NaCl.

2.3.5 DNA induced desorption

To study cDNA induced DNA desorption, FAM-DNA2 (10 nM) was incubated with ITO NPs (50 µg/mL) for 2 h and then dispersed in buffer solution (HEPES 10 mM, pH 7.6, NaCl 150 mM). After adding cDNA and 1 h reaction, the fluorescence was recorded. For the selectivity study, same amount of cDNA and the same DNA (10 nM) was added. To compare ITO with In₂O₃, the DNA-oxides conjugates were prepared in the same buffer condition. The concentration of probe DNA (FAM-DNA2) and cDNA were both 10 nM. The concentrations of In₂O₃ was 50 µg/mL.

2.4 Summary

In summary, a systematic study was carried out to understand DNA adsorption by ITO NPs. We show that fluorescently labeled ssDNA can be adsorbed by ITO NPs, inducing fluorescence quenching. The surface charge of ITO is important in maximizing the DNA loading. From displacement experiments, DNA adsorption is mainly through the phosphate backbone via electrostatic interaction with the ITO surface. The ITO-DNA conjugate can be used to detect cDNA down to 0.7 nM. Interestingly, ITO shows an averaged behavior of SnO₂ and In₂O₃. Doping the tin component has weakened DNA binding affinity, making it possible to directly detect cDNA. This study provided fundamental insights into DNA interaction with ITO, which is an important transparent electrode material useful for biosensor development.

Chapter 3 DNA Adsorption by Magnetic Iron Oxide Nanoparticles and Its Application for Arsenate Detection

The results presented in this chapter have been published as part of:

Biwu Liu and Juewen Liu, DNA Adsorption by Magnetic Iron Oxide Nanoparticles and Its Application for Arsenate Detection. *Chemical Communications*, 50, 8568-8570, 2014.

3.1 Introduction

Magnetic iron oxide nanoparticles have been intensively developed for environmental applications, including removal of heavy metal ions, oxyanion, and organic contaminants.⁸⁶ Removal of arsenic by iron oxide has been studied for decades. Iron oxide is ideal for this purpose because of its strong adsorption affinity and magnetic property, allowing for convenient separation. This method works in natural water samples, implying selectivity for arsenic in the environmental sample matrix. The interaction between arsenic species and iron oxide has been well-characterized by a diverse range of spectroscopic methods (see Section 1.3.2).

Arsenic is an extremely toxic element and arsenic contamination in many wells, lakes and rivers has caused serious adverse health effects,^{92,94,95} damaging skin, heart, liver and kidney and even leading to cancer and death.¹⁹⁹ To manage the arsenic poisoning problem, detection of arsenic is crucial. Currently, the detection task is mainly carried out using analytical instruments such as atomic emission²⁰⁰ or absorption spectroscopy,²⁰¹ inductively coupled plasma mass spectrometry (ICP-MS),²⁰² quartz crystal microbalance,²⁰³ surface enhanced Raman scattering, or electrochemistry.²⁰⁴ However, regions with arsenic contamination problems often lack centralized labs or equipment for

water analysis. In this regard, developing cost-effective biosensors might provide a more practical solution.

There are a few commercial kits based on simple inorganic reactions, which involve reducing arsenic species by zinc to produce highly toxic arsine (Gutzeit reaction).²⁰⁵ However, these sensors fail to measure arsenic accurately for various reasons.²⁰⁵ Therefore, efforts are still devoted to develop new sensors. On the biosensor side,⁹³ genetically engineered bacterial cells have been reported.²⁰⁶ In addition, assays were developed based on the inhibition of acetylcholinesterase,²⁰⁷ or cytochrome *c* activity by arsenic species.²⁰⁸ On the chemical sensor side, colorimetric assays were developed; they took advantage of the strong interaction between arsenite and thiol or noble metals.

Phosphate shares similar solution chemistry with arsenate and the free phosphate concentration in groundwater is very low (typically below 1 μM).²⁰⁹ We reason it may be possible to design sensors based on this. For example, DNA is a polyphosphate and it may be adsorbed by iron oxide, and then arsenate can displace the adsorbed DNA. Given the vast amount of knowledge on DNA detection, high sensitivity might be achieved. In this chapter, we report DNA-functionalized magnetic iron oxide nanoparticle for arsenate detection.

3.2 Results and Discussion

3.2.1 Sensor design and proof of concept

Given the similarity between phosphate and arsenate, we reason that DNA may also adsorb in a comparable way. Based on this assumption, we propose a scheme of sensor design (Figure 3.1D). Using a fluorescently labeled DNA, adsorption onto iron oxide

results in fluorescence quenching; arsenate competition then releases DNA and restores fluorescence, providing simultaneous arsenate detection and removal.

To test this hypothesis, we employed Fe_3O_4 NPs with an average size of ~ 25 nm (see Figure 3.1C for TEM). These NPs carry a negative charge at neutral pH (ζ -potential = -10 mV in 10 mM HEPES buffer, pH 7.6). Mixing Fe_3O_4 with a FAM-labeled DNA indeed resulted in strong fluorescence quenching (Figure 3.1E), indicating that DNA can be adsorbed and Fe_3O_4 is a fluorescence quencher. Addition of arsenate produced strong fluorescence, suggesting displacement of the adsorbed DNA by arsenate as shown in Figure 3.1E. In the subsequent work, we aim to optimize the DNA adsorption/desorption conditions and study the sensor performance.

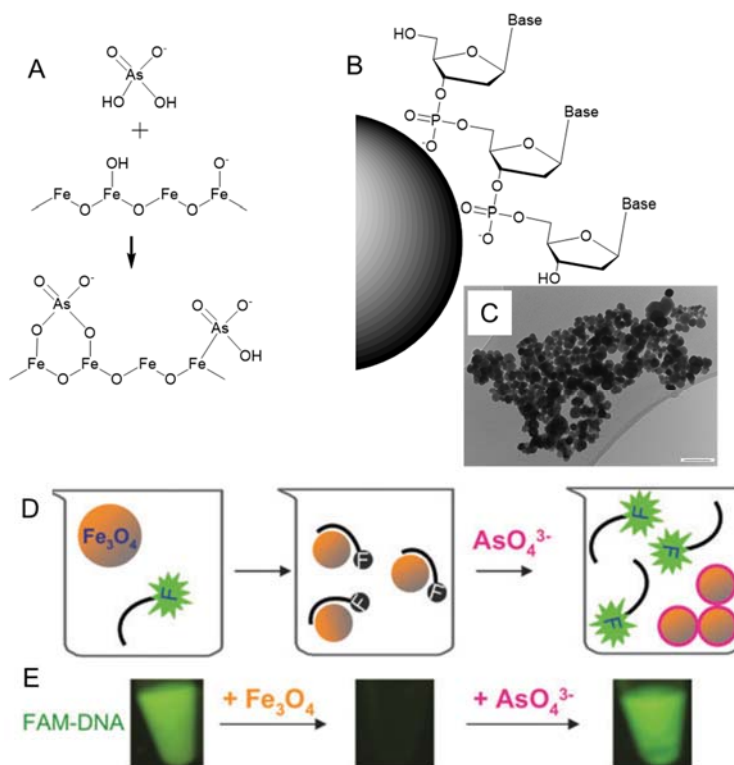


Figure 3.1 Design and proof of concept for arsenate sensor using DNA/ Fe_3O_4 NPs. (A) Adsorption of arsenate by iron oxide. (B) The structure of DNA, where its phosphate backbone can also bind to iron oxide. (C) TEM micrograph of iron oxide nanoparticles.

The scale bar is 100 nm. (D) Schematics of sensing and removal of arsenate by DNA-functionalized iron oxide NPs. DNA fluorescence is quenched upon adsorption. The NPs with adsorbed arsenate can be collected with a magnet. (E) Fluorescence photographs demonstrating the sensing scheme in (D) using a FAM-labelled 24-mer DNA (500 nM DNA in 25 mM HEPES, pH 7.6). $\text{Fe}_3\text{O}_4 = 10 \text{ mg/mL}$; final arsenate concentration = 40 mM.

3.2.2 Optimization of DNA adsorption

We first optimized the salt concentration. Fluorescence quenching provides a convenient assay to study DNA adsorption. In addition to iron oxide, many other nanomaterials also quench fluorescently labeled DNA, such as graphene oxide,¹⁸⁷ carbon nanotubes,²¹⁰ metal oxides,^{79,84} and AuNPs.²¹¹ Since both DNA and Fe_3O_4 NPs are negatively charged, no DNA was adsorbed in the absence of salt due to the charge repulsion (Figure 3.2A). Fast adsorption was achieved at higher ionic strength. We chose to perform DNA adsorption with 300 mM NaCl to achieve high adsorption efficiency. Next we studied the effect of DNA length (Figure 3.2B). Considering the scheme in Figure 3.1D, an ideal sensor should use shorter DNA to achieve a high probe density. The probe needs to cover the NP surface as much as possible, so that arsenate can directly compete with DNA binding instead of occupying free surface sites. However, FAM-A₅ adsorbed much less than FAM-A₁₅, which is attributed to the weaker affinity of shorter DNA. In other words, longer DNA is needed to achieve a stable multivalent interaction. FAM-A₃₀ also adsorbed less DNA, which is attributed to its larger size and thus occupying more footprint. Therefore, 15-mer DNA is an optimal length.

Using 15-mer DNA, the effect of DNA sequence was further studied (Figure 3.2C). We assumed that adsorption takes place via the phosphate backbone, and therefore DNA sequence should play a minor role. Indeed, all the four types of homopolymers can be adsorbed by Fe₃O₄ NPs. FAM-C₁₅ adsorbed with the fastest rate, giving also the lowest background. However, only ~60% FAM-G₁₅ was adsorbed. This may be caused by the formation of a G-quadruplex structure, impeding DNA adsorption.

DNA adsorption isotherm was next measured using FAM-C₁₅ (Figure 3.2E). When the added DNA was below 30 nM (Fe₃O₄ concentration = 25 µg/mL), adsorption was quantitative. Further increase of DNA concentration resulted in an overall Langmuir type of isotherm, which is reasonable since the adsorption should stop at a monolayer of DNA and adsorption is reversible based on the above phosphate displacement assay. The final capacity is 105 nM DNA for Fe₃O₄ NP of 25 µg/mL, corresponding to 55 FAM-C₁₅ DNA molecules per 20 nm Fe₃O₄ NP. This capacity is lower than adsorption of thiolated DNA by gold NPs, where each 20 nm NP can adsorb ~200 DNA.⁴¹ This lower capacity also indicates that DNA wraps around Fe₃O₄ NPs instead of adopting an upright conformation as in the AuNP system.

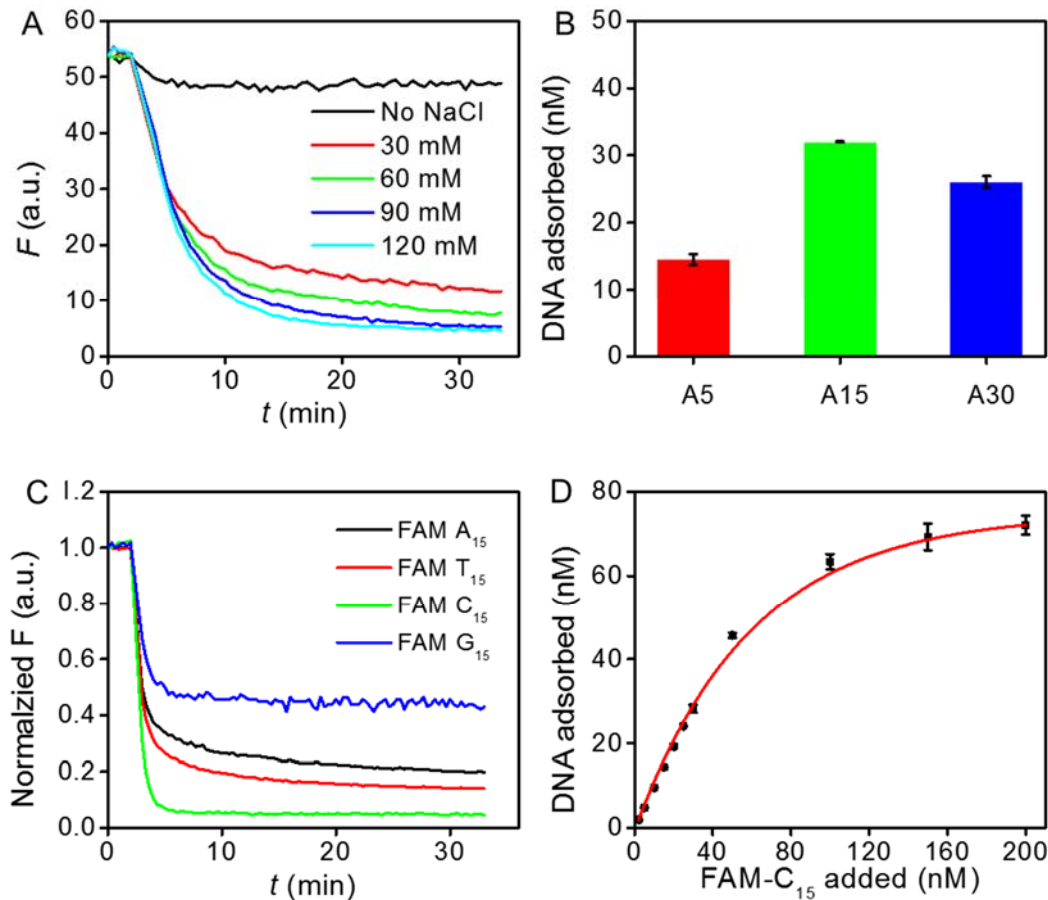


Figure 3.2 DNA adsorption behaviour by Fe₃O₄ NPs. (A) Adsorption kinetics of FAM-labeled 24-mer DNA by Fe₃O₄ NPs in the presence of different NaCl concentrations. (B) Adsorption capacity of FAM-labeled poly-A DNA as a function of DNA length. The NP concentration was 25 μ g/mL and the DNA concentration was 50 nM. The buffer contains 10 mM HEPES, pH 7.6 with 300 mM NaCl. (C) Adsorption of FAM-labeled 15-mer DNA with different sequences. (D) Adsorption isotherm of FAM-C₁₅ DNA.

To further confirm the adsorption mechanism, a displacement assay was performed. FAM-T₁₅ was first adsorbed and the sample was treated with free phosphate or thymidine (Figure 3.3). Strong fluorescence enhancement was observed only with phosphate. Therefore, the base is unlikely to be important for DNA adsorption by iron oxide.

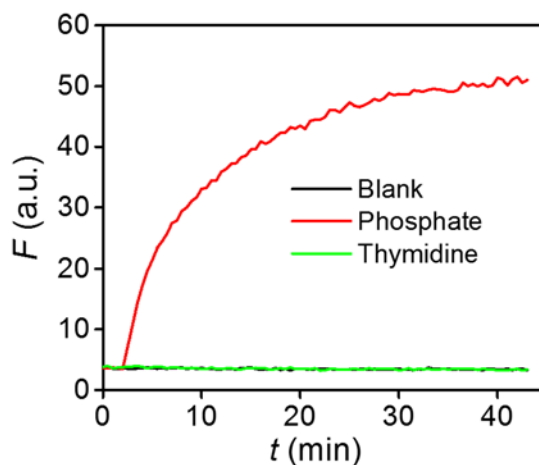


Figure 3.3 Desorption of the FAM-T₁₅ from Fe₃O₄ NPs by free phosphate or thymidine, demonstrating DNA adsorption occurs via the phosphate backbone.

3.2.3 Sensor performance

After optimizing DNA adsorption by Fe₃O₄ NPs for sensor preparation, we next studied the sensor performance in arsenic detection (Figure 3.4). The sensor was prepared using FAM-C₁₅. Since both arsenate and arsenite can bind to Fe₃O₄ NPs, we tested the sensor response for both species. As shown in Figure 3.4A and D, without arsenate or arsenite, the DNA/Fe₃O₄ NPs conjugate has a consistent and low signal, indicating the probe DNA adsorption was stable. In the presence of arsenate or arsenite, the sensor fluorescence gradually increased. The kinetics was initially fast followed by a slower phase. A large signal was achieved in just 10 min. Higher concentration of arsenate or arsenite produced stronger fluorescence enhancement. The signal increase reached ~35-fold with 500 μM arsenate and ~25-fold with 500 μM arsenite. This is among the highest signal increase in DNA-based sensors.^{212,213,214} The dynamic range goes up to 100 μM arsenate (Figure 3.4B) and the detection limit (LOD) was determined to be 300 nM based on the signal higher than three times of background variation (Figure 3.4C). The sensor is less

sensitive for arsenite, with a linear range up to 500 μM (Figure 3.4E). However, it has a weak response in the low concentration range (below 5 μM , Figure 3.4F). Therefore, our sensor is preferred to arsenate detection. The LOD is slightly higher than the current 130 nM WHO guideline, but below the 670 nM action limit by many developing countries. Another method to further improve sensitivity will be discussed next.

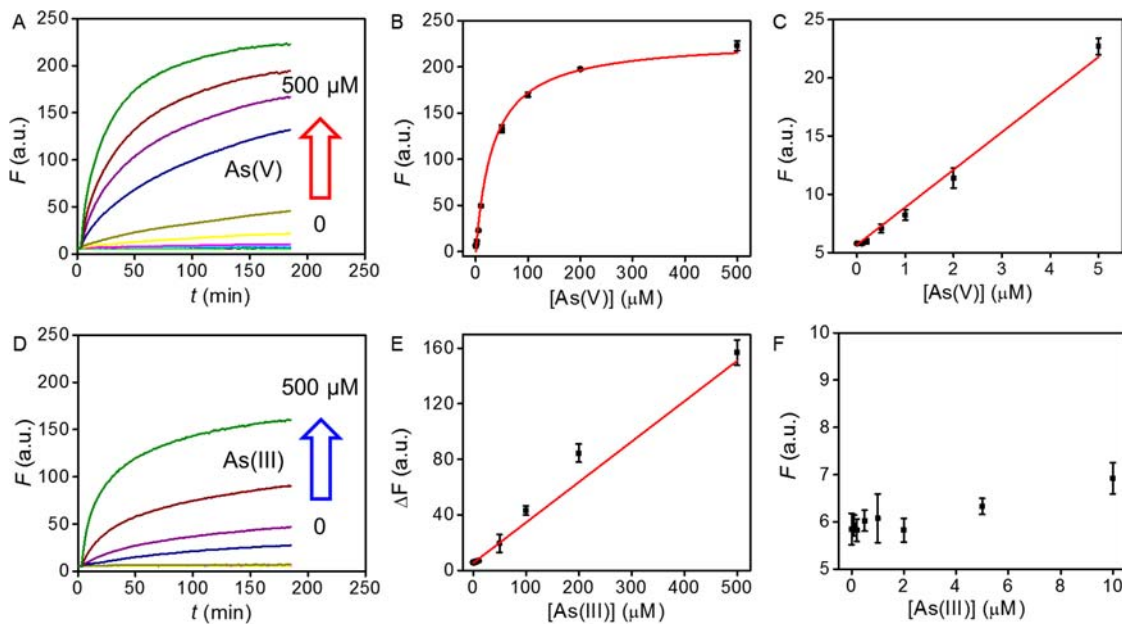


Figure 3.4 Performance of FAM-C₁₅/Fe₃O₄ conjugates as a sensor for arsenate and arsenite. Kinetics of sensor fluorescence increase with increasing of (A) arsenate and (D) arsenite. Sensitivity of FAM-C₁₅/Fe₃O₄ conjugates in (B) arsenate and (E) detection. The initial part Figure (B) and (D) are plotted in Figure (C) and (F), respectively.

To test the selectivity of the sensor, we incubated the prepared DNA/Fe₃O₄ NPs with various anions and only phosphate showed a high response (Figure 3.5A). This is expected since phosphate can also bind to the surface. Systematic comparison of phosphate and arsenate adsorption by iron oxide was previously reported, with arsenate adsorbing

slightly more strongly.¹¹⁹ Since the buffer already contained 300 mM NaCl, we did not test the further addition of chloride. Other common anions such as bromide, iodide, nitrate, perchlorate, acetate, bicarbonate, sulphate and sulphite did not produce much signal. As mentioned above, arsenite showed a relatively low response at the tested concentration. Therefore, this sensor is the most selective for arsenate.

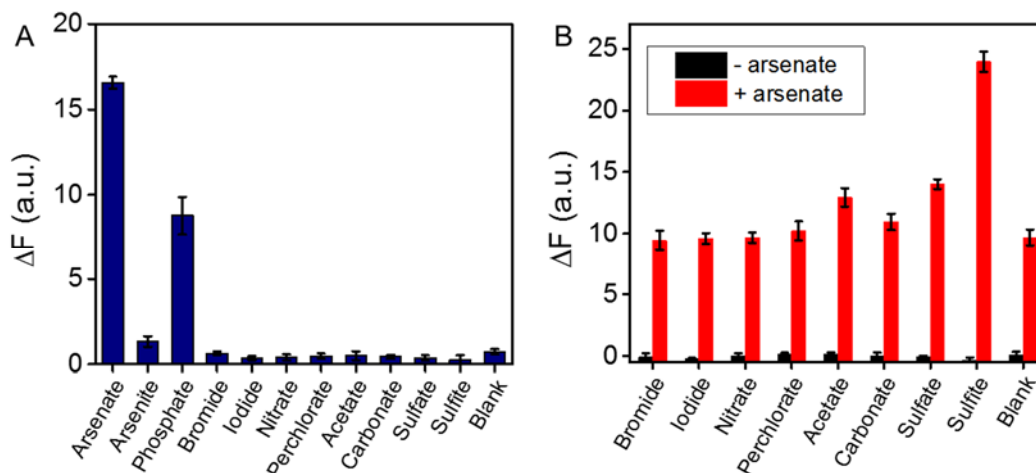


Figure 3.5 Selectivity of sensor in arsenate detection. (A) Selectivity against 10 μM other anions. The buffer contained 300 mM NaCl, 10 mM HEPES, pH 7.6. (B) Response of the sensor to other 1 mM anions with or without 10 μM arsenate.

Since phosphate is a limiting nutrient for organism growth and it can be easily precipitated by many cations, its concentration in water is very low (e.g., 1 μM being the upper limit in normal potable water).²⁰⁹ For other water samples with higher phosphate concentrations, a pre-treatment to precipitate phosphate or a separate phosphate sensor will be needed. We next tested a higher concentration of other anions (1 mM each) and still none of them showed much response (Figure 3.5B). When 10 μM arsenate was added to these samples, a high response was observed. The response in the presence of sulfite was

even higher than that in the absence. This might be related to its weak blocking effect to allow arsenate specifically displacing DNA instead of binding to the free iron oxide surface.¹¹⁵

3.2.4 Improved sensitivity

An alternative method is to incubate iron oxide NPs with the water sample first, where high removal capacity can be achieved with a large quantity of NPs. Adsorption of arsenate might inhibit DNA adsorption to achieve detection (Figure 3.6A). After harvesting the NPs with a magnet, only a small portion of the NPs needs to be used for detection. For the sensing aspect, this method also allows higher sensitivity since a large volume of water sample can be used without worrying about diluting DNA. Indeed, using the method, the detection limit was improved to 50 nM arsenate (Figure 4B). This sensitivity is comparable with those of many other arsenic sensors.^{206,215,216,217} In addition, the arsenate in solution was simultaneously removed by the adsorption process. We confirmed the removal efficiency using ICP-MS. After adsorption by Fe₃O₄ NPs, the arsenate concentration was below the detection limit (< 0.1 μg/L). We further tested the sensor response when it was dispersed in Lake Ontario water samples (Figure 3.6C). A similar response curve was observed.

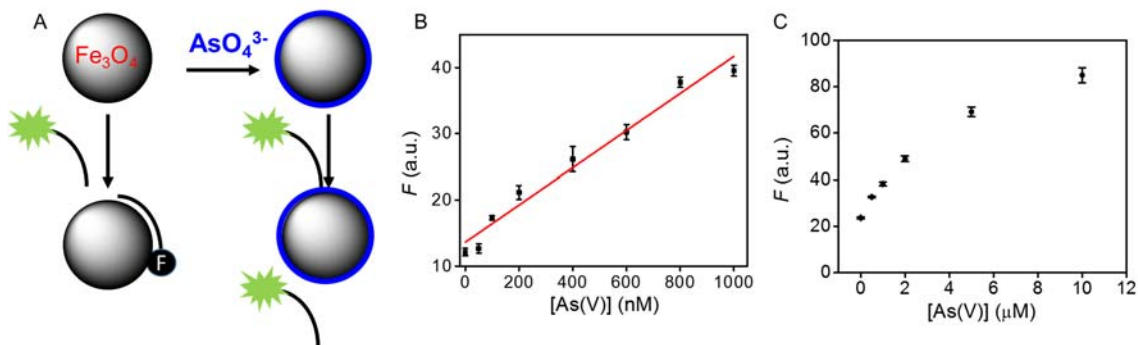


Figure 3.6 Improved sensitivity by pre-adsorbing arsenate. (A) A scheme of detecting arsenate by adsorbing it first before adding probe DNA. This allows high capacity arsenate removal and only a small portion of the NP is needed for detection. (B) Sensitivity of arsenate detection by this arsenate pre-adsorption method. (C) Sensor response in the Lake water matrix.

3.3 Materials and Methods

3.3.1 Chemicals

All of the DNA samples were purchased from Integrated DNA Technologies (IDT, Coralville, IA) and were purified by standard desalting. Their sequences and modifications are FAM-24 mer (FAM-ACG CAT CTG TGA AGA GAA CCT GGG), FAM-A₁₅ (FAM-AAA AAA AAA AAA AAA), FAM-T₁₅ (FAM-TTT TTT TTT TTT TTT), and FAM-C₁₅ (FAM-CCC CCC CCC CCC CCC). For the DNA homopolymers, FAM was labeled on the 5'-end. Sodium chloride, sodium bromide, sodium iodide, sodium nitrate, sodium bicarbonate, sodium acetate, sodium citrate, sodium phosphate dibasic heptahydrate, and 4-(2-hydroxyethyl) piperazine-1-ethanesulfonic acid (HEPES) were from Mandel Scientific (Guelph, ON, Canada). Sodium (meta)arsenite, sodium arsenate dibasic heptahydrate, sodium sulfate, sodium sulfite, sodium perchlorate were purchased from Sigma. Milli-Q water was used for all of the experiments.

3.3.2 Characterization of Fe₃O₄ NPs

To measure the ζ -potential of Fe₃O₄ NPs, 100 $\mu\text{g/mL}$ Fe₃O₄ NPs was dispersed in 10 mM buffer (HEPES, pH 7.6). The ζ -potential was then recorded using Zetasizer Nano

90 (Malvern). The TEM image was acquired on a Philips CM10 transmission electron microscope.

3.3.3 DNA adsorption by Fe₃O₄ NPs

To study the effect of NaCl concentration on DNA adsorption kinetics, FAM-24 mer (10 nM) was dissolved in HEPES buffer (pH 7.6, 10 mM) containing varying concentration of NaCl. After quickly adding the Fe₃O₄ NPs, the fluorescence was monitored for 30 min by a microplate reader (Infinite F200 Pro, Tecan). To study the effect of DNA length, 50 nM FAM-labeled DNA (A₅, A₁₅, or A₃₀) was dissolved in buffer A (10 mM HEPES, pH 7.6, 300 mM NaCl). After adding Fe₃O₄ NPs (final concentration = 25 µg/mL) and 30 min incubation, the fluorescence was recorded and compared to the initial intensity to calculate the adsorbed DNA. To test the effect of DNA sequence, 10 nM FAM-A₁₅, T₁₅, C₁₅, or G₁₅ was used. To obtain the adsorption isotherm, FAM-C₁₅ was used. For the displacement experiment, 2 mM phosphate or thymidine was added to the FAM-T₁₅/Fe₃O₄ NPs conjugate in buffer A followed by fluorescence recording for 40 min.

3.3.4 Arsenate detection (method 1)

The sensor was prepared by adsorbing FAM-C₁₅ (30 nM) onto Fe₃O₄ NPs (25 µg/mL) in buffer A in a total volume of 10 mL. The adsorption was allowed to take place for 1 h. This mixture was then divided into 100 µL aliquots in a 96-well plate. Then a small volume (1-5 µL) of arsenate with designed concentrations was added into 100 µL of the conjugate to induce desorption. The kinetics were obtained by monitoring the fluorescence for 3 h in triplicate. The response of arsenite was carried out using the same method.

For the selectivity test, a final concentration of 10 μM anions (arsenate, arsenite, phosphate, bromide, iodide, nitrate, perchlorate, acetate, carbonate, sulfate, or sulfite) were added, and the fluorescence was recorded after 1 h. The detection of arsenate (10 μM) in the presence of high anion concentration (1 mM) was also tested.

3.3.5 Arsenate detection (method 2)

Alternatively, Fe_3O_4 NPs (25 $\mu\text{g}/\text{mL}$) were incubated with various concentrations of arsenate in buffer A with a volume of 10 mL for 1 h. After that, the samples were agitated to fully disperse the Fe_3O_4 NPs, and 100 μL was taken out to mix with FAM- C_{15} probe DNA (30 nM). The fluorescence was measured after 1 h incubation. Lake Ontario water samples were collected from Colonel Samuel Smith Park in Toronto, Ontario, Canada. Arsenate was spiked into the Lake water sample and other operations were the same.

3.3.6 Arsenate removal

Arsenate (1 μM) was incubated with Fe_3O_4 NPs (10 $\mu\text{g}/\text{mL}$) 25 at pH 7 with a volume of 40 mL. After overnight incubation, the Fe_3O_4 NPs was precipitated using a magnet and the supernatant was diluted to 120 mL. The concentration of arsenic was tested by ICP-AES in the ALS facility in Waterloo, Ontario.

3.4 Summary

In summary, we studied DNA adsorption by iron oxide and demonstrated its application for detecting arsenate from water. DNA has been widely used to develop biosensors in the past two decades.⁴ In particular, many metal ions are detected using

aptamers and DNAzymes,^{4,218} where the DNA bases play a crucial role for metal recognition. Since DNA is a polyanion, DNA has not been very successful in detecting anions, possibly due to charge repulsion. Although arsenate aptamers have been claimed,²¹⁹ and a few related sensors have been developed,²²⁰ the binding mechanism responsible has not been elucidated. This work provides a new direction for anion sensing using DNA. DNA adsorption by nanomaterials is a popular way of signaling. Compared to adsorption reported previously for most other nanomaterials, the mechanism here is quite different. Binding of DNA to iron oxide is through the phosphate group, which is different from binding to gold (chemisorption through base nitrogen) or carbon (π - π stacking and hydrophobic force).⁷ Despite this simple interaction, the sensitivity and specificity of the sensor is quite remarkable. This is attributed to the strong affinity between arsenate and iron oxide.

Chapter 4 A Comprehensive Screen of Metal Oxide Nanoparticles for DNA Adsorption, Fluorescence Quenching, and Anion Discrimination

The results presented in this chapter have been published as part of:

Biwu Liu and Juewen Liu, A Comprehensive Screen of Metal Oxide Nanoparticles for DNA Adsorption, Fluorescence Quenching, and Anion Discrimination. *ACS Applied Materials & Interfaces*, 7, 24833-24838, 2015.

4.1 Introduction

DNA is highly attractive for designing hybrid materials due to its programmability, cost-effectiveness, ease of modification, and ability to recognize a broad range of analytes.^{51,176,178,221,222,223} While DNA has been interfaced with metal and carbon-based nanomaterials,^{4,7,51,224} limited work was carried out on metal oxide nanoparticles (MONPs).^{79,82,83,84,85,197,225,226,227,228,229} MONPs represent a very important class of materials due to their unique electronic, optical, magnetic and catalytic properties. DNA-functionalized MONPs might be useful as a sensor platform for anion detection. For example, when a fluorescently labeled DNA is adsorbed by iron oxide nanoparticles, the fluorescence is quenched.²²⁶ Arsenate adsorbs very strongly on iron oxide,^{108,119} displacing adsorbed DNA and regaining fluorescence.

We hypothesize that other metal oxides might have different adsorption affinity trends towards different anions, allowing their distinction using a sensor array. Array-based sensing is a strategy to differentiate multiple targets with high similarities. It mimics the

mammalian olfaction and is called “chemical nose”.²³⁰ Typically, the sensor array is composed of sets of receptors. Analytes are exposed to the sensor array to generate patterns of response. Then statistical analysis tools (e.g., linear discriminant analysis, LDA) are used to process the data. Different MONPs may have different affinities with DNA. At the same time, they also adsorb anions differently. Such differences may allow a pattern-recognition-based sensor array for anion discrimination. Arsenic is a highly toxic heavy metalloid inorganic arsenic exists in two forms in water: As(V) (arsenate) and As(III) (arsenite). For environmental science, it is important to know arsenic speciation.²³¹ Detection of phosphate is important on its own. Most river water has a low phosphate level, and elevated phosphate leads to water eutrophication problem.²³²

In this chapter, we screen a total of 19 MONPs with the intention to find different adsorption affinity patterns as a general way for anion discrimination. While various array-based methods have been reported,^{233,234,235,236,237,238,239,240} this is the first based on metal oxides.

4.2 Results and Discussions

4.2.1 Rationale of sensor design

Our experiment design is described in Figure 4.1. We started with nineteen commercially available MONPs, covering early and later transition metals as well as lanthanides. The detailed information about the nanomaterials are listed in Table 4.1. The final candidates need to offer different adsorption affinities for arsenate, arsenite, and phosphate. At the same time, they need to adsorb DNA, quench adsorbed fluorophore and

allow displacement of adsorbed DNA by target anions. Therefore, our screen of the MONPs is based on these criteria.

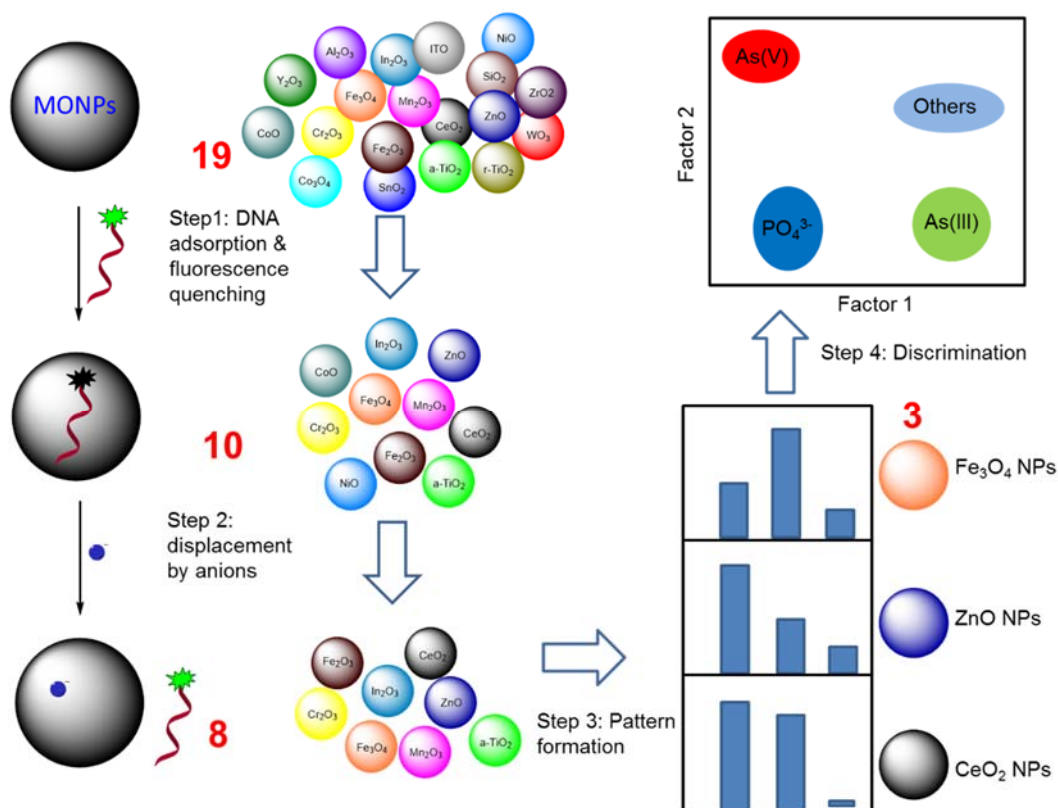


Figure 4.1 Schematics of the sensing strategy. Nineteen commercial MONPs were individually tested for adsorbing DNA and quenching fluorescence, from which eight were selected. These eight MONPs were tested with the different anions for DNA displacement, selectivity, and signalling. Finally, data from CeO₂, ZnO and Fe₃O₄ were used for discriminating arsenate, arsenite and phosphate using linear discriminant analysis. The numbers in red indicate the remaining number of MONPs after each screening step. The signalling scheme is included on the left side of the figure.

Table 4.1 Information of metal oxides nanoparticles (MONPs) used in this work

| Materials | Size**a | Hydrodynamic | ζ-Potential | Vendor**b | Catalog |
|------------------------------------|----------------|---------------------|--------------------|------------------|----------------|
| | (d, nm) | Size (d, nm) | (mV) | | Number |
| Al₂O₃ | 30-60 | 234.1 ± 3.03 | -68.27 ± 1.69 | S | 642991 |
| CeO₂ | 5 | 5.86 ± 0.39 | -4.23 ± 0.55 | S | 289744 |
| CoO | 50 | 591.17 ± 145.00 | -21.43 ± 3.18 | U. | US3051 |
| Co₃O₄ | 10-30 | 127.57 ± 21.34 | -30.53 ± 1.27 | U | US3056 |
| Cr₂O₃ | 60 | 614.2 ± 47.31 | -29.80 ± 0.88 | U | US3060 |
| Fe₂O₃ | 50 | 321.47 ± 27.30 | -29.80 ± 1.19 | U | US3200 |
| Fe₃O₄ | 50 | 534 ± 23.58 | -29.08 ± 2.99 | S | 637106 |
| In₂O₃ | 20-70 | 282.83 ± 38.70 | -22.08 ± 2.02 | U | US3250 |
| ITO | 20-70 | 332.17 ± 11.29 | -32.83 ± 1.10 | U | US3855 |
| Mn₂O₃ | 30 | 285.67 ± 14.26 | -50.00 ± 0.92 | U | US3340 |
| NiO | 10-20 | 433.5 ± 81.65 | 17.23 ± 0.21 | U | US3356 |
| SiO₂ | 12 | 171.9 ± 16.55 | -38.07 ± 0.74 | S | 718483 |
| SnO₂ | 18 | 261.83 ± 1057 | -40.5 ± 1.65 | U. | US3470 |
| a-TiO₂ (anatase) | 25 | 255.63 ± 9.99 | -25.80 ± 0.41 | S | 637254 |
| r-TiO₂ (rutile) | 30 | 175.87 ± 24.37 | -41.77 ± 0.67 | U | US3520 |
| WO₃ | 23-65 | 179.6 ± 4.75 | -49.6 ± 1.41 | U | US3540 |
| Y₂O₃ | 20-40 | 701.8 ± 283.97 | -8.79 ± 0.38 | U | US3550 |
| ZnO | 35 | 70.19 ± 3.90 | 23.45 ± 0.68 | S | 721077- |
| ZrO₂ | 100 | 174.5 ± 105.15 | -32.33 ± 1.96 | S | 544760 |

a: the information is provided the vendors.

b: U is US Research Nano, S is Sigma-Aldrich.

4.2.2 Screen for DNA adsorption

We first screened the MONPs for DNA adsorption and fluorescence quenching. A FAM (6-carboxyfluorescein) labeled DNA (named FAM-24 mer) was incubated with each MONP at pH 7.6. The buffer also included 300 mM NaCl to screen electrostatic interactions. After centrifugation to precipitate the MONPs, the samples were observed under 470 nm excitation (Figure 4.2A). The supernatant in each sample was also measured using a microplate reader for quantification of DNA adsorption efficiency (Figure 4.2B, black bars). Little DNA adsorbed on Al₂O₃, SiO₂, SnO₂, WO₃ or ZrO₂. The rest of the MONPs adsorbed DNA to various degrees. To test whether the poor DNA adsorption by some MONPs is attributable to insufficient particle concentration, we also measured the DNA adsorption at a lower pH (pH adjusted with 10 mM HCl). MONPs are more protonated at lower pH and should bind negatively charged DNA more tightly. Indeed, all the samples achieved quantitative DNA adsorption using the same amount of MONPs (Figure 4.2B, red bars), indicating the lack of adsorption at pH 7.6 (e.g., Co₃O₄, and r-TiO₂) is not related to surface area. Since we intend to use the sensors at neutral pH, Al₂O₃, SiO₂, SnO₂, WO₃, ZrO₂, Co₃O₄, and r-TiO₂ were ruled out after this step of screening.

The remaining MONPs are divided into two groups. Most MONPs strongly quench fluorescence upon DNA adsorption as indicated by the dark pellets and dark supernatants in Figure 4.2A. The remaining four (In₂O₃, ITO, Y₂O₃, and ZnO) display fluorescent pellets and dark supernatant, indicating that these MONPs might be poor fluorescence quenchers. A low quenching efficiency is attributed to a large band gap and disfavored electron

transfer (e.g., band gap of $\text{Y}_2\text{O}_3 = 5.85 \text{ eV}$).^{241,242} Among these four oxides, In_2O_3 can adsorb DNA and quench fluorescence better than ITO.²²⁵ We are particularly concerned about Y_2O_3 and ZnO , since they can efficiently adsorb DNA and are potential good candidates for anions sensing. After dispersing in buffer, the quenching efficiency of ZnO and Y_2O_3 was quantified to be $\sim 90\%$ and $\sim 50\%$, respectively (Figure 4.3). Since quenching is critical for our sensor design, Y_2O_3 and ITO were also ruled out. After this round of screening, only ten MONPs were left (Figure 4.1).

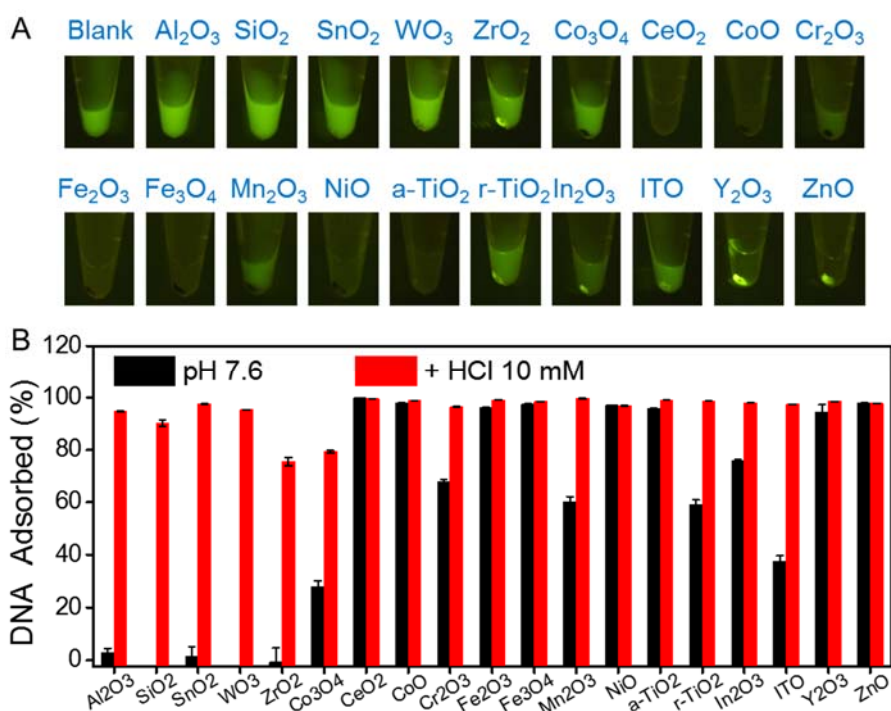


Figure 4.2 DNA adsorption and fluorescence quenching by various MONPs. The FAM-24 mer DNA (200 nM) was mixed with each MONP (0.5 mg/mL) in Buffer A (HEPES 10 mM, pH 7.6, 300 mM NaCl). (A) Photographs showing the samples under LED light excitation (470 nm) after centrifugation. Bright pellets indicate DNA adsorption with poor quenching, while bright supernatants indicate poor DNA adsorption. (B) Quantitative measurement of adsorbed DNA based on the free DNA remaining in the supernatant in

Buffer A (black bars) and in in HCl solution (10 mM). The error bars represent the standard deviation from three independent measurements.

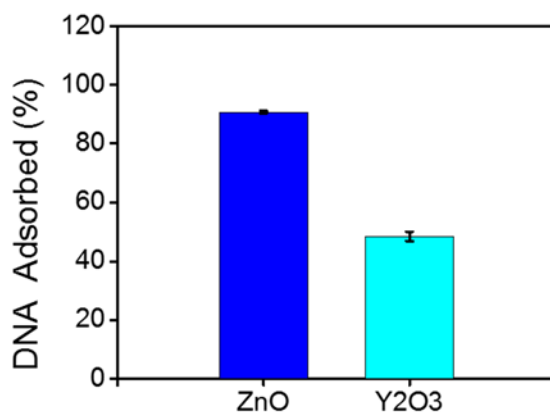


Figure 4.3 Fluorescence quenching efficiency of the FAM-24 mer DNA by ZnO NPs and Y₂O₃ NPs. The DNA/MONP conjugates were prepared by incubating 200 nM DNA with ZnO or Y₂O₃ (0.5 mg/mL) in Buffer A. The fluorescence was measured without centrifugation.

4.2.3 Screen for DNA desorption

After efficient DNA probe adsorption and fluorescence quenching, the adsorbed probe needs to be displaced by target anions for signaling (see the left side of Figure 4.1 for the sensing scheme). Therefore, we next measured anion-induced DNA release using the remaining ten MONPs. For this experiment, we started with the free FAM-24 mer DNA, which displayed strong fluorescence (the black spectra in Figure 4.4). After adding each MONP, all the samples were quenched efficiently (the red spectra in Figure 4.4); this is consistent with our above screening results. Then 0.5 mM phosphate was added to each sample to induce DNA displacement (green spectra in Figure 4.4). The DNA on CoO and

NiO was not displaced much by phosphate (less than 5%) and these two were ruled out for further studies (Figure 4.4B,H). It is likely that they interact too strongly with DNA. All other MONPs released the DNA probe upon adding phosphate, and they might be useful candidates for further biosensor development.

This displacement assay is also useful for understanding the interaction mechanism between DNA and MONPs. DNA has two structural elements for adsorption by surfaces: 1) negatively charged phosphate and 2) nucleobases. For metallic nanoparticles (e.g., AuNPs) and carbon-based nanomaterials (e.g., graphene oxide and carbon nanotubes), DNA adsorption is achieved mainly via base interaction.^{7,60,224,243,244} For example, adding phosphate has little effect on DNA adsorbed by these materials. Many MONPs (e.g., TiO₂, CeO₂, ITO) adsorb DNA mainly via the phosphate backbone.^{79,84,225,227} Here, we confirmed that phosphate backbone binding is also important for DNA adsorption onto Cr₂O₃, Mn₂O₃ and ZnO.

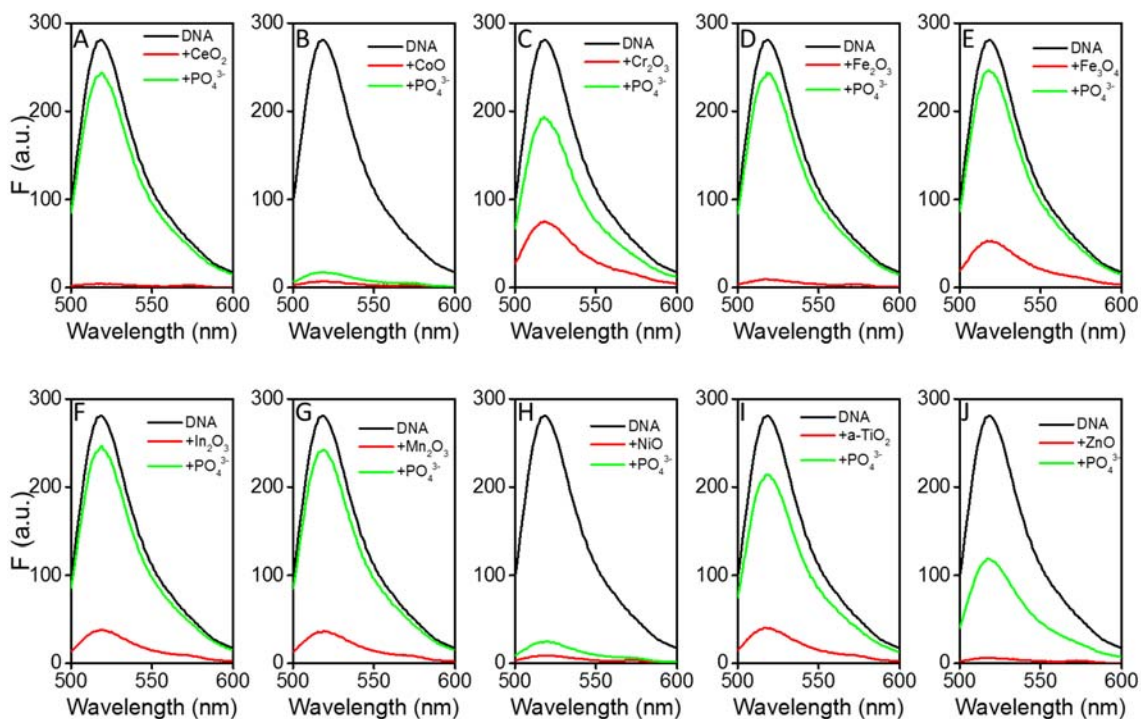


Figure 4.4 Phosphate-induced DNA release from various MONPs: (A) CeO_2 , (B) CoO , (C) Cr_2O_3 , (D) Fe_2O_3 , (E) Fe_3O_4 , (F) In_2O_3 , (G) Mn_2O_3 , (H) NiO , (I) $\alpha\text{-TiO}_2$, and (J) ZnO . The ten MONPs were added to FAM-24 mer DNA (100 nM) in Buffer A to achieve fluorescence quenching (red spectra). After adding phosphate (0.5 mM) and centrifugation, the fluorescence spectra of the DNA in the supernatant were then measured (green spectra). The free DNA spectra are in black.

In addition to phosphate, we also tested DNA displacement by other common oxyanions: arsenate, arsenite, and silicate (Figure 4.5A). They are all environmentally important analytes and may share a similar binding mechanism on MONPs. Interestingly, it is difficult to displace DNA from CoO and NiO using any of these anions. Other oxides allowed easier DNA displacement. Anion adsorption was also confirmed by the ζ -potential change of MONPs (Figure 4.5B). For example, the slightly negative charged CeO_2 (-4.23

± 0.55 mV) becomes much more negative (~ 50 mV) after adsorbing oxyanions. The positive surface of ZnO becomes negative after adsorbing phosphate, arsenate, or arsenite.

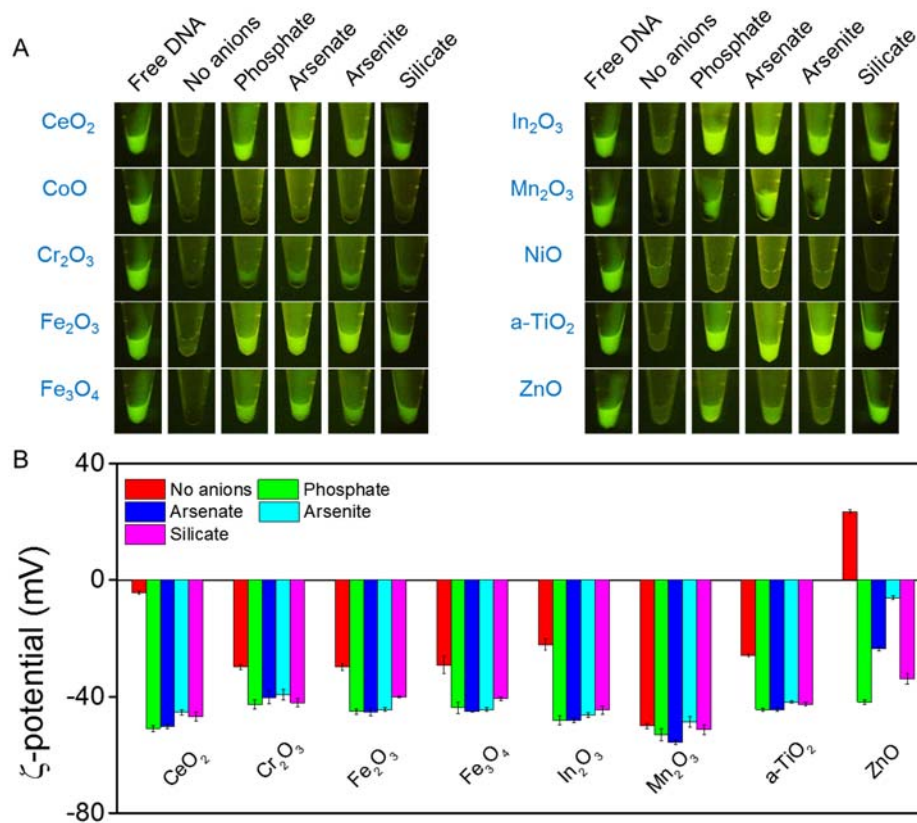


Figure 4.5 Effect of other oxyanions on DNA desorption. (A) Fluorescence images of anion-induced DNA desorption from MONPs. FAM-24 mer DNA (100 nM) was incubated with various MONPs (CeO₂ 0.01 mg/mL, CoO 0.25 mg/mL, Cr₂O₃ 0.25 mg/mL, Fe₂O₃ 0.1 mg/mL, Fe₃O₄ 0.15 mg/mL, In₂O₃ 0.4 mg/mL, Mn₂O₃ 0.4 mg/mL, NiO 0.1 mg/mL, a-TiO₂ 0.1 mg/mL, and ZnO 0.12 mg/mL) in Buffer A. After DNA adsorption, the fluorescence was quenched. Besides phosphate anion, other anions (arsenate, arsenite, and silicate) were also tested. The concentration of all anions was 0.5 mM. (B) ζ-potential of eight MONPs in the absence and presence of various anions. MONPs were dispersed in HEPES buffer

(10 mM, pH 7.6). The ζ -potential measurement was carried out after incubating each MONPs with each anion (0.5 mM) for 1 h.

While many MONPs enhanced fluorescence upon anion addition, they do so in a non-specific way; various anions can all produce fluorescence signal. Therefore, it is difficult to use single DNA/MONP complexes for selective anion detection, and the remaining eight MONPs were used to form a sensor array to solve the selectivity problem.

4.2.4 Sensor optimization

After screening for DNA adsorption and desorption, we next optimized the signaling conditions. First, we evaluated the effect of DNA sequence. While the interaction between DNA and MONPs are mainly through the DNA phosphate backbone, DNA sequence may still be important due to possible secondary structures and weak base interactions. The previously used FAM-24 mer is a random DNA containing all the four types of nucleobases. We then compared FAM-A₁₅, FAM-T₁₅, and FAM-C₁₅ as probes for signalling. FAM-G₁₅ was not tested since poly-guanine strongly quenches fluorescence. A fixed concentration of phosphate (50 μ M) was added to induce DNA desorption. The fold of fluorescence enhancement (F/F_0-1) is plotted for various MONPs (Figure 4.6A). Interestingly, DNA sequence indeed has a huge influence on sensor signaling. The DNA sequence induced the largest signal enhancement was chosen for further sensor development (i.e., A₁₅ for Cr₂O₃; C₁₅ for In₂O₃; T₁₅ for Mn₂O₃, α -TiO₂, and ZnO). We did not study the other three MONPs here since they were optimized in previous work; the

optimal sequences are T₁₅ for CeO₂; and C₁₅ for Fe₃O₄ and Fe₂O₃.^{226,227} Therefore, DNA bases also appear to influence DNA adsorption and desorption.

For sensing applications, signaling kinetics are also a very important parameter and this was tested next (Figure 4.6B). After 4 min background fluorescence scan, phosphate was added and the kinetics of fluorescence increase were monitored. All the samples showed fast fluorescence recovery, achieving a plateau within 10 min (Figure 4.6B). Therefore, we quantified the fluorescence signal at 5 min after adding target anions for further investigation.

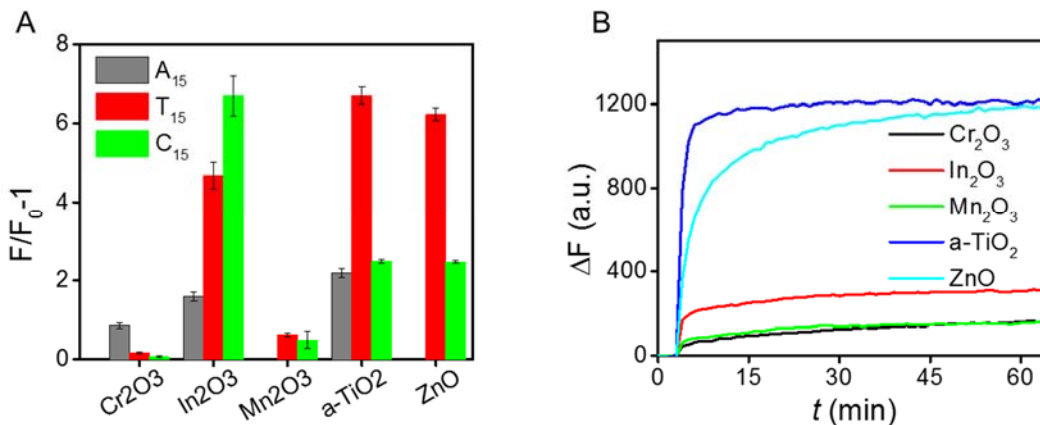


Figure 4.6 Optimization of sensor performance. Effect of (A) DNA sequence and (B) reaction time for different metal oxides. DNA (15-mer poly-A, T, C) was incubated with five MONPs. Phosphate (50 μ M) was used to induce fluorescence recovery.

4.2.5 Array-based anion sensing

After screening MONPs and optimizing DNA sequence, we next tested the sensor responses in the presence of various common anions. To obtain a training data set, each target anion (phosphate, arsenate, and arsenite) was repeated six times, and other anions

were run in triplicates. As shown in Figure 4.7, each MONP shows a differential response to each target anion. As reported previously, DNA/Fe₃O₄ (Figure 4.7E) and Fe₂O₃ (Figure 4.7D) have the strongest response to arsenate.²²⁶ A main goal of this work is to screen for MONPs with preferred binding towards phosphate and arsenite. After several steps of screening, we indeed found MONPs with selectivity for phosphate over arsenate, including CeO₂ (Figure 4.7A), ZnO (Figure 4.7H), Cr₂O₃ (Figure 4.7B), In₂O₃ (Figure 4.7F), and α-TiO₂ (Figure 4.7G). However, other anions caused significant interference. For example, fluoride, carbonate, and sulfite resulted in even more DNA desorption than phosphate using Cr₂O₃. Carbonate also induced significant fluorescence enhancement in the Fe₂O₃ and In₂O₃ samples. Furthermore, while Mn₂O₃ shows a slightly higher affinity to arsenite (Figure 4.7C), bromide, nitrate, and sulfate also induce similar signal enhancement. Therefore, these MONPs were also ruled out and only three were selected in this final step.

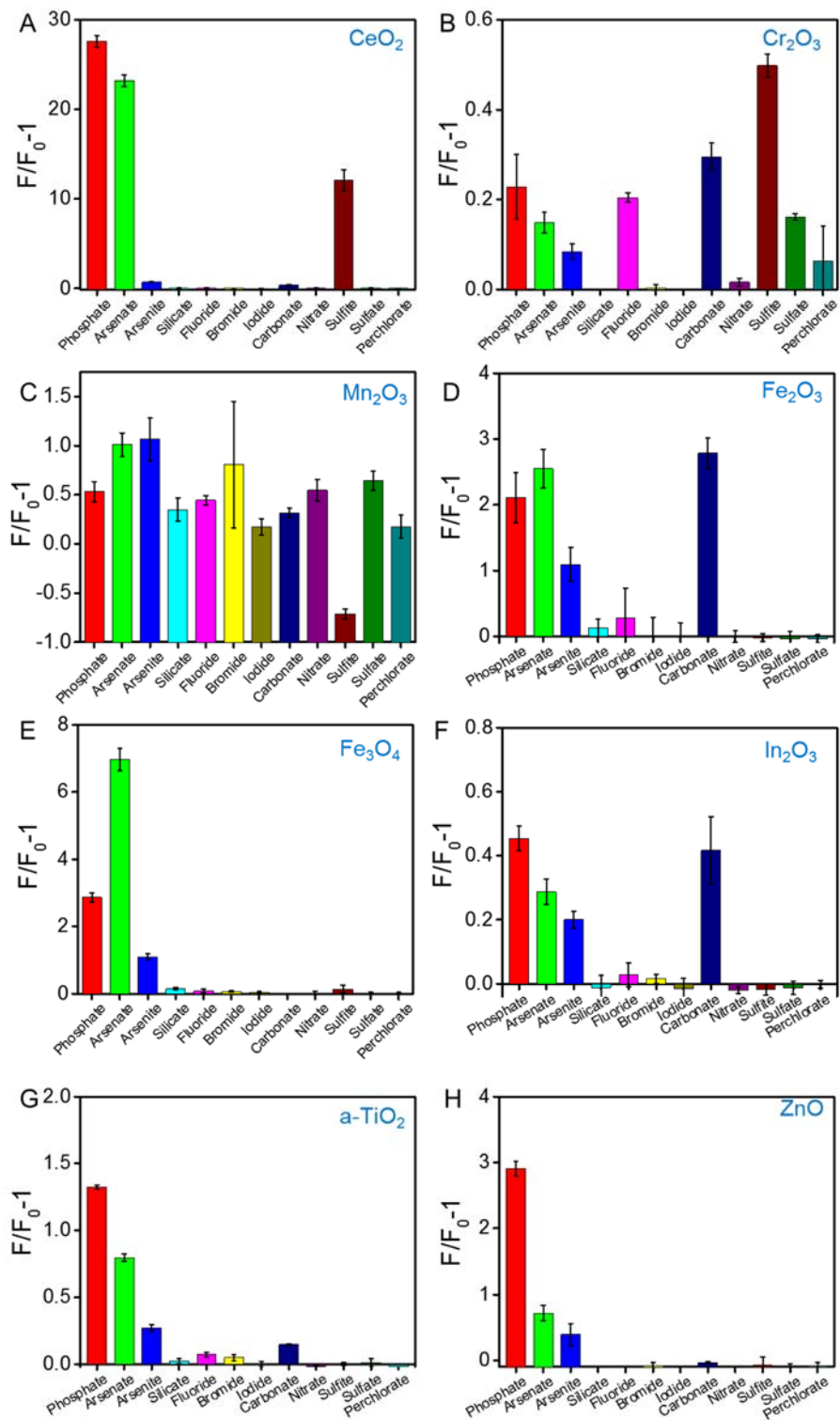


Figure 4.7 Signal enhancement of FAM-labeled DNA adsorbed onto various MONPs: (A) CeO_2 , (B) Cr_2O_3 , (C) Mn_2O_3 , (D) Fe_2O_3 , (E) Fe_3O_4 , (F) In_2O_3 , (G) $\alpha-TiO_2$, and (H) ZnO

NPs for various anions. The concentration of phosphate, arsenate, arsenite and silicate was 10 μ M, and that of all other anions was 1 mM.

While the selectivity of a single DNA/MONP sensor is limited, this difference might be large enough to form a pattern recognition based detection method. Our main goal is to identify phosphate, arsenate and arsenite. We chose to use an array formed by CeO₂, Fe₃O₄, and ZnO. They gave selective responses to arsenate, arsenite and phosphate, while other anions do not give much signal. Using this array, we obtained a training set of data. As a proof of concept, it is quite easy to separate the three anions and other anions using the canonical score plot (Figure 4.8).

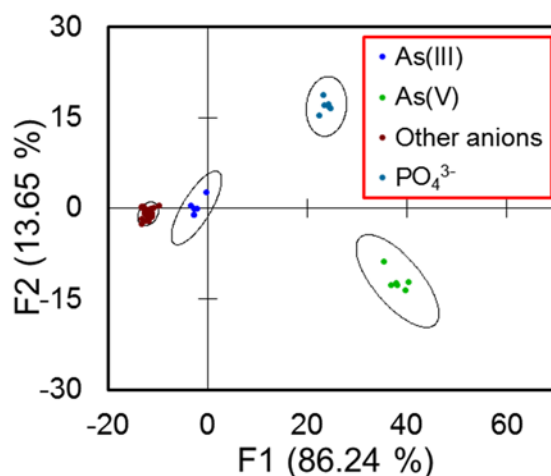


Figure 4.8 The canonical score plot for fluorescence enhancement using three DNA/MONP (CeO₂, Fe₃O₄, and ZnO) sensors for the discrimination of phosphate, arsenate, and arsenite in the presence of interference anions. The ‘other anions’ include fluoride, bromide, iodide, silicate, carbonate, nitrate, sulfite, sulfate, and perchlorate.

4.3 Materials and Methods

4.3.1 Chemicals

All of the DNA samples were purchased from Integrated DNA Technologies (IDT, Coralville, IA) and were purified by standard desalting. Their sequences and modifications are FAM-24 mer (FAM-ACG CAT CTG TGA AGA GAA CCT GGG), FAM-A₁₅ (FAM-AAA AAA AAA AAA AAA), FAM-T₁₅ (FAM-TTT TTT TTT TTT TTT), and FAM-C₁₅ (FAM-CCC CCC CCC CCC CCC). For the DNA homopolymers, FAM was labeled on the 5'-end. Metal oxide nanoparticles (MONPs) were purchased from Sigma or US Research Nano. The detailed information of the MONPs is shown in Table 4.1. Sodium fluoride, sodium chloride, sodium bromide, sodium iodide, sodium nitrate, sodium bicarbonate, sodium acetate, sodium citrate, sodium phosphate dibasic heptahydrate, and 4-(2-hydroxyethyl) piperazine-1-ethanesulfonic acid (HEPES) were from Mandel Scientific (Guelph, ON, Canada). Sodium (meta)arsenite, sodium arsenate dibasic heptahydrate, sodium sulfate, sodium sulfite and sodium perchlorate were purchased from Sigma. Sodium silicate solution (40 wt %) was from Ward's Science. Milli-Q water was used for all of the experiments.

4.3.2 Instrumentation

The hydrodynamic size and ζ -potential of MONPs in the aqueous environment were measured using Zetasizer Nano 90 (Malvern). Typically, 50 $\mu\text{g/mL}$ of MONPs were dispersed in Milli-Q water for the size measurement or in HEPES buffer (10 mM, pH 7.6) for the ζ -potential measurement. To evaluate the effect of anion adsorption on surface

charge, 0.5 mM of anions (phosphate, arsenate, arsenite, and silicate) were incubated with each MONP for 1 h before the measurement.

4.3.3 DNA adsorption capability of MONPs.

To screen MONPs for effective DNA adsorption, 200 nM of FAM-24 mer DNA was mixed with different MONPs (0.5 mg/mL) in Buffer A (HEPES 10 mM, pH 7.6, NaCl 300 mM). After 2 h incubation, each MONP was centrifuged (CeO₂, 100,000 rpm for 10 min; other nanoparticles, 10,000 rpm for 10 min). The DNA/MONP conjugates were prepared in a similar way for the following experiments unless otherwise indicated. The fluorescence images were taken using a digital camera under the 470 nm LED light excitation. The fluorescence intensity of the supernatant after adsorption was measured using a microplate reader (Infinite F200 Pro, Tecan; excitation: 485 nm, emission: 535 nm). The DNA adsorption on MONPs at low pH was performed using a similar procedure and the same DNA/particle ratio. pH was adjusted by adding HCl to a final of 10 mM. After 10 min incubation and centrifugation, the pH of supernatant was adjusted to neutral by adding NaOH (10 mM). Next, the fluorescence of supernatant was measured after dilution with Buffer A.

4.3.4 DNA desorption by anions.

To measure the DNA displacement by anions, the DNA/MONP conjugate was firstly prepared using the method as described above. Typically, FAM-24 mer DNA (100 nM) was mixed with MONPs (CeO₂, 0.01 mg/mL; CoO, 0.25 mg/mL; Cr₂O₃, 0.25 mg/mL; Fe₂O₃, 0.1 mg/mL; Fe₃O₄, 0.15 mg/mL; In₂O₃, 0.4 mg/mL; Mn₂O₃, 0.4 mg/mL; NiO, 0.1

mg/mL; α -TiO₂, 0.1 mg/mL; and ZnO, 0.12 mg/mL) in Buffer A and the mixtures were incubated for 1 h. Afterwards, phosphate (1 mM) was introduced to the DNA/MONP conjugates. After another 1 h incubation and centrifugation, the fluorescence spectra from the supernatants were recorded. The fluorescence images of DNA/MONP in the presence of different anions (0.5 mM each) were taken using the camera under 470 nm light excitation.

4.4.5 Effect of DNA sequence on desorption.

To evaluate the effect of DNA sequence on the signal enhancement, FAM A₁₅, T₁₅, or C₁₅ (10 nM each) was incubated with five MONPs (Cr₂O₃, 0.05 mg/mL; In₂O₃, 0.05 mg/mL; Mn₂O₃, 0.03mg/mL; α -TiO₂, 0.03 mg/mL; and ZnO, 0.02 mg/mL) in Buffer A, respectively. Phosphate (50 μ M) was added to induce fluorescence recovery. Desorption kinetics were recorded for 1 h. The fluorescence enhancement (F/F_0-1) was plotted as a function of DNA sequence.

4.4.6 Sensor array for anion discrimination.

The response of each sensor is plotted by the fluorescence enhancement (F/F_0-1) from different anions. The concentrations of MONPs and DNA are listed in Table 4.2. The concentration of target anions (PO₄³⁻, As(V), and As(III)) was 10 μ M, and all other anions was 1 mM. Target anions were replicated six times, and other anions were in triplicate. The fluorescence was recorded after adding the anions for 10 min. The training data were analyzed using canonical discriminate analysis from the software OriginLab.

Table 4.2 DNA sequences and concentrations for MONPs in the final sensor array.

| MONP | [MONP] ($\mu\text{g/mL}$) | DNA sequence | [DNA] (nM) |
|--|---|---------------------|-------------------|
| CeO₂ | 2.5 | FAM-T ₁₅ | 50 |
| Cr₂O₃ | 50 | FAM-A ₁₅ | 10 |
| Fe₂O₃ | 20 | FAM-C ₁₅ | 30 |
| Fe₃O₄ | 25 | FAM-C ₁₅ | 30 |
| In₂O₃ | 50 | FAM-C ₁₅ | 10 |
| Mn₂O₃ | 30 | FAM-T ₁₅ | 10 |
| α-TiO₂ | 30 | FAM-T ₁₅ | 30 |
| ZnO | 20 | FAM-T ₁₅ | 30 |

4.4 Summary

In summary, we demonstrated a large potential for using DNA and MONPs for anion discrimination and sensing. We screened nineteen types of common MONPs for their DNA adsorption, fluorescence quenching, and anion-induced DNA displacement property. Based on the anion selectivity pattern, we chose to use CeO₂, Fe₃O₄, and ZnO to form a sensor array, which successfully discriminated phosphate, arsenate, arsenite and other interference anions. This study provides a comprehensive understanding on the interaction between DNA and metal oxides, and the influence of environmentally important analytes on DNA adsorption.

Chapter 5 DNA/Cerium Oxide Nanoparticles with Catalase-like Activity: Detection of H₂O₂ and Glucose

The results presented in this chapter have been published as part of:

Biwu Liu, Ziyi Sun, Po-Jung Jimmy Huang and Juewen Liu, Hydrogen Peroxide Displacing DNA from Nanoceria: Mechanism and Detection of Glucose in Serum. *Journal of the American Chemical Society*, 137, 1290-1295, 2015.

5.1 Introduction

Cerium oxide nanoparticles (nanoceria, CeO₂) possess a few types of enzyme-like activities.^{245,246,247,248} This is probably related to the co-existence of both Ce³⁺ and Ce⁴⁺ on the surface, where the Ce³⁺ species is coupled with oxygen vacancies. As an oxidase mimic, nanoceria oxidizes many common substrates including TMB.^{127,249} It also has peroxidase, superoxide dismutase, and catalase activities under different conditions.^{247,250} Its reaction with reactive oxygen species (ROS) makes it useful as an anti-oxidant.^{123,170,251,252}

Hydrogen peroxide (H₂O₂) plays critical roles in a diverse range of biological processes including biosynthesis, host defense, and cell signaling.²⁵³ An elevated H₂O₂ concentration often links to oxidative stress. In addition, being an incomplete reduction product of oxygen, H₂O₂ is a by-product of many enzymatic reactions. The most well-known example is the oxidation of glucose by glucose oxidase (GOx), where H₂O₂ is the actual target molecule of most glucose sensors. For these reasons, detecting H₂O₂ has long attracted the interest of many chemists,²⁵⁴ and a number of sensing methods were developed. For example, as a co-substrate for peroxidases, H₂O₂ can be measured using chromogenic substrates such as Amplex Red or TMB. Intracellular detection relies on

fluorescent probes that light up by reacting with H_2O_2 .²⁵⁵ When nanoceria is mixed with H_2O_2 , its color changes to orange. Direct detection of H_2O_2 based on this color change was reported.¹⁷³ However, the sensitivity is limited since an obvious color change requires a high H_2O_2 concentration. In addition, a similar color change may arise by reacting nanoceria with other biological molecules such as ascorbate and dopamine.²⁵⁶ These reactions may interfere with color-based detection.

With the progresses of nanoceria as enzyme-mimics, our fundamental understanding on the interaction between H_2O_2 and nanoceria is still far from complete, which hinders further developments. While many spectroscopic methods have been used, we reason that DNA might be a simple probe to study surface interactions.¹⁷⁶ Since cerium is a hard metal that likes phosphate containing ligands, nanoceria strongly binds to DNA and nucleotides.^{84,246} The tunable length and sequence of DNA also facilitates systematic studies. In this chapter, we probed H_2O_2 and nanoceria interaction using DNA. Although H_2O_2 is often linked to oxidative DNA damage in the presence of redox metals (e.g., in the Fenton chemistry), we emphasize on a simple ligand role of H_2O_2 , displacing adsorbed DNA without cleavage. This study contributes new knowledge to the interaction between H_2O_2 and inorganic surfaces and also expands the scope of DNA-based sensing.¹⁷⁶ With a DNA/nanoceria complex, we detected H_2O_2 and glucose (when coupled with the GOx) with very high sensitivity and selectivity.

5.2 Results and Discussions

5.2.1 Sensor rationale and proof of concept

Our nanoceria has a size of ~5 nm as characterized by high resolution transmission electron microscopy (HR-TEM, Figure 5.1A). Dynamic light scattering (DLS) indicates a similar average size with a relatively high polydispersity (Figure 5.1B). Upon addition of H₂O₂, the color of nanoceria changes from colorless to orange (Figure 5.1C,D), which is also reflected by UV-vis measurement (Figure 5.1F).^{173,257} The increased absorption at ~400 nm explains the orange color, allowing H₂O₂ to be detected down to ~10 μM.¹⁷³ Due to the small UV-vis spectral shift and high background, we reason that better sensitivity might be achieved using fluorescence-based detection. Figure 5.1E (left panel) shows the fluorescence image of a FAM (carboxyfluorescein) labeled DNA. After adding nanoceria, the fluorescence was completely quenched, suggesting DNA adsorption. Interestingly, the fluorescence was fully recovered immediately after adding H₂O₂. The fluorescence spectra of these samples are shown in Figure 5.1G. This proof-of-concept study indicates the possibility of using DNA-functionalized nanoceria to directly detect H₂O₂ (Figure 5.1C), which may allow much higher sensitivity compared to the colorimetric detection. At the same time, DNA can serve as a mechanistic probe.

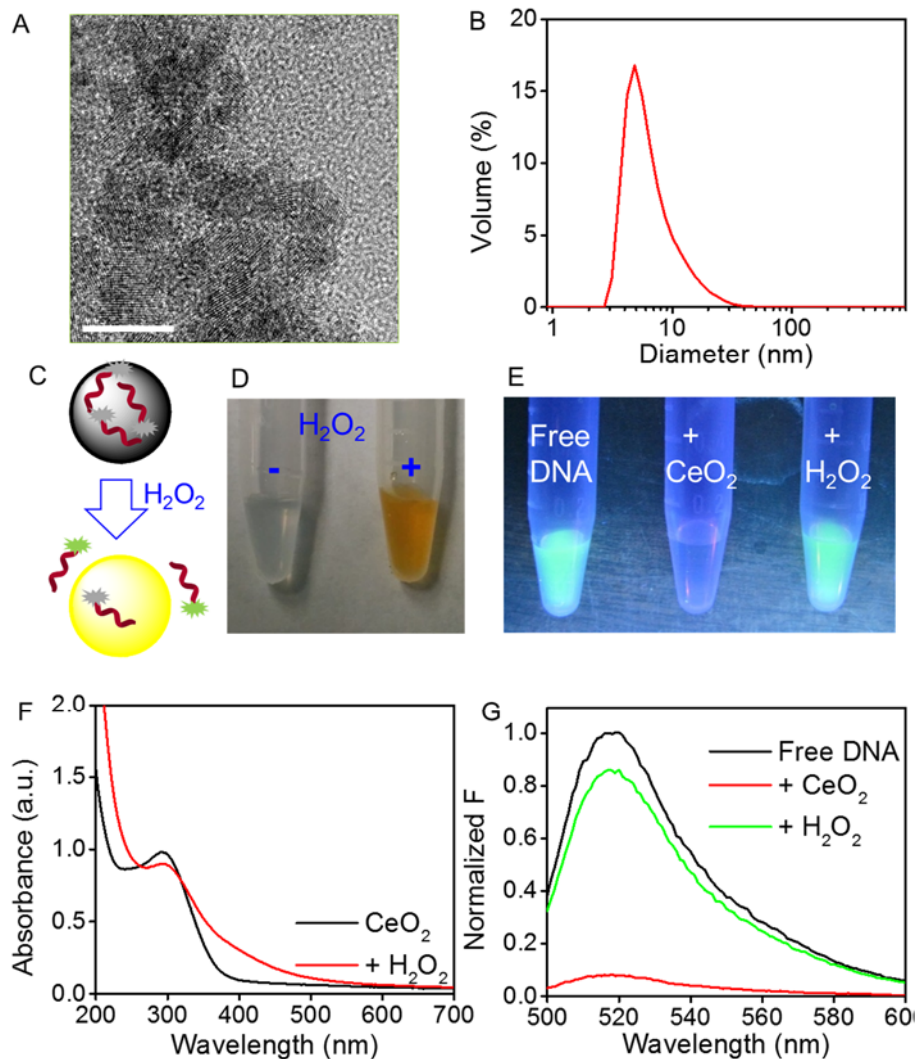


Figure 5.1 Fluorescent sensing H_2O_2 by a DNA/nanoceria complex. (A) HR-TEM image and (B) hydrodynamic size of nanoceria. (C) Schematics of H_2O_2 inducing the color change of nanoceria, and displacing DNA from nanoceria surface. (D) A photo of the untreated nanoceria (1 mg/mL) and after reacting with H_2O_2 (10 mM) and (F) the corresponding UV-vis absorbance spectra (25 times diluted). (E) A fluorescence photo of free FAM- A_{15} DNA (200 nM), after adding nanoceria (10 $\mu\text{g}/\text{mL}$) and then adding H_2O_2 (10 mM). The corresponding spectra were shown in (G). The scale bar in A is 10 nm.

5.2.2 Effect of ionic strength

Nanoceria is slightly negatively charged at neutral pH (ζ -potential = -6.2 mV). Efficient DNA adsorption occurred even in the absence of additional salt and complete adsorption was achieved with just 30 mM NaCl (Figure 5.2A). This indicates a strong affinity between DNA and nanoceria. Such low background fluorescence is ideal for sensing since it allows a large signal increase and low noise. After adsorbing DNA, the H₂O₂ signaling kinetics as a function of salt concentration were measured. All the samples maintained a stable background in the absence of H₂O₂ (Figure 5.2B). At 2 min, H₂O₂ was added. It is interesting to note that a higher salt concentration produced stronger fluorescence enhancement, while barely any fluorescence was generated in the absence of salt. It is unlikely that the interaction between nanoceria and H₂O₂ is affected by such low NaCl concentrations. We reason that the salt effect is mainly on the DNA. With a higher ionic strength, DNA tends to adopt a more compact structure (e.g., screening intramolecular charge repulsion), thus reducing the number of contacting points on nanoceria and facilitating DNA desorption.

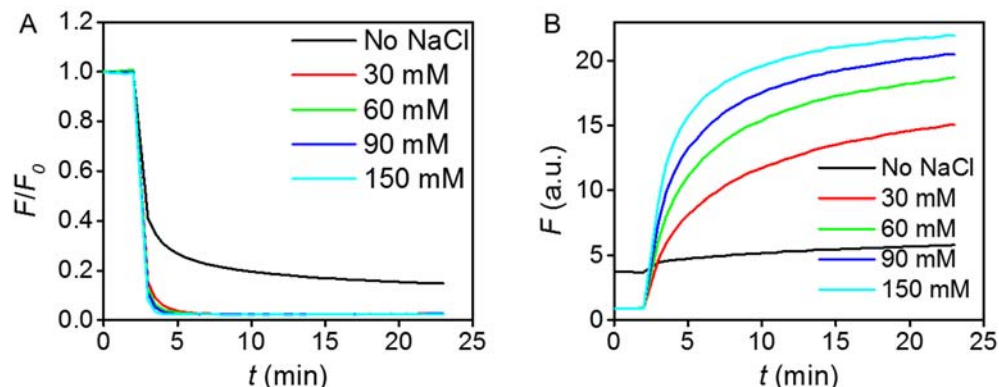


Figure 5.2 Effect of salt concentration on DNA recovery by H₂O₂. (A) Adsorption kinetics and (B) H₂O₂-induced desorption kinetics of FAM-A₁₅ as a function of NaCl concentration at pH 7.6.

5.2.3 Effect of pH

The effect of pH is also very pronounced (Figure 5.3A). H₂O₂ induces the fastest signaling at pH 8, and this first-order rate decreases by 4-fold at pH 7. Barely any fluorescence change occurs at pH 6 or lower. To understand this, we measured the ζ -potential of nanoceria as a function of pH, and the point of zero charge (PZC) is between pH 6 to 7 (Figure 5.3B, black dots). We reason that as the surface of nanoceria becomes more positively charged at lower pH, electrostatic attraction inhibits DNA release. Since pH 8 already shows some background signal, we did not test even higher pH. The optimal value should be between pH 7 and 8, which is ideal for detecting H₂O₂ in physiological conditions.

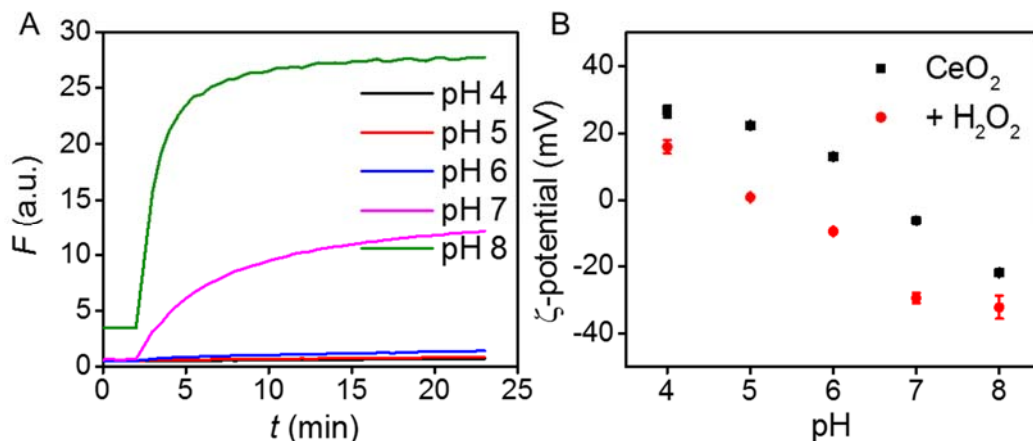


Figure 5.3 Effect of pH on DNA recovery by H_2O_2 . (A) Desorption kinetics as a function of pH. (B) ζ -potential of nanoceria as a function of pH in the absence of and presence of H_2O_2 , respectively. Alexa Fluor 488-labeled DNA was used at different pH (150 mM NaCl).

5.2.4 Effect of DNA sequence and length

The effect of DNA sequence was studied next. Ideally, short DNA should be used, allowing higher probe density and thus better sensitivity. Therefore, 5-mer FAM-labeled DNAs were tested (Figure 5.4A). Since guanine is a quencher, FAM-G₅ has very low fluorescence intensity as a free DNA, while the other three give much stronger emission (blue bars). After adding nanoceria, T₅ and C₅ quenched most significantly (red bars). Fluorescence recovery was achieved after adding H_2O_2 for all the samples (green bars), but the increase with C₅ and G₅ was very moderate. Overall, A₅ and T₅ appears to be optimal.

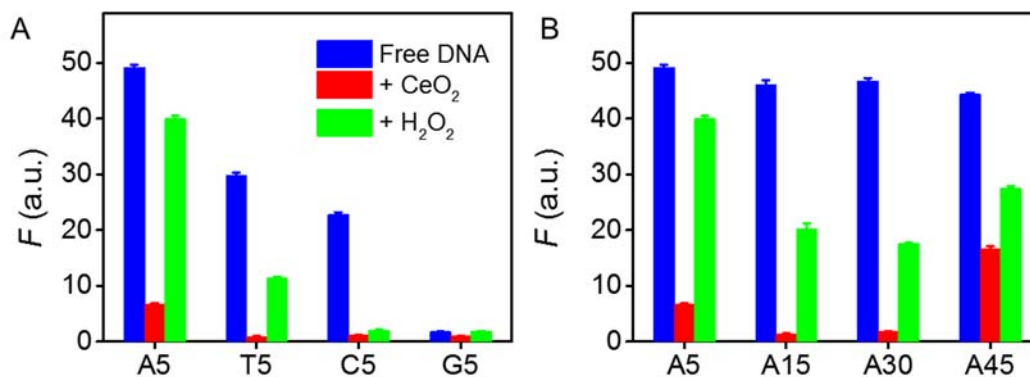


Figure 5.4 Effect of DNA and length. Fluorescence quenching by CeO₂ (red bars) and recovery by H₂O₂ (green bars) as a function of DNA (A) sequence and (B) length (all with FAM labels).

To test the effect of DNA length, a few poly-A DNAs were employed (Figure 5.4B). More efficient adsorption was observed with A₁₅ and A₃₀ compared to A₅, possibly due to more interaction points, leading to stronger adsorption and lower background. However A₄₅ showed a high background and poor fluorescence recovery by H₂O₂, which might be related to its large size and some fluorophores are far away from the nanoceria surface after DNA adsorption.

5.2.5 Mechanistic investigations

It is quite unexpected that H₂O₂ enhances the fluorescence. Two mechanisms may explain this: 1) oxidative DNA cleavage, or 2) H₂O₂-induced DNA desorption. H₂O₂ is reservoir for ROS and it can convert to more reactive hydroxyl radicals in the presence of redox active metals to oxidatively cleave DNA (e.g. Fenton chemistry with Fe²⁺). Given the redox property of cerium, oxidative DNA cleavage appears to be a quite possible mechanism.

To test this, a gel electrophoresis experiment was carried out (Figure 5.5). The first lane is a ladder of 30, 15 and 5-mer FAM-labeled poly-A DNA. Lane 2 is the FAM-A₃₀ DNA without any treatment. Lane 3 is the DNA incubated with 1 mM H₂O₂. Lane 4 is the DNA/nanoceria complex, and Lane 5 is DNA/nanoceria treated with 1 mM H₂O₂, mimicking the sensing condition. However, no DNA cleavage was observed for any of these samples. Therefore, the oxidative DNA cleavage mechanism is ruled out and the reaction is likely to be simply H₂O₂-induced DNA desorption. In fact, some reports show that nanoceria can decrease the oxidative stress by reacting with ROS,²⁵⁸ thus avoiding DNA cleavage. However, the oxidative damage to the DNA bases without backbone cleavage cannot be excluded in this stage.

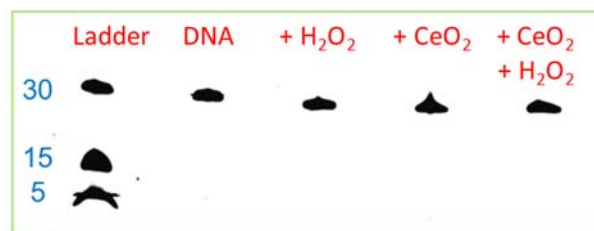


Figure 5.5 Gel electrophoresis to check DNA integrity. [H₂O₂] = 1 mM.

The nanoceria surface becomes more negatively charged after the H₂O₂ treatment compared to the original nanoceria (e.g., PZC = ~5, Figure 5.3B). This could explain its decreased DNA binding affinity. To further understand the surface chemistry of CeO₂ after H₂O₂ treatment, a pH and conductivity titration experiment was performed to measure the pK_a of surface groups on nanoceria. Untreated nanoceria has a pK_a of 8.62, while after the H₂O₂ treatment; two pK_a's were observed (Figure 5.6). The one at 8.85 is similar to the untreated sample, and the other value is 7.61. This new and more acidic group on nanoceria

after the H₂O₂ treatment explains the shift of the PZC to lower pH from the ζ -potential measurement in Figure 5.3B.

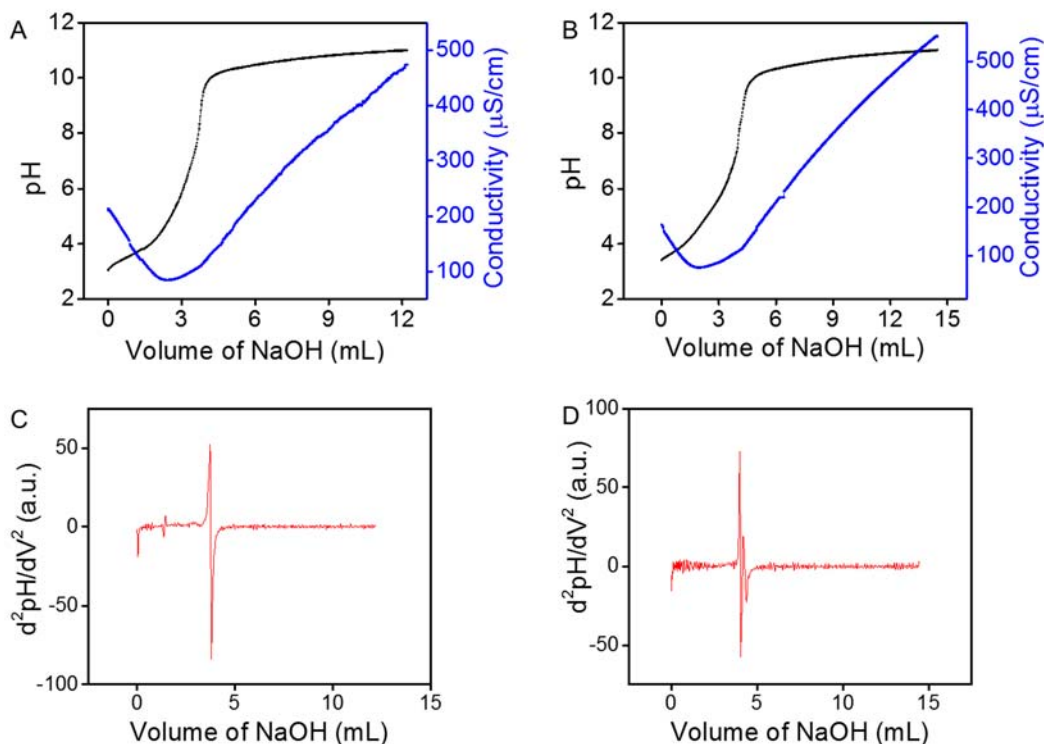


Figure 5.6 Potentiometric and conductometric titration of (A) nanoceria and (B) H₂O₂ treated nanoceria . (C) and (D) are the corresponding second derivative of curve (A) and (B), respectively, to determine the pK_a values.

To further explore the mechanism of DNA desorption, we followed pH change in a non-buffered solution. After mixing H₂O₂ and nanoceria, pH dropped by ~1 unit in less than 1 min (black squares, Figure 5.7), and this initial pH drop was also observed by others.²⁵⁹ This time scale agrees with that for the color change and DNA desorption. It is generally accepted that the color change is due to oxidation of Ce³⁺ to Ce⁴⁺.^{173,247,252,260} However, the pH drop cannot be explained by direct oxidation by H₂O₂. Instead, pH should

have increased if H_2O_2 were to oxidize Ce^{3+} (e.g. $\text{H}_2\text{O}_2 + 2\text{e}^- \rightarrow 2\text{OH}^-$). This pH change was very moderate (equal to producing $\sim 40 \mu\text{M}$ protons), and is completely masked by 10 mM HEPES (red circles, Figure 5.7). We reason this initial pH drop might be due to the remaining acetic acid in our nanoceria sample or nanoceria reacting with a trace amount of OH radicals.¹⁶⁸

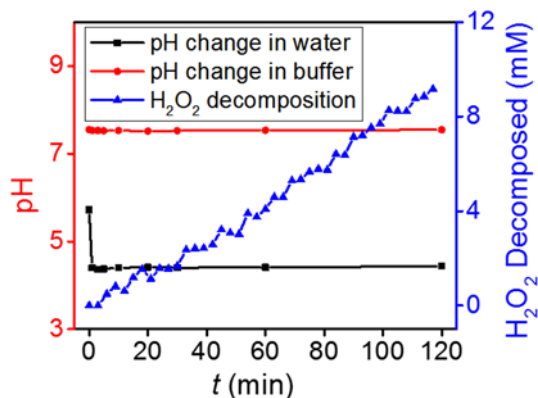


Figure 5.7 Kinetics of pH change after mixing H_2O_2 and nanoceria (1.5 mg/mL) in water or in 10 mM HEPES (pH 7.6) (left axis) and kinetics of H_2O_2 decomposition with 3 $\mu\text{g}/\text{mL}$ nanoceria (right axis).

We also monitored the rate of H_2O_2 decomposition using UV-vis spectrometry (Figure 5.7, blue triangles). In 2 h, $\sim 10 \text{ mM}$ H_2O_2 was decomposed with 3 $\mu\text{g}/\text{mL}$ nanoceria (the rate is faster with more nanoceria). Therefore, H_2O_2 decomposition does not involve pH change.^{123,259} Ghibelli and co-workers proposed a $\text{Ce}^{4+}/\text{Ce}^{3+}$ cycle for H_2O_2 decomposition.¹²³ However, based on a rigorous spectroscopy study, Cafun *et al.* argued that the catalase activity of nanoceria does not involve discrete Ce^{3+} centers;²⁵⁹ Ce^{4+} species in the whole particle acts as an electron sponge to perform catalysis.

Taken together, we reason that after adding H_2O_2 , Ce^{3+} is quickly oxidized to Ce^{4+} , producing the orange color. The Ce^{4+} surface is further capped by H_2O_2 (Figure 5.8), producing a more acidic peroxo proton ($\text{pK}_a = 7.61$). This capping reaction on one hand shields the cerium center from DNA phosphate binding, and on the other hand, increases the negative charge density. The peroxo ligand was reported in small molecule cerium complexes as well.²⁶¹ It was also reported that phosphate affinity with Ce^{4+} is much weaker than that with Ce^{3+} .²⁶² All these factors favor DNA desorption. Note that after DNA desorption occurs in the first minute. Once desorbed, further decomposition of H_2O_2 should proceed as free nanoceria. The peroxo capped species is relatively stable. After consuming all H_2O_2 , it slowly converts back to the original light colored state over many days.^{168,259}

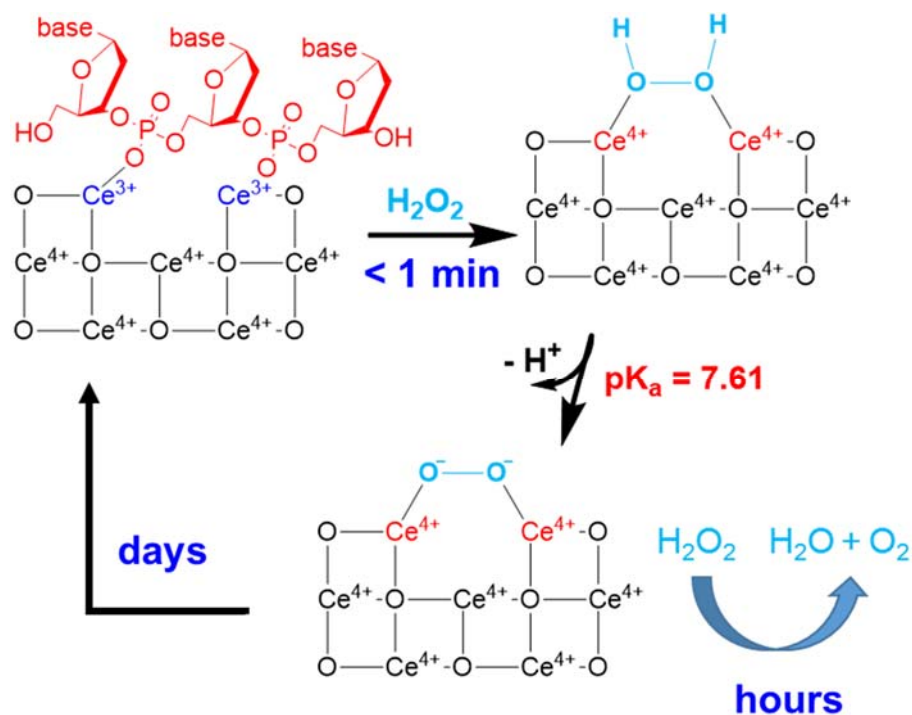


Figure 5.8 A proposed mechanism of H_2O_2 -induced DNA release by capping the nanoceria surface. For the three time scales marked in the scheme, DNA release is related to the one on the order of 1 min.

5.2.6 Detection of H_2O_2 and glucose

After the mechanistic work, we next tested this system as a biosensor for H_2O_2 . Using FAM-T₅ as the probe, the fluorescence intensity was followed after adding various concentrations of H_2O_2 (Figure 5.9A). With a high concentration of H_2O_2 (e.g., 1 mM), saturated signal was achieved in less than 1 min. The signal-to-background ratio reaches >20-fold, and over 80% of adsorbed DNA can be released. The fluorescence intensity at 5 min is plotted as a function of the H_2O_2 concentration (Figure 5.9B). The dynamic range reached ~ 1 mM H_2O_2 , and the detection limit is 130 nM H_2O_2 (4.4 ppb,

$3\sigma/\text{slope}$, inset). This is one of the most sensitive sensors for H_2O_2 based on nanoparticle optical detection (e.g. ~ 80 -fold more sensitive than the previous colorimetric detection). For selectivity test, we measured a few common metabolites (1 mM each, Figure 5.9C). Only ascorbate gave an obvious signal, but 50 μM ascorbate (the physiological concentration) is silent, indicating highly specificity.

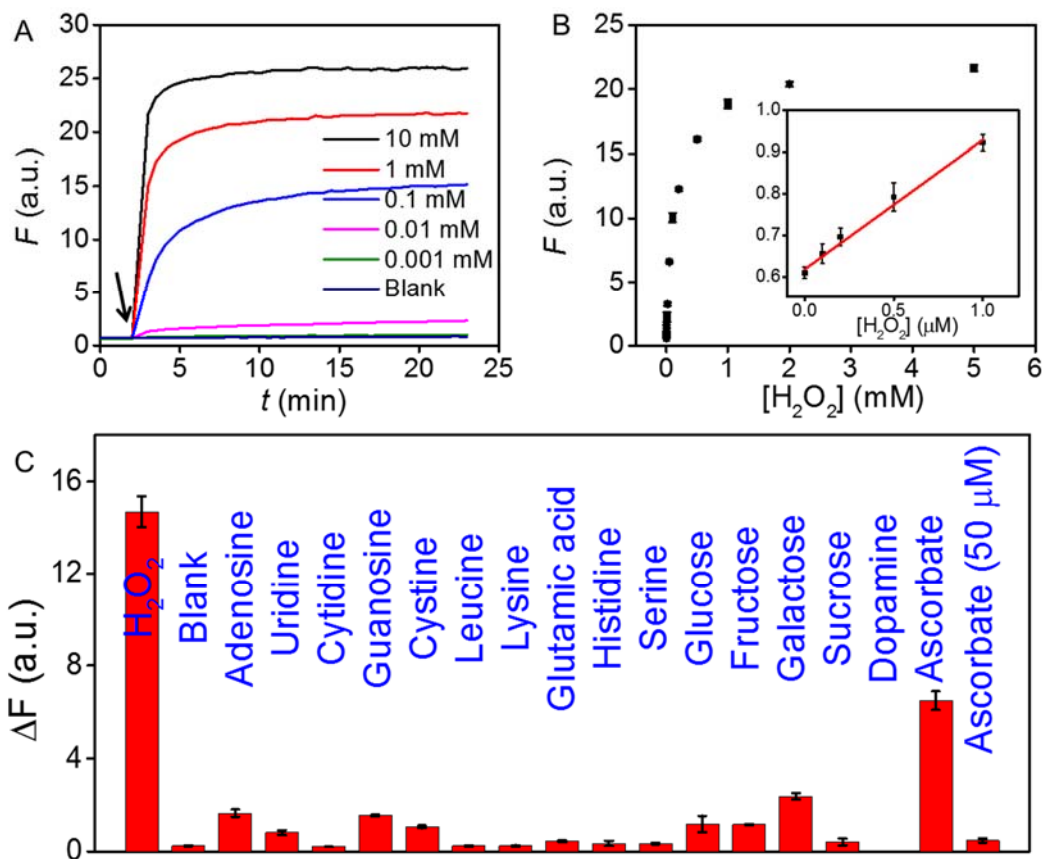


Figure 5.9 Sensor performance in H_2O_2 detection. (A) Kinetics of sensor signaling. Arrowhead indicates H_2O_2 addition. (B) Sensor calibration curve. Inset: the initial linear response. (C) Selectivity test of H_2O_2 detection towards sugars, L-amino acids, nucleosides, and other metabolites (1 mM). The last bar is ascorbate at 50 μM .

Given the sensor performance for H₂O₂, we next tested glucose detection. H₂O₂ was *in situ* generated using GOx and glucose. By varying the glucose concentration, a linear response was observed with a detection limit of 8.9 μM glucose in buffer (Figure 5.10A). Only glucose produced signal, while the other sugars were silent (Figure 5.10B), consistent with the high specificity of GOx. Finally, we challenged the sensor by glucose measurement in blood serum. A commercial glucose meter was used to determine the concentration of glucose in undiluted serum and a value of 4.57 ± 0.06 mM was obtained. The serum was then analyzed by our sensor based on the GOx reaction. Due to its opaque optical appearance, we diluted the serum in buffer. Since our sensor is highly sensitive, accurate measurement was still possible after dilution. The standard addition method was used to minimize the sample matrix effect and a value of 4.37 ± 0.32 mM was obtained (see Figure 5.10C for the titration). Within the error range, this result is the same as that from the glucose meter, indicating this sensor works in complex sample matrix.

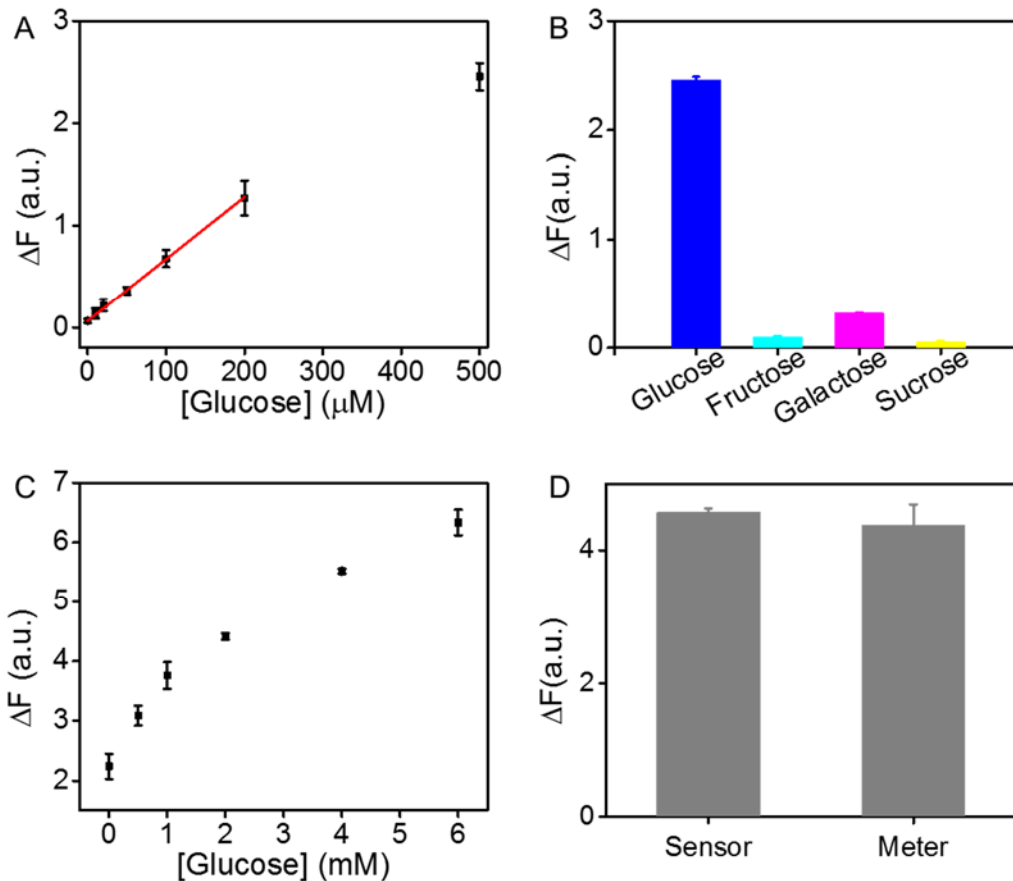


Figure 5.10 Sensor performance for glucose detection. (A) Sensor calibration curve for glucose detection in buffer. (B) Sensor selectivity test for glucose detection in buffer. Glucose concentration = 0.5 mM and the other sugars are 5 mM. (C) Titration of glucose into serum sample to determine the glucose concentration using the DNA/nanoceria based sensor. (D) Detection of glucose in serum by the nanoceria/DNA based sensor and by a commercial glucose meter.

5.3 Materials and Methods

5.3.1 Chemicals

All of the DNA oligomers were purchased from Integrated DNA Technologies (IDT, Coralville, IA, USA). The DNA sequences and modifications are listed in Table 5.1. Sodium acetate, sodium chloride, 4-(2-hydroxyethyl) piperazine-1-ethanesulfonic acid (HEPES), 2-(N-morpholino) ethanesulfonic acid (MES), the amino acids, and nucleosides were from Mandel Scientific (Guelph, ON, Canada). Glucose, fructose, galactose, sucrose, 30 wt% H₂O₂ solution, dopamine, sodium ascorbate, amino acids and nanoceria dispersion (catalog number: 289744, 20% dispersed in 2.5% acetic acid) were purchased from Sigma-Aldrich. The solution pH was controlled using designated buffers (acetate buffer for pH 4 and 5, MES for pH 6, and HEPES for pH 7 and 8) for most experiments unless otherwise specified. Milli-Q water was used for all the experiments.

Table 5.1 The sequences and modification of DNA used in this work

| DNA | Sequences (from 5' to 3') and modifications |
|---------------------------|---|
| Alexa-DNA | TCA CAG ATG CGT-Alexa Fluoro 488 |
| FAM-A₅ | FAM-AAA AA |
| FAM-T₅ | FAM-TTT TT |
| FAM-C₅ | FAM-CCC CC |
| FAM-G₅ | FAM-GGG GG |
| FAM-A₁₅ | FAM-AAA AAA AAA AAA AAA |
| FAM-A₃₀ | FAM-AAA AAA AAA AAA AAA AAA AAA AAA AAA AAA |

5.3.2 Washing CeO₂ nanoparticles

Our nanoceria sample was a 20% suspension containing 2.5% acetic acid as stabilizer. For applications related to pH change measurement, it was washed three times using ultracentrifugation (rpm 10, 000 10 min). For other applications, the nanoceria was much diluted and the effect of acetic acid is minimal.

5.3.3 Transmission electron microscopy and UV-vis spectroscopy

The size and morphology of nanoceria were studied using high resolution transmission electron microscopy (HR-TEM) (Zeiss Libra 200MC). The TEM sample was prepared by dropping nanoceria dispersion (10 µg/mL) on a copper grid. The grid was allowed to dry overnight at room temperature. The UV-vis spectra of nanoceria were acquired using a UV-vis spectrometer (Agilent 8453A). To obtain the orange colored product, nanoceria (1 mg/mL) was incubated with H₂O₂ (10 mM) for 15 min. The photo was taken by a digital camera and the sample was diluted 25 times (40 µg/mL) for the UV-vis measurement.

5.3.4 Kinetics of H₂O₂ decomposition

To obtain the reaction kinetics of H₂O₂ decomposition, nanoceria (3 µg/mL) was added into 50 mM H₂O₂ solution. The UV-vis absorbance of the solution was then followed at 240 nm.

5.3.5 Dynamic light scattering (DLS) measurement

The hydrodynamic diameter and ζ -potential of nanoceria were measured using a Malvern Nanosizer ZS90. To obtain pH-dependent ζ -potential values, normal or washed nanoceria (50 $\mu\text{g/mL}$) was dispersed in designed buffer solutions of various pH (10 mM). The solution pH was controlled using designated buffers (acetate buffer for pH 4 and 5, MES for pH 6, and HEPES for pH 7 and 8). The temperature was maintained at 25 $^{\circ}\text{C}$ for all the measurements.

5.3.6 DNA adsorption kinetics and capacities

To study salt-dependent DNA adsorption, FAM-A₁₅ (50 nM) was dissolved in HEPES buffer (pH 7.6, 10 mM) containing varying concentration of NaCl. After scanning the free DNA for 2 min (excitation at 485 nm, emission at 535 nm) using a microplate reader (Infinite F200Pro, Tecan), a small volume of nanoceria (final concentration = 3 $\mu\text{g/mL}$) was added to induce DNA adsorption. The fluorescence was recorded for another 20 min by the microplate reader. The fluorescence intensity was normalized based on the initial intensity before adding nanoceria. The DNA loading capacity as a function of pH was measured by comparing the fluorescence before and after adding nanoceria (3 $\mu\text{g/mL}$) to an Alexa Fluoro 488 labeled DNA (Alexa-DNA, 200 nM, see Table 5.1 for sequence).

5.3.7 H₂O₂-induced DNA desorption

The desorption kinetics were obtained in a similar way as the adsorption kinetics. Typically, the DNA-nanoceria conjugate was first prepared at designed conditions as described above, and after recording the background, H₂O₂ was added to induce DNA

desorption. In the NaCl concentration and pH dependent studies, the final concentration of H₂O₂ added was 1 mM. To investigate the effect of DNA sequence and length, homo FAM-labeled DNA (5-mer poly A, poly T, poly C, poly G, and 15-mer, 30-mer, 45-mer poly A) (50 nM) were respectively adsorbed onto nanoceria (4 µg/mL) in buffer (HEPES 10 mM, pH 7.6, NaCl 150 mM). After 1 h incubation, H₂O₂ was introduced to release DNA. The fluorescence intensity at each state (free DNA, after DNA adsorption, and after desorption) was recorded. The fluorescence picture of H₂O₂ induced DNA release from nanoceria was taken under a UV lamp (365 nm excitation). FAM-A₁₅ (200 nM) was used as the probe DNA and the final H₂O₂ concentration was 10 mM. The corresponding fluorescence spectra were collected using a Varian Eclipse fluorometer. To test the sensitivity of DNA-nanoceria for H₂O₂ detection, various concentrations of H₂O₂ (from 100 nM to 5 mM) were added into the FAM-T₅ DNA/nanoceria conjugate solution. The fluorescence intensity at 5 min after H₂O₂ addition was plotted as a function of H₂O₂ concentration. Sugars (sucrose, galactose, fructose, and glucose), L-amino acids (serine, histidine, glutamic acid, lysine, leucine, and cysteine), sodium ascorbate, dopamine and nucleosides (guanosine, cytidine, uridine, and adenosine) were also used to test the selectivity. The concentrations of all these molecules are 1 mM (50 µM of sodium ascorbate was also tested).

5.3.8 Potentiometric and Conductometric Titration.

Conductivity and pH were measured simultaneously using a Metrohm 809 Titrandot autotitrator. The stock nanoceria and H₂O₂ treated nanoceria were centrifuged for 10 min (100,000 rpm) to remove the supernatant and then dispersed in Milli-Q water. This is to remove the free acetic acid present in the original solution. Then, the pH of the nanoceria

sample (0.1 wt%) was adjusted to ~ 3 by adding HCl. The sample was then titrated with 0.02 M NaOH until the pH approached a plateau. The pK_a values were calculated after taking the second derivative of the titration traces.

5.3.9 Gel Electrophoresis

For denaturing gels, DNA-nanoceria in the absence or the presence of H_2O_2 was dispersed in 15% glycerol and loaded onto 10% polyacrylamide gel with 8 M urea. The conjugate was prepared by mixing FAM-A₃₀ (200 nM) and nanoceria (15 $\mu\text{g}/\text{mL}$) in HEPES buffer (pH 7.6, 10 mM, NaCl 150 mM) and 10 mM H_2O_2 was added to induce DNA desorption. The gels were then imaged using blue LED epi excitation (Bio-Rad, Chemidoc MP).

5.3.10 pH monitoring.

Washed nanoceria (1.5 mg/mL, 0.15 wt %) was used to react with H_2O_2 (50 mM) and the pH of the reaction solution was monitored by a pH meter for 2 h at various time points. In addition, the same reaction was carried out in 10 mM HEPES (pH 7.6) (nanoceria 3 $\mu\text{g}/\text{mL}$, H_2O_2 50 mM).

5.3.11 Detection of glucose in buffer and in serum

Detection of glucose in buffer solution was performed as following steps: (1) various concentrations of glucose (from 10 μM to 500 μM) was incubated with glucose oxidase (GOx, 50 $\mu\text{g}/\text{mL}$) in HEPES buffer (pH 7, 20 mM) at 37 °C for 40 min; (2) 50 μL of the solution after incubation was added into 50 μL DNA-nanoceria conjugate. The

fluorescence intensity after 5 min was recorded. For the selectivity test, 5 mM fructose, galactose, and sucrose were respectively incubated with GOx in the same way, and the fluorescence was compared with that of glucose (500 μ M). To test the feasibility of sensing glucose in serum, fetal bovine serum (FBS) was chosen as the incubation matrix and the standard addition method was used to derive the glucose concentration in FBS. Glucose was added into the FBS with varying concentration (0.5 mM to 6 mM). Then, 10 μ L of FBS with or without additional glucose was added into 990 μ L of incubation buffer containing GOx (50 μ g/mL) in HEPES buffer (pH 7, 20 mM) at 37 °C for 40 min as mentioned above. The calculated value was multiplied by 100 to obtain the glucose concentration in serum. For comparison, a commercial glucose meter (BAYER, Contour® next EZ) was used to measure the glucose in FBS following the vendor recommended protocol.

5.4 Summary

In summary, by studying the interaction between H₂O₂ and nanoceria using DNA, we developed a highly sensitive sensor for H₂O₂. H₂O₂ acts as a capping ligand and it quickly releases DNA from the particle surface, generating fluorescence signal for H₂O₂ and glucose detection even in blood serum samples. This study opens up many new ways of using H₂O₂ for interfacing with inorganic nanoparticles, and also expands the scope of DNA-based biosensors.

Chapter 6 DNA/Iron Oxide Conjugates with Enhanced Peroxidase-like Activity

The results presented in this chapter have been published as part of:

Biwu Liu and Juewen Liu, Accelerating Peroxidase Mimicking Nanozymes Using DNA. *Nanoscale*, 33, 13831-13835, 2015.

6.1 Introduction

Nanomaterials as enzyme mimics (nanozymes) have received considerable attention recently.^{121,122,123} A wide range of nanomaterials including gold nanoparticles,^{124,125} metal oxides,^{126,127,128,129} and carbon-based materials^{130,131} have been reported to have oxidase, peroxidase, catalase, and superoxide dismutase like activity. Among these nanozymes, iron oxide nanoparticles (e.g., Fe₃O₄ NPs) are particularly interesting because of their unique magnetic properties and applications in magnetic resonance imaging, drug delivery, and separation.¹²² Fe₃O₄ NPs were first reported to have peroxidase activity in 2007.¹²⁶ Based on the peroxidase activity of Fe₃O₄ NPs, colorimetric biosensors for H₂O₂ detection have been developed using chromogenic substrates.¹⁵⁰ When glucose oxidase is combined with Fe₃O₄ NPs, glucose can also be selectively detected.²⁶³ For practical applications and fundamental mechanistic understanding, factors affecting the peroxidase activity need to be fully addressed.^{164,264,265,266} For example, the surface Fe²⁺ content was found to be vital in its oxidation activity.¹²⁶ Prussian blue modified γ -Fe₂O₃ NPs have an elevated surface Fe²⁺ content and thus a higher enzymatic activity.²⁶⁵ Also, the role of surface charge on substrate oxidation was investigated and electrostatic interaction was found to be crucial for substrate binding.²⁶⁴ The activity of unmodified

particles is often quite low, and an important challenge in this field is to promote their catalytic activity. We reason this goal might be achieved via understanding the surface chemistry of the reactions.

DNA-functionalized NPs represent an important hybrid material in bionanotechnology.^{2,10,37,52} Since the seminal work by the Mirkin and the Alivisatos groups,^{38,39} a plethora of DNA-NP conjugates have been reported for various applications, such as directed assembly of nanostructures,^{182,185,267} biosensing,^{4,51,176,187} and drug delivery.¹⁷⁹ DNA functionalization not only improves the colloidal stability of NPs, but also provides additional molecular recognition ability (e.g. aptamers) toward metal ions, small molecules and proteins.^{4,221,223} DNA-functionalized Fe₃O₄ NPs have been successfully used for detecting arsenate ions,²²⁶ and biomolecules.⁸⁰ However, the effect of DNA modification on the intrinsic properties of Fe₃O₄ NPs is less explored. In this chapter, we report that DNA-modified Fe₃O₄ NPs exhibit significantly enhanced peroxidase activity for TMB oxidation compared the bare NPs. Further studies show that both surface charge and DNA base composition are important for modulating the substrate affinity to Fe₃O₄ NPs, and thus the catalytic activity.

6.2 Results and Discussions

6.2.1 Characterization of Fe₃O₄ NPs

We first characterized our Fe₃O₄ NPs using TEM (Figure 6.1A). The NPs are roughly spherical and have a size around 25 nm (also see Chapter 3). Aggregation was observed attributable to the unmodified surface. We are interested in studying naked NPs without strong capping ligands, so that the surface property can be better controlled. No

obvious light absorption features were observed using UV-vis spectroscopy in the visible region from 400 to 800 nm (Figure 6.1B). At low NP concentrations used in this study, this low background absorption does not interfere with visual observation of color change from chromogenic substrates or quantitative spectroscopic measurements. Surface charge is another important parameter in determining the property of colloidal nanoparticles. Therefore, we also measured the ζ -potential of Fe₃O₄ NPs at various conditions (Table 6.1) and the surface of bare Fe₃O₄ NPs show a positive charge at pH 4.

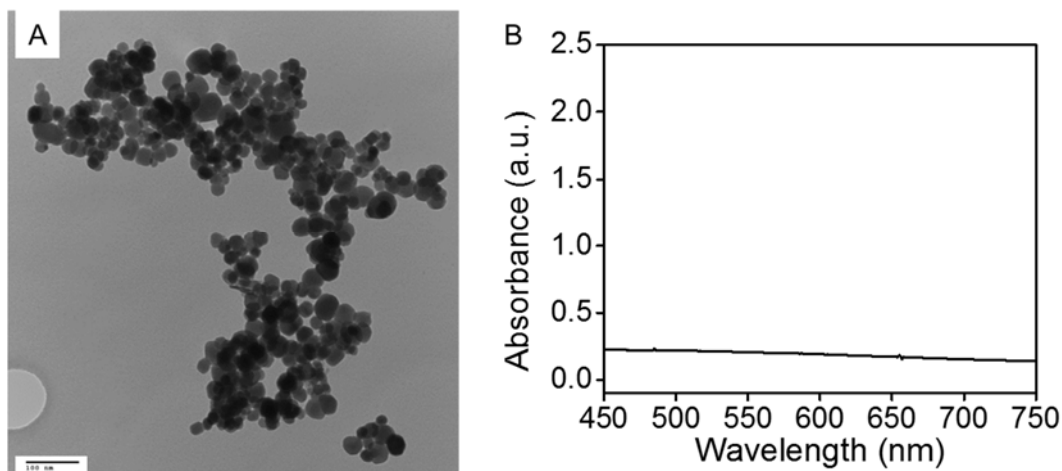


Figure 6.1 Characterization of Fe₃O₄ NPs used in this work. (A) TEM and (B) UV-vis absorbance spectroscopy.

Table 6.1 ζ -potential of iron oxide NPs at various conditions

| pH | Nanoparticles | Buffer | Surface Modification | Substrate | ζ -potential (mV) |
|-----|--------------------------------|---------|----------------------|-----------|-------------------------|
| 4.0 | Fe ₃ O ₄ | Acetate | No | No | 12.91 ± 3.66 |
| 4.0 | Fe ₃ O ₄ | Acetate | No | TMB | 28.70 ± 0.98 |
| 4.0 | Fe ₃ O ₄ | Acetate | DNA | No | -36.68 ± 1.71 |

| | | | | | |
|-----|--------------------------------|-----------|-----|-----|---------------|
| 4.0 | Fe ₃ O ₄ | Acetate | DNA | TMB | -25.30 ± 0.14 |
| 4.0 | Fe ₃ O ₄ | Acetate | PAA | No | -34.80 ± 1.17 |
| 4.0 | Fe ₃ O ₄ | Acetate | PSS | No | -34.80 ± 1.28 |
| 4.0 | Fe ₃ O ₄ | Phosphate | No | No | -20.37 ± 0.23 |
| 7.6 | Fe ₃ O ₄ | HEPES | No | No | -27.40 ± 0.61 |
| 7.6 | Fe ₃ O ₄ | Phosphate | No | No | -47.60 ± 1.15 |
| 4.0 | Fe ₂ O ₃ | Acetate | No | No | 12.33 ± 0.67 |
| 4.0 | Fe ₂ O ₃ | Acetate | DNA | No | -34.17 ± 0.51 |

6.2.2 Proof of concept

Peroxidase can catalyse the oxidation reaction in the presence of H₂O₂. TMB is a commonly used peroxidase substrate. It is colorless in the reduced state and blue in the oxidized state. We next tested the effect of DNA adsorption on the oxidation of TMB by H₂O₂ using Fe₃O₄ NPs as a peroxidase mimic. In the presence of unmodified Fe₃O₄ NPs, TMB was slowly oxidized by H₂O₂, producing a moderate blue colour after 15 min (Figure 6.2A). Interestingly, a strong blue color appeared when DNA was added to the reaction mixture. The change of absorbance at 652 nm is around 8-fold higher with DNA than that with only the unmodified Fe₃O₄ NPs (Figure 6.2B). The difference in TMB oxidation indicates that DNA has promoted the activity of Fe₃O₄ NPs as a peroxidase. To verify the role of DNA, more control tests were performed (Figure 6.2C,D) Without Fe₃O₄ NPs, the

TMB oxidation by H_2O_2 was slow, and adding DNA did not accelerate the reaction. Also, Fe_3O_4 NPs or DNA alone did not oxidize TMB. Therefore, the enhanced TMB oxidation was due to DNA promoted peroxidase activity of Fe_3O_4 NPs.

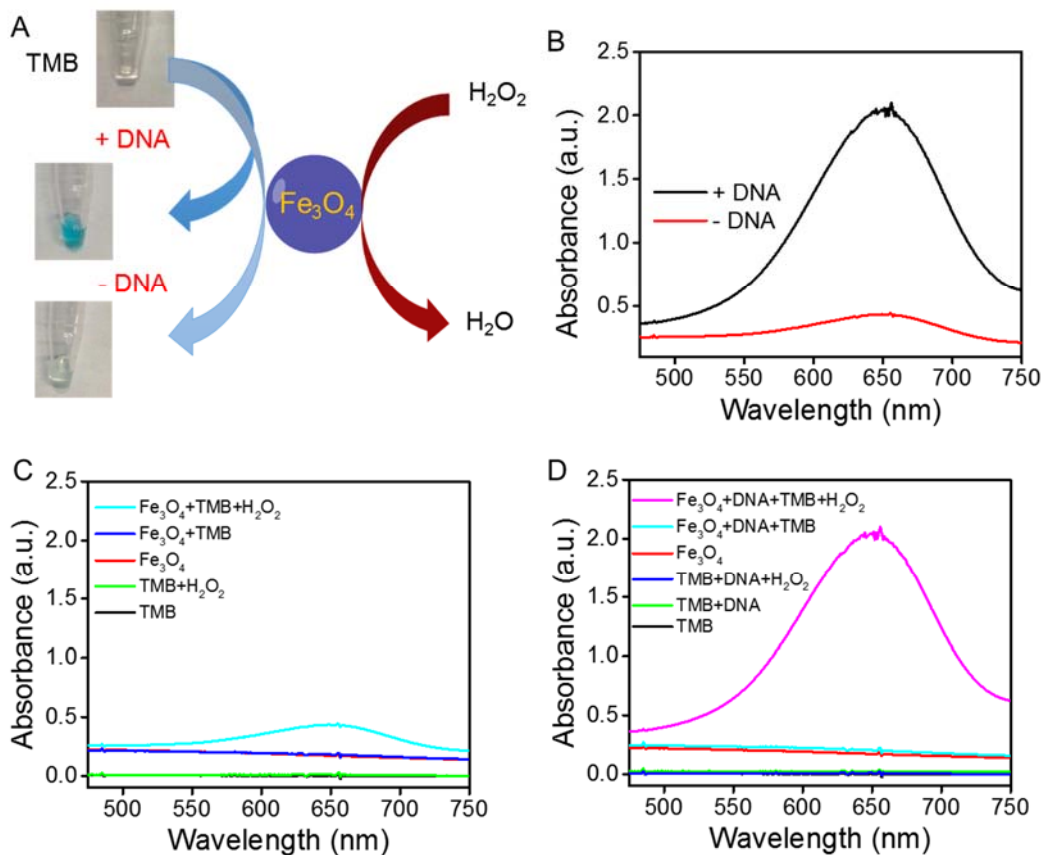


Figure 6.2 Proof of concept study of the effect of DNA on the TMB oxidation. (A) Accelerated oxidation of TMB using the C_{30} DNA-modified Fe_3O_4 NPs as a peroxidase mimic. The photographs of the reaction substrate and product are shown. (B) UV-vis spectra of the reaction products with and without DNA after 15 min reaction. Control experiments showing the TMB oxidation (C) in the absence and (D) presence of DNA, respectively.

6.2.3 Effect of DNA sequence, length, and concentration

Our previous work has indicated that DNA is tightly adsorbed by Fe₃O₄ NPs mainly via the phosphate backbone of DNA at neutral pH (Chapter 3).²²⁶ From ζ -potential measurement, Fe₃O₄ NPs carry a negative charge at pH 7.6 and a positively charge at pH 4 (Table 6.1). Our TMB oxidation experiment was carried out at pH 4, and thus electrostatic interaction might also contribute to DNA adsorption. To evaluate the effect of DNA on the peroxidase property of Fe₃O₄ NPs, we first tested the kinetics of TMB oxidation as a function of DNA sequence. Fe₃O₄ NPs were incubated with 15-mer homo DNAs (A₁₅, T₁₅, C₁₅, G₁₅) at pH 4 (acetate buffer, 10 mM) for 10 min, followed by adding the substrate TMB. In the absence of H₂O₂, oxidation of TMB was slow and the added DNA did not alter the reaction (Figure 6.2D). After adding H₂O₂, the reaction showed a DNA sequence dependent kinetics (Figure 6.3A). The order of reaction kinetics is: C > G > T > A > No DNA. The initial rate of the C₁₅-Fe₃O₄ NP conjugate is 9 times faster than that of unmodified Fe₃O₄ NPs, showing a significant enhancement effect. While we reported the major binding between DNA and Fe₃O₄ NPs are from the phosphate backbone, the secondary structure of homo-DNAs may cause different interactions. C₁₅ was also found to be the most effective probe used for arsenate detection.²²⁶ The pK_a of cytosine is 4.5, and a large fraction of the base at pH 4 is protonated, which may assist charge neutralization on the particle surface and reduce repulsion among DNA, allowing the packing of more DNA and accelerate the oxidation activity.

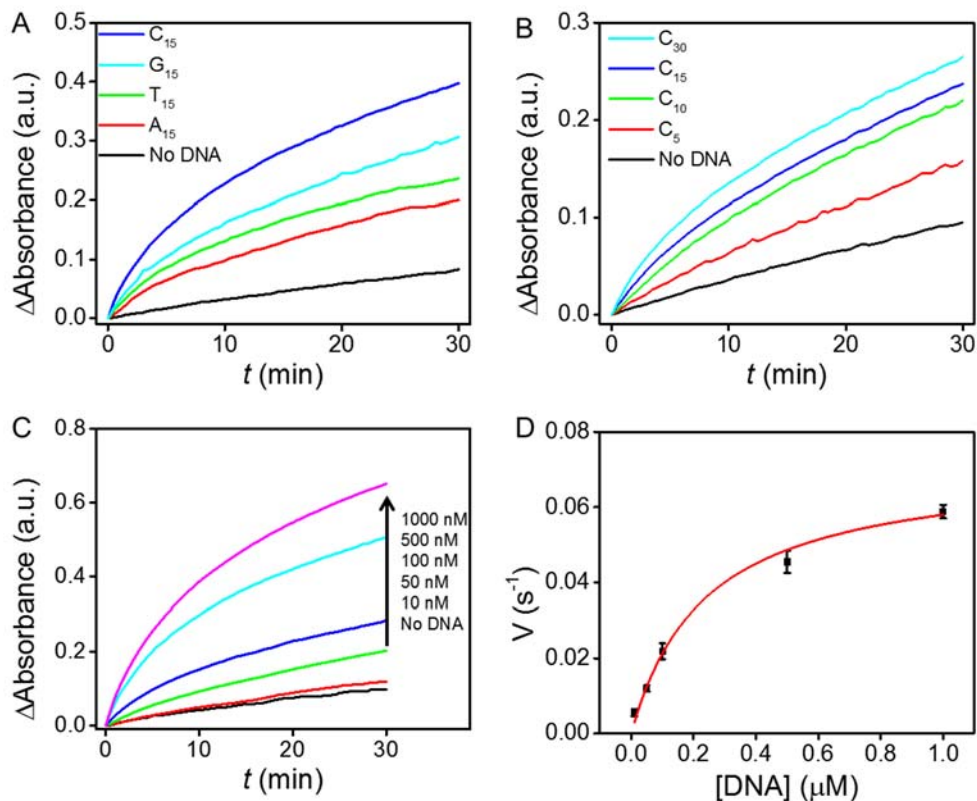


Figure 6.3 Effects of DNA on the kinetics of TMB oxidation catalysed by DNA-modified Fe₃O₄ NPs as a function of (A) sequence, (B) length, and (C) concentration. (D) The initial reaction rate as a function of DNA concentration.

Next, we tested the effect of DNA length on the rate enhancement. By fixing the total concentration of nucleosides, we used poly C_n ($n = 5, 10, 15,$ and 30) to modify Fe₃O₄ NPs (e.g. the concentration of C₅ is six times higher than that of C₃₀). The initial rate exhibits a DNA length-dependent increase (Figure 6.3B). Poly C₃₀, the longest DNA tested here, shows the largest enhancement, even though its molar concentration is the lowest. Longer DNAs have higher affinity with the Fe₃O₄ NPs due to the presence of more binding sites (e.g., polyvalent binding effect). This experiment strongly indicates that DNA

adsorption affinity is crucial for activity enhancement. The fact that longer DNA provided higher activity suggests that the activity enhancement is from surface bound DNA.

We further examined the effect of DNA concentration. As shown in Figure 6.3C, higher DNA concentration induced faster TMB oxidation. When the concentration is higher than 500 nM, the enhancement is less significant, likely due to surface saturation (Figure 6.3D). This experiment also indicates that it is the surface adsorbed DNA instead of free DNA in this system to increase the peroxidase activity of Fe₃O₄ NPs.

6.2.4 Effect of pH

Since the peroxidase activity of Fe₃O₄ NPs is pH-dependent¹²⁶ and pH may affect DNA adsorption, the effect of pH on the TMB oxidation was also tested. For the free Fe₃O₄ NPs (Figure 6.4A), the reaction is more effective at lower pH (e.g., pH 4) as reported in the literature. The presence of DNA does not alter the pH-dependent activity trend (Figure 6.4B). To compare the DNA effect at each pH, we plotted the absorbance (652 nm) after 1 h reaction. It clearly shows that the DNA adsorption enhanced the TMB oxidation at each pH (Figure 6.4C). Notice that at pH 6, the color change of TMB with DNA modified NPs is comparable to that at pH 4 with the unmodified Fe₃O₄ NPs. Attaching DNA can expand the application of Fe₃O₄ NPs over a broader pH range.

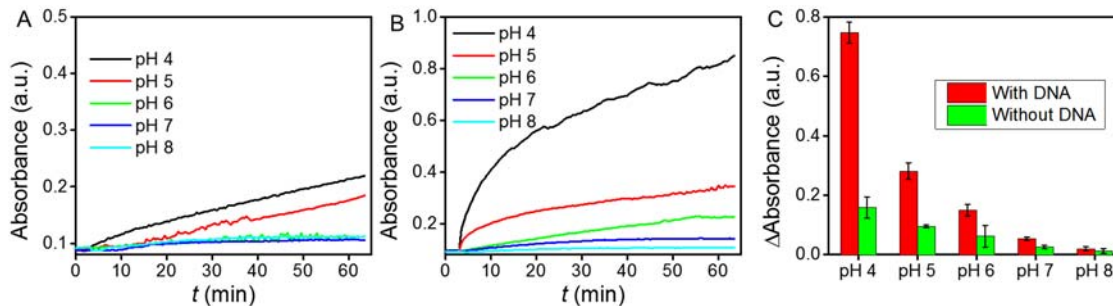


Figure 6.4 Effects of pH on the DNA-induced enhancement. Reaction kinetics of TMB oxidation as a function of pH in the (A) absence and (B) presence of DNA, respectively. (C) The variation of absorbance at 652 nm as a function of pH after 1 h reaction.

6.2.5 Mechanistic investigation

Using polymer coatings to modulate nanozymes activity was also reported in a few other systems.²⁶⁴ In those examples, electrostatic interaction between Fe₃O₄ NPs and the substrates (TMB and ABTS) was found to be important for the enzyme activity. If TMB (positively charged) was used as a substrate, more negatively charged particles showed higher k_{cat} values.²⁶⁴ In another example, DNA from PCR products was reported to inhibit o-phenylenediamine oxidation, as the electrostatic interaction between the positively charged substrate and the negatively charged Fe₃O₄ NP surface is blocked by free DNA in solution and on particle surface.²⁶⁸ To understand the mechanism here, we first studied whether H₂O₂ and TMB can compete with DNA adsorption. We recently reported that H₂O₂ can efficiently displace DNA adsorbed by CeO₂ NPs due to the strong affinity between H₂O₂ and CeO₂.²²⁷ However, H₂O₂ only inhibited DNA adsorption by Fe₃O₄ NPs at a very high concentration (1 M) and no adsorption inhibition was observed at our experimental conditions (Figure 6.5A). TMB did not block and even slightly facilitated DNA adsorption onto Fe₃O₄ NPs (Figure 6.5B).

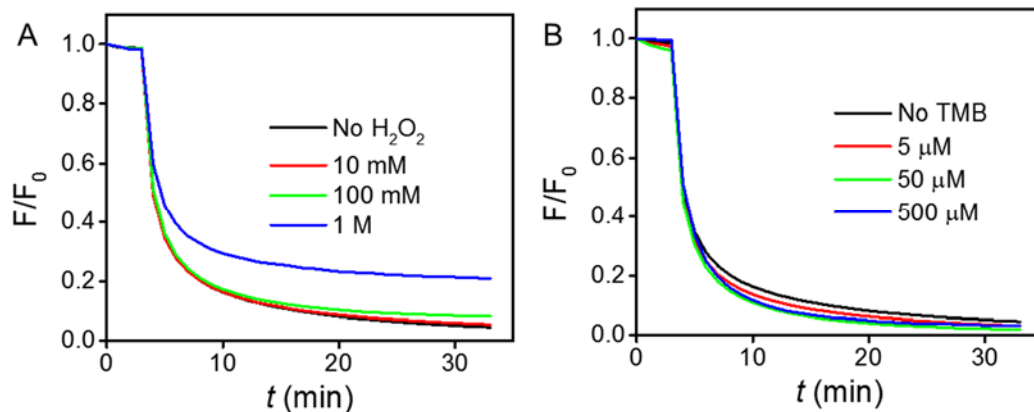


Figure 6.5 Kinetics of Alexa-DNA (50 nM) adsorption onto Fe_3O_4 NPs (25 $\mu g/mL$) at pH 4 (acetate buffer, 10 mM) in the presence of varying concentrations of (A) H_2O_2 and (B) TMB. The lack of obvious kinetic changes indicate that H_2O_2 and TMB do not inhibit DNA adsorption.

Second, we examined the integrity of DNA by gel electrophoresis. One concern is that DNA might be degraded in the presence of H_2O_2 and iron species (e.g. via the Fenton chemistry). The control group (Fe^{2+}/H_2O_2 , lane 6, Figure 6.6) indeed shows that the fluorophore tag on DNA (6-carboxyfluorescein, FAM) might be damaged due to generated hydroxyl free radicals indicated by the weak fluorescence intensity. However, DNA on the Fe_3O_4 NPs surface was not cleaved and the fluorophore was not damaged at our experimental conditions (lane 5, Figure 6.6). Combined with fluorescence-based results, DNA remained intact on the surface during and after the peroxidase reaction.

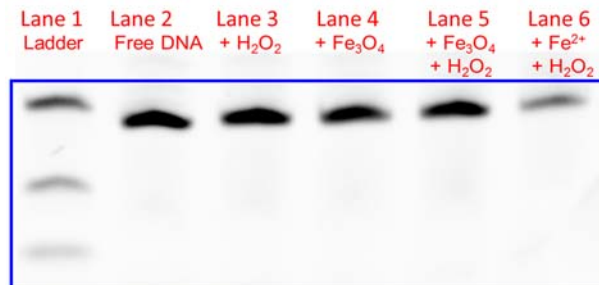


Figure 6.6 Gel image of DNA-Fe₃O₄ treated with H₂O₂. Lane 1 is a DNA ladder with FAM-A₅, FAM-A₁₅ and FAM-A₃₀. Lane 2 is an untreated FAM-labeled 24 mer DNA. Lane 3-6 are the FAM DNA treated with various chemicals as indicated in the lanes. Acetate buffer (pH 4, 10 mM) was used for all samples. FAM-24 mer DNA (200 nM) was incubated with Fe₃O₄ NPs (25 μg/mL) or Fe²⁺ (50 μM) and H₂O₂ (10 mM) was added if necessary.

One possibility is that DNA facilitates the adsorption of TMB by Fe₃O₄ NPs. With two amino groups, the non-oxidized TMB has a pK_a of ~ 4.2 and is partially positive charged at pH 4 (Figure 6.7A). This may explain its affinity for DNA. If this hypothesis is true, the activity of Fe₃O₄ NPs should decrease when a negatively charged substrate is used. To test this hypothesis, we then employed another peroxidase substrate, ABTS. ABTS is negative charged due to the dual sulfate anions (Figure 6.7A). As shown in Figure 6.7A, after adding H₂O₂ (10 min), ABTS was oxidized by the unmodified Fe₃O₄ NPs but not by the DNA-modified Fe₃O₄ NPs. DNA modification alters the surface charge of Fe₃O₄ NPs from positive to negative (Table 6.1). The charge repulsion between ABTS and DNA surface inhibits the oxidation reaction. To further prove the charge repulsion mechanism, we monitored the oxidation of ABTS at different ionic strengths. In the absence of DNA, increasing NaCl concentration slightly inhibited TMB oxidation. In the presence of DNA, we found that the enzymatic performance was gradually recovered by increasing NaCl

concentration to screen charge repulsion and the activity is even higher than unmodified Fe_3O_4 NPs without additional NaCl (Figure 6.7C,D).

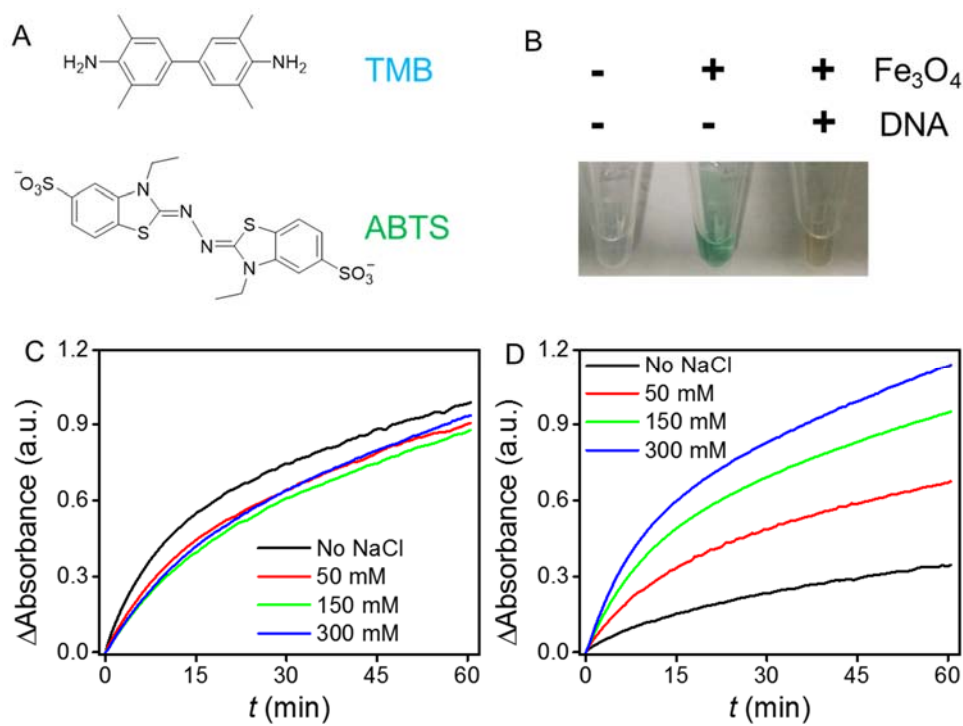


Figure 6.7 Effect of electrostatic interaction on the DNA-induced enhancement. (A) Chemical structures of TMB and ABTS. (B) A photograph showing oxidation of ABTS (1 mM) in the presence of Fe_3O_4 NPs (50 $\mu\text{g}/\text{mL}$) at pH 4 producing a green colour. Kinetics of ABTS oxidation at various NaCl concentrations catalysed by (C) bare Fe_3O_4 NPs and (D) DNA-capped Fe_3O_4 NPs, respectively. The absorbance at 420 nm was monitored.

Aside from the negatively charged backbone, DNA can also provide hydrogen bonding, π - π interactions via DNA bases. To test if DNA bases are involved in substrate binding, we compared DNA with other negatively charged polymers for coating Fe_3O_4 NPs. Polyacrylic acid (PAA) and polystyrene sulfonate (PSS) were respectively used to modify Fe_3O_4 NPs. The surface charge alternation at pH 4 was confirmed by ζ -potential

measurement and all modified Fe₃O₄ NPs exhibit similar negative charge values (Table 6.1). Compared to unmodified Fe₃O₄ NPs, negatively charged NPs all enhanced the activity and DNA modification provides the highest enhancement, followed by PSS and PAA (Figure 6.8A). To further emphasize the importance of DNA bases, we compared Fe₃O₄ NPs modified by phosphate, guanosine monophosphate (GMP), and G₁₅ (Figure 6.8B). Phosphate also changes the surface charge of Fe₃O₄ NPs to be negative (Table 6.1); however, the activity increase is minimal. As expected, GMP-modified Fe₃O₄ NPs facilitate TMB oxidation, confirming the role the DNA bases. The further increased activity by G₁₅ functionalization is consistent with our observation that the enhancement is DNA length-dependent (Figure 6.3B). We propose that DNA bases also facilitate the substrate binding via hydrogen bonding with the amino groups of TMB, and/or the nucleobase interacting with the benzene rings of TMB via π - π stacking.

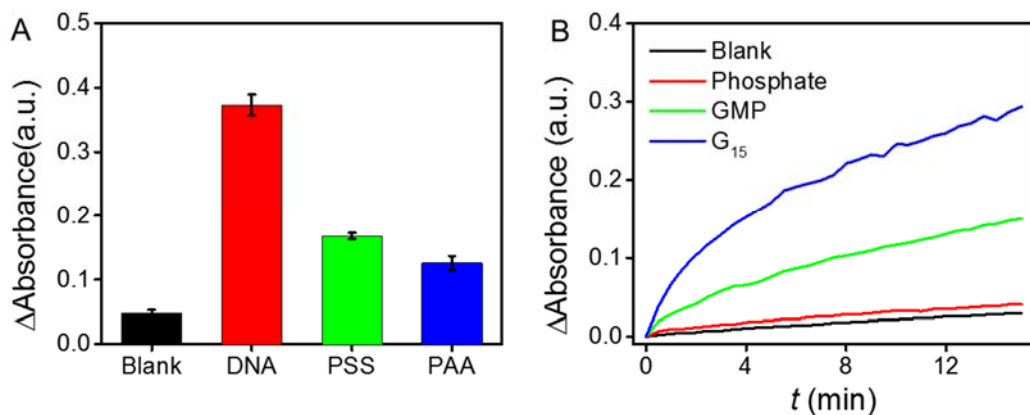


Figure 6.8 Effect of surface coating the peroxidase activity of Fe₃O₄ NPs. Comparison of the peroxidase activity of DNA-Fe₃O₄ NPs with (A) various negatively charged polymers coated Fe₃O₄ NPs and (B) phosphate and GMP modified Fe₃O₄ NPs.

Now that we have changed the polymer coating and substrate, we finally also tested a different type of NP, CeO₂ NPs. We previously reported that the oxidase activity of CeO₂ is inhibited by adsorbed DNA for oxidation of TMB.⁸⁴ However, the peroxidase activity of CeO₂ is actually enhanced by DNA modification (Figure 6.9). This might be attributed to that TMB needs to be directly adsorbed by CeO₂ to be oxidized in the absence of H₂O₂ (i.e., CeO₂ surface works as an oxidizing agent).²⁴⁹ However, in the presence of H₂O₂, CeO₂ can mediate the oxidation at a distance from the surface. As an oxidase, the substrate TMB needs to get onto the particle surface since the oxidizing agent is the particle surface. As a peroxidase, the actual oxidizing agent is derived from H₂O₂ (e.g., reactive oxygen species), which can diffuse near the particle surface. The activity of Fe₃O₄ NPs we studied here is the peroxidase activity. In this case, the surface is likely to react with H₂O₂ and then the reactive oxygen species produced in this process is used to oxidize TMB. H₂O₂ is a much smaller molecule and DNA does not block its access to the Fe₃O₄ NPs.

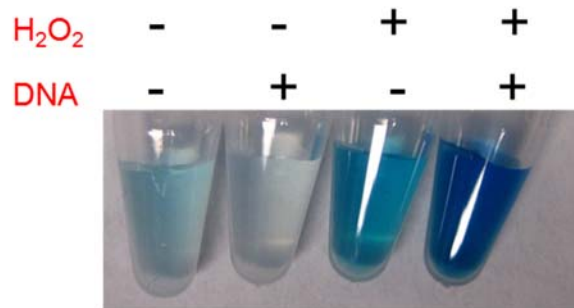


Figure 6.9 Effect of DNA on the oxidase and peroxidase-like activity of nanoceria.

6.3 Materials and Methods

6.3.1 Chemicals

All of the DNA samples were from Integrated DNA Technologies (IDT, Coralville, IA, USA). Their sequences and modifications are shown in Table S1. Fe₃O₄ NPs (637106), nanoceria (catalog number: 289744, 20% dispersed in 2.5% acetic acid), 3,3',5,5'-tetramethylbenzidine (TMB), 2,2'-azino-bis(3-ethylbenzothiazoline-6-sulfonic acid) diammonium salt (ABTS), 30 wt % H₂O₂ solution, polystyrene sulfonate (PSS, catalog number: 527483), polyacrylic acid, sodium salt (PAA, catalog number: 416037), guanosine monophosphate (GMP) were purchased from Sigma-Aldrich. Fe₂O₃ NPs (Stock number: US3200) were purchased from US Research Nanomaterials. Sodium acetate, sodium citrate, sodium phosphate, sodium chloride, 4-(2-hydroxyethyl) piperazine-1-ethanesulfonic acid (HEPES), 2-(N-morpholino) ethanesulfonic acid (MES) were from Mandel Scientific (Guelph, ON, Canada). Milli-Q water was used for all of the experiments

Table 6.2 The sequences and modification of DNA used in this work

| DNA names | Sequences (from 5' to 3') and modifications |
|---------------------------|---|
| Alexa-DNA | TCA CAG ATG CGT-Alexa Fluoro 488 |
| FAM-A₅ | FAM-AAA AA |
| FAM-A₁₅ | FAM-AAA AAA AAA AAA AAA |
| FAM-A₃₀ | FAM-AAA AAA AAA AAA AAA AAA AAA AAA AAA AAA |
| FAM-24 mer | FAM-ACG CAT CTG TGA AGA GAA CCT GGG |
| A₅ | AAA AA |

| | |
|-----------------------|---|
| C₅ | CCC CC |
| C₁₀ | CCC CCC CCC C |
| A₁₅ | AAA AAA AAA AAA AAA |
| T₁₅ | TTT TTT TTT TTT TTT |
| C₁₅ | CCC CCC CCC CCC CCC |
| G₁₅ | GGG GGG GGG GGG GGG |
| C₃₀ | CCC |

6.3.2 Modification of iron oxide NPs

To coat Fe₃O₄ NPs with polymers, PSS or PAA (final concentration 10 mg/mL) was mixed with 1 mg/mL of NPs. After overnight stirring, excess polymer was removed by centrifugation (10, 000 rpm, 10 min) and the conjugates were washed with Milli-Q water three times. PSS modified Fe₂O₃ NPs were prepared in a similar way. Phosphate (1 mM), GMP (1 mM), and DNA (G₁₅, 500 nM) modified nanoparticles were prepared by incubating designed concentration of Fe₃O₄ NPs and capping agents at acetate buffer (pH 4) for at least 10 min without further purification.

6.3.3 Transmission Electron Microscopy (TEM) and UV-vis spectroscopy

The particle size and morphology of Fe₃O₄ NPs was studied using TEM (Philips CM10). The TEM sample was prepared by dropping Fe₃O₄ NPs dispersion (50 µg/mL) into a copper grid and was allowed to dry overnight at room temperature. The UV-vis spectra of Fe₃O₄ NPs, TMB and oxidized TMB were scanned after reacting H₂O₂ (20 mM) with TMB (0.5 mM) at different conditions for 15 min using a UV-vis spectrometer

(Agilent 8453A). Poly C₃₀ (500 nM) was used to modify Fe₃O₄ NPs. The concentration of Fe₃O₄ NPs was 50 µg/mL for most experiments unless otherwise specified. The visual images were taken by a digital camera.

6.3.4 ζ-potential measurement

The ζ-potential was measured by dynamic light scattering (DLS) using Malvern Nanosizer ZS90. Effects of pH, buffer, and surface modification on the ζ-potential of Fe₃O₄ NPs and Fe₂O₃ NPs were tested and the reaction conditions were specified in Table S2. The temperature was maintained at 25 °C during measurement.

6.3.5 Inhibition of DNA adsorption

To study the effect of H₂O₂ and TMB on adsorption kinetics, Alexa-DNA (50 nM) was dissolved into the pH 4 buffer (acetate buffer, 10 mM) with varying concentrations of H₂O₂ or TMB. The initial fluorescence of free DNA (F₀) was monitored for 3 min (excitation at 485 nm, emission at 535 nm) using a microplate reader (Infinite F200Pro, Tecan). After a quick addition of Fe₃O₄ NPs dispersion (final concentration 25 µg/mL), the fluorescence was monitored for another 30 min. The fluorescence was then normalized based on the initial intensity (F/F₀).

6.3.6 Peroxidase activity assays of Fe₃O₄ NPs

In a typical assay, 1 µL of TMB in DMSO solution (50 mM) was added into 100 µL of Fe₃O₄ NPs (final concentration 50 µg/mL) with or without DNA at pH 4 (acetate buffer, 10 mM), followed by a quick mixing to avoid TMB precipitation. The absorbance

at 652 nm was recorded in a kinetic mode using a microplate reader. Afterwards, H₂O₂ (10 mM) was added to induce the reaction and the absorbance was monitored for another 30 min. The effect of DNA sequence was studied using homo poly DNAs with different bases (A₁₅, T₁₅, C₁₅, G₁₅ concentration = 500 nM). Poly C_n (n = 5, 10, 15, 30) was used to investigate the DNA length effect. The total concentration of nucleosides of cytosine was set as 3 μM. For the DNA concentration and pH effect studies, C₃₀ was used as the capping agent. The solution pH was controlled by using designed buffers (acetate buffer for pH 4 and 5, MES for pH 6, and HEPES for pH 7 and 8). The oxidation kinetics of ABTS at various salt concentrations were studied in a similar way expect that the final concentration of ABTS was 1 mM. The absorbance at 420 nm was recorded. NaCl was used to adjust the ionic strength of the reaction.

6.3.7 Activity of CeO₂ NPs

DNA (A₅, 5 μM) was incubated with CeO₂ NPs (0.1 mg/mL) for 15 min before adding TMB (1 mM). To study the DNA effect on the peroxidase activity of CeO₂, a mixture of TMB and H₂O₂ solution was added into CeO₂ or DNA-CeO₂. The final concentration of H₂O₂ was 10 mM. All reactions were performed at pH 4 acetate buffer. The photographs were taken after 30 min.

6.3.8 Gel electrophoresis

For denaturing gels, DNA-Fe₃O₄ NPs in the absence or the presence of H₂O₂ was dispersed in 15% glycerol and loaded onto 15% polyacrylamide gel with 8 M urea. The conjugate was prepared by mixing FAM-24 mer (200 nM) and Fe₃O₄ NPs (25 μg/mL) in

acetate buffer (pH 4.0, 10 mM) and 10 mM H₂O₂ was added. As a control, 50 μM of Fe²⁺ was used to cleave DNA at the same reaction condition. The gels were then imaged using blue LED epi excitation (Bio-Rad, Chemidoc MP).

6.4 Summary

In summary, we observed a significant rate enhancement brought by DNA for the peroxidase activity of Fe₃O₄ NPs for TMB oxidation. Such a rate enhancement will make such a nanozyme a better material for biosensor development and catalysis. Starting from this observation, we investigated the effect of DNA adsorption on enhancing the peroxidase-like activity of Fe₃O₄ NPs. DNA/Fe₃O₄ forms a stable hybrid material, and neither H₂O₂ nor TMB can displace DNA from the particle surface under our experimental conditions. Among all the tested anionic polymers, DNA affords the highest rate enhancement. This is attributed to both electrostatic attraction and aromatic stacking with the substrate TMB. The hypothesis is further supported by using a negative charged substrate ABTS and with CeO₂ NPs. The insight from this work will be useful for further rational improving nanozyme activity via surface modification.

Chapter 7 Conclusions and Future Work

7.1 Conclusions

DNA can be used as a functional molecule to interface with nanomaterials to construct bio-nano conjugates. The majority of previous work on DNA/MONPs has focused on indirect conjugation with the help of cross-linkers or surface coating layers. Previous work also focused on metal nanoparticles and carbon-based nanomaterials, while relatively little was explored for MONPs. In this thesis, I explored the direct adsorption of DNA by naked MONPs, including ITO, Fe₃O₄, CeO₂, and other sixteen oxides.

In Chapter 2, I have systematically investigated the adsorption of DNA by ITO NPs. ITO NPs are shown to adsorb fluorescently labeled DNA and quench fluorescence. DNA adsorption is more efficient at acidic conditions due to the positive surface charge of ITO. DNA binds to ITO mainly through the phosphate backbone based on displacement assays. Interestingly, cDNA can induced desorption of adsorbed DNA, allowing DNA detection down to 0.7 nM. Doping the tin component into In₂O₃ has weakened the DNA binding affinity, making it possible to directly detect cDNA. The study in this chapter provided fundamental insights into DNA interaction with ITO NPs, which is an important transparent electrode material useful for biosensor development.

In Chapter 3, I have studied DNA adsorption by Fe₃O₄ NPs and demonstrated its application for detecting arsenate from water as low as 130 nM. The work in this chapter provides a new direction for sensing anions using DNA. Different from DNA adsorption by gold or carbon nanomaterials, binding of DNA to iron oxide is through the phosphate group.

In Chapter 4, I have screened nineteen types of MONPs for the DNA adsorption, fluorescence quenching, and anion-induced DNA desorption. Three oxide, CeO₂, Fe₃O₄, and ZnO, were obtained to form a sensor array to successfully discriminate phosphate, arsenate, arsenite and other interference anions. This study is an extension of the study of Chapter 2, and provides a comprehensive understanding on the interaction between DNA and MONPs.

In Chapter 5, I have studied the interaction between H₂O₂ and nanoceria using DNA. A highly sensitive sensor for H₂O₂ has been developed. I demonstrated that H₂O₂ acts as a capping ligand and it displaces the surface adsorbed DNA quickly. The fluorescently labeled DNA serves as signaling molecule. H₂O₂ and glucose detection in blood serum samples were achieved based on the DNA release induced fluorescence recovery. The study opens up many new ways of using H₂O₂ for interfacing with nanozymes, and also expands the scope of DNA-based sensors.

In Chapter 6, I have investigated the role of DNA in enhancing the peroxidase-like activity of Fe₃O₄ NPs for TMB oxidation. As demonstrated in Chapter 3, DNA/Fe₃O₄ forms a stable hybrid, and neither H₂O₂ nor TMB can displace DNA from the particle surface. DNA exhibits the highest enhancing effect among various modification methods. The rate enhancement is attributed to both electrostatic and aromatic stacking with the substrate. The insight from this work will be useful for further rational improving nanozyme activity via surface modification.

7.2 Original Contributions

This thesis provides important insights into the surface chemistry of bio-nano interface, and offers new strategy to analytical chemistry in designing sensors to detect some challenging analytes.

First, I have further established the methodology used in investigating the interaction between DNA and nanomaterials. Methods used in previous works are time-consuming, need complicated sample preparation, and mostly perform under non-aqueous environment. In my thesis, fluorescently labeled DNA were used to probe the *in situ* adsorption and desorption processes on MONPs with high sensitivity. Importantly, several MONPs I tested, for example, ITO, Fe₃O₄, and CeO₂, are fluorescence quenchers. Using this fluorescence method, both kinetic and thermodynamic information of the surface reaction can be easily obtained.

Second, the fundamental interaction between DNA and MONPs provide important insights into bio-nano interface. These understandings serve as baseline for the further design of functional biosensors. For example, the adsorption kinetics and capacity of probe DNA on ITO surface, as revealed in Chapter 2 rely on the solution pH, ionic strength, probe sequence and length. To design a biosensor with high sensitivity, all of these parameters should be examined. Also, even though ITO NPs bind to DNA via the phosphate backbone, they still can differentiate ssDNA and dsDNA. The difference may be due to the flexibility of DNA strands that ssDNA is more flexible than dsDNA. As a result, ssDNA have more binding sites on oxides surface. This interesting finding could server as the basis in cDNA detection biosensors. Actually, after our work, several groups have reported the design of DNA/oxides biosensors for DNA and protein detection.^{80,81} While the sensors are

constructed successfully, the underlying mechanism is studied by us. A common feature for all these oxides is that they adsorb DNA via the DNA phosphate backbone.

Third, functional sensors have been developed with some unique features. DNA probe has been widely used as the recognition element to construct biosensor. While DNA can recognize a wide range of targets, such as metal ions, small molecules (e.g., adenosine), and proteins (e.g., thrombin), it still fails to target certain analytes (e.g., anions, H_2O_2 , glucose). These analytes either repel DNA due to the like-charge or lack functional groups to interface with DNA. This problem can be partially solved by using modified DNA bases or cofactors to increase the binding affinity.^{237,269} But only certain research groups can perform this now. In my thesis, I have developed a simple strategy to solve this problem. Rather than directly interfacing DNA with targets, I chose to use fluorescently labeled DNA as signaling molecule. The recognition processes rely on the surface activity of MONPs. In Chapter 3, the arsenate adsorption ability of iron oxide was utilized to displace DNA. One minor issue of such design is that the selectivity. Phosphate is very similar to arsenate, and may also induce false positive signal. This problem was solved by designing a chemical sensor array to discriminate the three similar anions, phosphate, arsenate, and arsenite, which is described in Chapter 4. As a proof of concept, I demonstrate the first metal oxide based sensing array for anion discrimination. In Chapter 5, based on the strong interaction between H_2O_2 and nanocerium, I developed another sensor for H_2O_2 with high sensitivity and selectivity. While many organic dyes have been used to probe H_2O_2 , the sensor proposed here represents a new design strategy.

Another feature of using nanomaterials rather than DNA as recognition element is the ability to remove molecules from water. With surface adsorption and magnetic

separation of iron oxide, arsenate in water can be removed down to the safe level. With surface capping and decomposition ability of nanoceria, toxic H_2O_2 can be scavenged. Therefore, the sensing platforms developed in this thesis provide: 1) a new sensing strategy; 2) sensitive sensors for analytes previously difficult to detect with DNA; and 3) simultaneous detection and removal of toxins.

Last but not least, I have demonstrated a new way to modulate the peroxidase-like activity of iron oxide using DNA. Different from the sensors developed in Chapter 3, 4, and 5, DNA used here is not displaced by the two substrates. Alternatively, DNA serves as a promoter in enhancing the substrate affinity. The effect of DNA revealed here suggests that it is possible to improve the selectivity of nanozymes by combining the recognition ability of DNA.

7.2 Future Work

The results presented in this thesis have proved that interfacing DNA with non-modified MONPs has both fundamental and practical importance. Extension of current work can be carried out in the future.

First, more mechanistic work is needed to understand the interaction between DNA and MONPs. For example, the phosphate backbone has been shown to be the main binding sites. However, it is also suggested that DNA bases facilitate the adsorption.⁸⁵ MONPs encompass a large range of materials, and they may adsorb DNA differently. In addition, the size, shape, and structure of MONP affect the DNA adsorption.

Second, MONPs are able to adsorb not only anions, but also heavy metal ions.⁸⁷ Such metal ions adsorption is expected to alter the surface chemistry of MONPs. The

alternation can be probed again by fluorescently labeled DNA. In this way, we expanded the use of DNA/MONPs to both small anions and cations.

Third, the functionality of DNA has not been incorporated into the DNA/metal oxide conjugates. Further investigation may combine aptamer binding to improve the substrate oxidation reaction. In Chapter 6, I have demonstrated that DNA serves as linker to facilitate the substrate binding. If an aptamer rather than random DNA is used, the specific oxidation of substrate can be expected. For example, dopamine has been used as chromogenic substrate, the corresponding aptamer has also been identified. The definition of nanozymes has always been challenged due to the lack of substrate specificity. However, if receptors, such as DNA aptamers, antibodies, and molecular imprinted polymers, can be involved in the design of nanozyme-based assays, nanozymes will have competitive activity to real protein enzymes.

Fourth, DNAzymes can also be coupled to MONPs to obtain functional hybrids. Some other nanomaterials, for example, AuNPs, GO have been conjugated with aptamers and DNAzymes. But metal oxides surface provides a chemically different interaction modes with the DNA. Whether such binding affects DNAzymes activity needs careful studies.

Last but not least, DNA can be used as template to assemble hybrid nanomaterials. For example DNA has been shown to assemble AuNPs on graphene oxides surface using the multiple interaction sites.²⁷⁰ At the same time, DNA has been used as template to grow various nanostructures.^{271,272,273} However, no hybrid materials have involved both the phosphate backbone and DNA bases.

References

1. Seeman, N. C. DNA in a Material World. *Nature* **2003**, *421* (6921), 427-431.
2. Wilner, O. I.; Willner, I. Functionalized DNA Nanostructures. *Chem. Rev.* **2012**, *112* (4), 2528-2556.
3. Ward, W. L.; Plakos, K.; DeRose, V. J. Nucleic Acid Catalysis: Metals, Nucleobases, and Other Cofactors. *Chem. Rev.* **2014**, *114* (8), 4318-4342.
4. Liu, J.; Cao, Z.; Lu, Y. Functional Nucleic Acid Sensors. *Chem. Rev.* **2009**, *109* (5), 1948-1998.
5. Huang, P.-J. J.; Liu, J. DNA-Length-Dependent Fluorescence Signaling on Graphene Oxide Surface. *Small* **2012**, *8* (7), 977-983.
6. Kool, E. T. Hydrogen Bonding, Base Stacking, and Steric Effects in DNA Replication. *Annu. Rev. Biophys. Biomol. Struct.* **2001**, *30* (1), 1-22.
7. Liu, J. Adsorption of DNA onto Gold Nanoparticles and Graphene Oxide: Surface Science and Applications. *Phys. Chem. Chem. Phys.* **2012**, *14* (30), 10485-10496.
8. Izatt, R. M.; Christensen, J. J.; Rytting, J. H. Sites and Thermodynamic Quantities Associated with Proton and Metal Ion Interaction with Ribonucleic Acid, Deoxyribonucleic Acid, and their Constituent Bases, Nucleosides, and nucleotides. *Chem. Rev.* **1971**, *71* (5), 439-481.
9. Sapsford, K. E.; Algar, W. R.; Berti, L.; Gemmill, K. B.; Casey, B. J.; Oh, E.; Stewart, M. H.; Medintz, I. L. Functionalizing Nanoparticles with Biological Molecules: Developing Chemistries that Facilitate Nanotechnology. *Chem. Rev.* **2013**, *113* (3), 1904-2074.

10. Tjong, V.; Tang, L.; Zauscher, S.; Chilkoti, A. "Smart" DNA Interfaces. *Chem. Soc. Rev.* **2014**, *43* (5), 1612-1626.
11. Gehring, K.; Leroy, J.-L.; Gueron, M. A Tetrameric DNA Structure with Protonated Cytosine-Cytosine Base Pairs. *Nature* **1993**, *363* (6429), 561-565.
12. Day, H. A.; Pavlou, P.; Waller, Z. A. E. I-Motif DNA: Structure, Stability and Targeting with Ligands. *Bioorg. Med. Chem.* **2014**, *22* (16), 4407-4418.
13. McKeague, M.; DeRosa, M. C. Challenges and Opportunities for Small Molecule Aptamer Development. *Journal of Nucleic Acids* **2012**, *2012*, 20.
14. Famulok, M.; Hartig, J. S.; Mayer, G. Functional Aptamers and Aptazymes in Biotechnology, Diagnostics, and Therapy. *Chem. Rev.* **2007**, *107* (9), 3715-3743.
15. Bock, L. C.; Griffin, L. C.; Latham, J. A.; Vermaas, E. H.; Toole, J. J. Selection of Single-stranded DNA Molecules that Bind and Inhibit Human Thrombin. *Nature* **1992**, *355* (6360), 564-566.
16. Huizenga, D. E.; Szostak, J. W. A DNA Aptamer That Binds Adenosine and ATP. *Biochemistry* **1995**, *34* (2), 656-665.
17. Lin, C. H.; Patei, D. J. Structural Basis of DNA Folding and Recognition in an AMP-DNA Aptamer Complex: Distinct Architectures but Common Recognition Motifs for DNA and RNA Aptamers Complexed to AMP. *Chem. Biol.* **1997**, *4* (11), 817-832.
18. Cruz-Toledo, J.; McKeague, M.; Zhang, X.; Giamberardino, A.; McConnell, E.; Francis, T.; DeRosa, M. C.; Dumontier, M. Aptamer Base: A Collaborative Knowledge Base to Describe Aptamers and SELEX Experiments. *Database* **2012**, *2012*.
19. Lee, J. F.; Hesselberth, J. R.; Meyers, L. A.; Ellington, A. D. Aptamer Database. *Nucleic Acids Res.* **2004**, *32* (suppl 1), D95-D100.

20. Thodima, V.; Pirooznia, M.; Deng, Y. RiboaptDB: A Comprehensive Database of Ribozymes and Aptamers. *BMC Bioinformatics* **2006**, *7* (2), 1-6.
21. Liu, J. Oligonucleotide-Functionalized Hydrogels as Stimuli Responsive Materials and Biosensors. *Soft Matter* **2011**, *7* (15), 6757-6767.
22. Kruger, K.; Grabowski, P. J.; Zaug, A. J.; Sands, J.; Gottschling, D. E.; Cech, T. R. Self-splicing RNA: Autoexcision and Autocyclization of the Ribosomal RNA Intervening Sequence of Tetrahymena. *Cell* **1982**, *31* (1), 147-157.
23. Guerrier-Takada, C.; Gardiner, K.; Marsh, T.; Pace, N.; Altman, S. The RNA Moiety of Ribonuclease P is the Catalytic Subunit of the Enzyme. *Cell* **1983**, *35* (3), 849-857.
24. Breaker, R. R.; Joyce, G. F. A DNA Enzyme That Cleaves RNA. *Chem. Biol.* **1994**, *1* (4), 223-229.
25. Silverman, S. K. In vitro Selection, Characterization, and Application of Deoxyribozymes That Cleave RNA. *Nucleic Acids Res.* **2005**, *33* (19), 6151-6163.
26. Seeman, N. C. Nucleic Acid Junctions and Lattices. *J. Theor. Biol.* **1982**, *99* (2), 237-247.
27. Kallenbach, N. R.; Ma, R.-I.; Seeman, N. C. An Immobile Nucleic Acid Junction Constructed from Oligonucleotides. *Nature* **1983**, *305* (5937), 829-831.
28. Zheng, J.; Birktoft, J. J.; Chen, Y.; Wang, T.; Sha, R.; Constantinou, P. E.; Ginell, S. L.; Mao, C.; Seeman, N. C. From Molecular to Macroscopic via the Rational Design of a Self-assembled 3D DNA Crystal. *Nature* **2009**, *461* (7260), 74-77.
29. Rothmund, P. W. K. Folding DNA to Create Nanoscale Shapes and Patterns. *Nature* **2006**, *440* (7082), 297-302.

30. Ke, Y.; Sharma, J.; Liu, M.; Jahn, K.; Liu, Y.; Yan, H. Scaffolded DNA Origami of a DNA Tetrahedron Molecular Container. *Nano Lett.* **2009**, *9* (6), 2445-2447.
31. Andersen, E. S.; Dong, M.; Nielsen, M. M.; Jahn, K.; Subramani, R.; Mamdouh, W.; Golas, M. M.; Sander, B.; Stark, H.; Oliveira, C. L. P.; Pedersen, J. S.; Birkedal, V.; Besenbacher, F.; Gothelf, K. V.; Kjems, J. Self-Assembly of a Nanoscale DNA Box with a Controllable Lid. *Nature* **2009**, *459* (7243), 73-76.
32. Han, D.; Pal, S.; Nangreave, J.; Deng, Z.; Liu, Y.; Yan, H. DNA Origami with Complex Curvatures in Three-Dimensional Space. *Science* **2011**, *332* (6027), 342-346.
33. Chen, J.; Seeman, N. C. Synthesis from DNA of a Molecule with the Connectivity of a Cube. *Nature* **1991**, *350* (6319), 631-633.
34. Nel, A. E.; Madler, L.; Velegol, D.; Xia, T.; Hoek, E. M. V.; Somasundaran, P.; Klaessig, F.; Castranova, V.; Thompson, M. Understanding Biophysicochemical Interactions at the Nano-bio Interface. *Nat. Mater.* **2009**, *8* (7), 543-557.
35. Ma, H.; Liu, J.; Ali, M. M.; Mahmood, M. A. I.; Labanieh, L.; Lu, M.; Iqbal, S. M.; Zhang, Q.; Zhao, W.; Wan, Y. Nucleic Acid Aptamers in Cancer Research, Diagnosis and Therapy. *Chem. Soc. Rev.* **2015**, *44* (5), 1240-1256.
36. Becerril, H. A.; Woolley, A. T. DNA-Templated Nanofabrication. *Chem. Soc. Rev.* **2009**, *38* (2), 329-337.
37. Saha, K.; Agasti, S. S.; Kim, C.; Li, X.; Rotello, V. M. Gold Nanoparticles in Chemical and Biological Sensing. *Chem. Rev.* **2012**, *112* (5), 2739-2779.
38. Mirkin, C. A.; Letsinger, R. L.; Mucic, R. C.; Storhoff, J. J. A DNA-Based Method for Rationally Assembling Nanoparticles into Macroscopic Materials. *Nature* **1996**, *382* (6592), 607-609.

39. Alivisatos, A. P.; Johnsson, K. P.; Peng, X.; Wilson, T. E.; Loweth, C. J.; Bruchez, M. P.; Schultz, P. G. Organization of 'Nanocrystal Molecules' Using DNA. *Nature* **1996**, *382* (6592), 609-611.
40. Hurst, S. J.; Lytton-Jean, A. K. R.; Mirkin, C. A. Maximizing DNA Loading on a Range of Gold Nanoparticle Sizes. *Anal. Chem.* **2006**, *78* (24), 8313-8318.
41. Hill, H. D.; Millstone, J. E.; Banholzer, M. J.; Mirkin, C. A. The Role Radius of Curvature Plays in Thiolated Oligonucleotide Loading on Gold Nanoparticles. *ACS Nano* **2009**, *3* (2), 418-424.
42. Li, J.; Zhu, B.; Zhu, Z.; Zhang, Y.; Yao, X.; Tu, S.; Liu, R.; Jia, S.; Yang, C. J. Simple and Rapid Functionalization of Gold Nanorods with Oligonucleotides Using an mPEG-SH/Tween 20-Assisted Approach. *Langmuir* **2015**, *31* (28), 7869-7876.
43. Zhang, X.; Servos, M. R.; Liu, J. Instantaneous and Quantitative Functionalization of Gold Nanoparticles with Thiolated DNA Using a pH-Assisted and Surfactant-Free Route. *J. Am. Chem. Soc.* **2012**, *134* (17), 7266-7269.
44. Shi, D.; Song, C.; Jiang, Q.; Wang, Z.-G.; Ding, B. A Facile and Efficient Method to Modify Gold Nanorods with Thiolated DNA at a Low pH Value. *Chem. Commun.* **2013**, *49* (25), 2533-2535.
45. Zhang, X.; Servos, M. R.; Liu, J. Fast pH-Assisted Functionalization of Silver Nanoparticles with Monothiolated DNA. *Chem. Commun.* **2012**, *48* (81), 10114-10116.
46. Li, H.; Rothberg, L. Colorimetric Detection of DNA Sequences Based on Electrostatic Interactions with Unmodified Gold nanoparticles. *Proc. Natl. Acad. Sci. U. S. A.* **2004**, *101* (39), 14036-14039.

47. Li, H.; Rothberg, L. J. Label-Free Colorimetric Detection of Specific Sequences in Genomic DNA Amplified by the Polymerase Chain Reaction. *J. Am. Chem. Soc.* **2004**, *126* (35), 10958-10961.
48. Rosi, N. L.; Giljohann, D. A.; Thaxton, C. S.; Lytton-Jean, A. K. R.; Han, M. S.; Mirkin, C. A. Oligonucleotide-Modified Gold Nanoparticles for Intracellular Gene Regulation. *Science* **2006**, *312* (5776), 1027-1030.
49. Lytton-Jean, A. K. R.; Mirkin, C. A. A Thermodynamic Investigation into the Binding Properties of DNA Functionalized Gold Nanoparticle Probes and Molecular Fluorophore Probes. *J. Am. Chem. Soc.* **2005**, *127* (37), 12754-12755.
50. Jin, R.; Wu, G.; Li, Z.; Mirkin, C. A.; Schatz, G. C. What Controls the Melting Properties of DNA-Linked Gold Nanoparticle Assemblies? *J. Am. Chem. Soc.* **2003**, *125* (6), 1643-1654.
51. Rosi, N. L.; Mirkin, C. A. Nanostructures in Biodiagnostics. *Chem. Rev.* **2005**, *105* (4), 1547-1562.
52. Cutler, J. I.; Auyeung, E.; Mirkin, C. A. Spherical Nucleic Acids. *J. Am. Chem. Soc.* **2012**, *134* (3), 1376-1391.
53. Chithrani, B. D.; Ghazani, A. A.; Chan, W. C. W. Determining the Size and Shape Dependence of Gold Nanoparticle Uptake into Mammalian Cells. *Nano Lett.* **2006**, *6* (4), 662-668.
54. Giljohann, D. A.; Seferos, D. S.; Patel, P. C.; Millstone, J. E.; Rosi, N. L.; Mirkin, C. A. Oligonucleotide Loading Determines Cellular Uptake of DNA-Modified Gold Nanoparticles. *Nano Lett.* **2007**, *7* (12), 3818-3821.

55. Zheng, D.; Giljohann, D. A.; Chen, D. L.; Massich, M. D.; Wang, X.-Q.; Iordanov, H.; Mirkin, C. A.; Paller, A. S. Topical Delivery of siRNA-based Spherical Nucleic Acid Nanoparticle Conjugates for Gene Regulation. *Proc. Natl. Acad. Sci. U. S. A.* **2012**, *109* (30), 11975-11980.
56. Cutler, J. I.; Zheng, D.; Xu, X.; Giljohann, D. A.; Mirkin, C. A. Polyvalent Oligonucleotide Iron Oxide Nanoparticle “Click” Conjugates. *Nano Lett.* **2010**, *10* (4), 1477-1480.
57. Cutler, J. I.; Zhang, K.; Zheng, D.; Auyeung, E.; Prigodich, A. E.; Mirkin, C. A. Polyvalent Nucleic Acid Nanostructures. *J. Am. Chem. Soc.* **2011**, *133* (24), 9254-9257.
58. Demers, L. M.; Östblom, M.; Zhang, H.; Jang, N.-H.; Liedberg, B.; Mirkin, C. A. Thermal Desorption Behavior and Binding Properties of DNA Bases and Nucleosides on Gold. *J. Am. Chem. Soc.* **2002**, *124* (38), 11248-11249.
59. Östblom, M.; Liedberg, B.; Demers, L. M.; Mirkin, C. A. On the Structure and Desorption Dynamics of DNA Bases Adsorbed on Gold: A Temperature-Programmed Study. *J. Phys. Chem. B* **2005**, *109* (31), 15150-15160.
60. Zhang, X.; Servos, M. R.; Liu, J. Surface Science of DNA Adsorption onto Citrate-Capped Gold Nanoparticles. *Langmuir* **2012**, *28* (8), 3896-3902.
61. Zhang, X.; Liu, B.; Servos, M. R.; Liu, J. Polarity Control for Nonthiolated DNA Adsorption onto Gold Nanoparticles. *Langmuir* **2013**, *29* (20), 6091-6098.
62. Nelson, E. M.; Rothberg, L. J. Kinetics and Mechanism of Single-Stranded DNA Adsorption onto Citrate-Stabilized Gold Nanoparticles in Colloidal Solution. *Langmuir* **2011**, *27* (5), 1770-1777.

63. Pei, H.; Li, F.; Wan, Y.; Wei, M.; Liu, H.; Su, Y.; Chen, N.; Huang, Q.; Fan, C. Designed Diblock Oligonucleotide for the Synthesis of Spatially Isolated and Highly Hybridizable Functionalization of DNA–Gold Nanoparticle Nanoconjugates. *J. Am. Chem. Soc.* **2012**, *134* (29), 11876-11879.
64. Liu, B.; Kelly, E. Y.; Liu, J. Cation-Size-Dependent DNA Adsorption Kinetics and Packing Density on Gold Nanoparticles: An Opposite Trend. *Langmuir* **2014**, *30* (44), 13228-13234.
65. Zhu, Y.; Jiang, X.; Wang, H.; Wang, S.; Wang, H.; Sun, B.; Su, Y.; He, Y. A Poly Adenine-Mediated Assembly Strategy for Designing Surface-Enhanced Resonance Raman Scattering Substrates in Controllable Manners. *Anal. Chem.* **2015**, *87* (13), 6631-6638.
66. Solanki, P. R.; Kaushik, A.; Agrawal, V. V.; Malhotra, B. D. Nanostructured Metal Oxide-Based Biosensors. *NPG Asia Mater.* **2011**, *3*, 17-24.
67. Scherer, F.; Anton, M.; Schillinger, U.; Henke, J.; Bergemann, C.; Kruger, A.; Gansbacher, B.; Plank, C. Magnetofection: Enhancing and Targeting Gene Delivery by Magnetic Force in Vitro and in Vivo. *Gene Ther.* **2002**, *9* (2), 102-109.
68. He, X.-x.; Wang, K.; Tan, W.; Liu, B.; Lin, X.; He, C.; Li, D.; Huang, S.; Li, J. Bioconjugated Nanoparticles for DNA Protection from Cleavage. *J. Am. Chem. Soc.* **2003**, *125* (24), 7168-7169.
69. Frey, N. A.; Peng, S.; Cheng, K.; Sun, S. Magnetic Nanoparticles: Synthesis, Functionalization, and Applications in Bioimaging and Magnetic Energy Storage. *Chem. Soc. Rev.* **2009**, *38* (9), 2532-2542.

70. Paunesku, T.; Rajh, T.; Wiederrecht, G.; Maser, J.; Vogt, S.; Stojicevic, N.; Protic, M.; Lai, B.; Oryhon, J.; Thurnauer, M.; Woloschak, G. Biology of TiO₂-Oligonucleotide Nanocomposites. *Nat. Mater.* **2003**, *2* (5), 343-346.
71. Ye, Q.; Zhou, F.; Liu, W. Bioinspired Catecholic Chemistry for Surface Modification. *Chem. Soc. Rev.* **2011**, *40* (7), 4244-4258.
72. Paunesku, T.; Vogt, S.; Lai, B.; Maser, J.; Stojićević, N.; Thurn, K. T.; Osipo, C.; Liu, H.; Legnini, D.; Wang, Z.; Lee, C.; Woloschak, G. E. Intracellular Distribution of TiO₂-DNA Oligonucleotide Nanoconjugates Directed to Nucleolus and Mitochondria Indicates Sequence Specificity. *Nano Lett.* **2007**, *7* (3), 596-601.
73. Armistead, P. M.; Thorp, H. H. Modification of Indium Tin Oxide Electrodes with Nucleic Acids: Detection of Attomole Quantities of Immobilized DNA by Electrocatalysis. *Anal. Chem.* **2000**, *72* (16), 3764-3770.
74. Armistead, P. M.; Thorp, H. H. Oxidation Kinetics of Guanine in DNA Molecules Adsorbed onto Indium Tin Oxide Electrodes. *Anal. Chem.* **2001**, *73* (3), 558-564.
75. Yang, I. V.; Thorp, H. H. Modification of Indium Tin Oxide Electrodes with Repeat Polynucleotides: Electrochemical Detection of Trinucleotide Repeat Expansion. *Anal. Chem.* **2001**, *73* (21), 5316-5322.
76. Liu, S.-Q.; Xu, J.-J.; Chen, H.-Y. A Reversible Adsorption-Desorption Interface of DNA Based on Nano-sized Zirconia and its Application. *Colloids Surf., B* **2004**, *36* (3-4), 155-159.
77. Solanki, P. R.; Kaushik, A.; Chavhan, P. M.; Maheshwari, S. N.; Malhotra, B. D. Nanostructured Zirconium Oxide Based Genosensor for Escherichia coli Detection. *Electrochem. Commun.* **2009**, *11* (12), 2272-2277.

78. Das, M.; Sumana, G.; Nagarajan, R.; Malhotra, B. D. Zirconia Based Nucleic Acid Sensor for Mycobacterium tuberculosis Detection. *Appl. Phys. Lett.* **2010**, *96* (13), 133703.
79. Zhang, X.; Wang, F.; Liu, B.; Kelly, E. Y.; Servos, M. R.; Liu, J. Adsorption of DNA Oligonucleotides by Titanium Dioxide Nanoparticles. *Langmuir* **2014**, *30* (3), 839-845.
80. Song, C.; Wang, G.-Y.; Kong, D.-M. A Facile Fluorescence Method for Versatile Biomolecular Detection Based on Pristine α -Fe₂O₃ Nanoparticle-Induced Fluorescence Quenching. *Biosens. Bioelectron.* **2015**, *68*, 239-244.
81. Yu, J.; Yang, L.; Liang, X.; Dong, T.; Liu, H. Bare Magnetic Nanoparticles as Fluorescence Quenchers for Detection of Thrombin. *Analyst* **2015**, *140* (12), 4114-4120.
82. Yuan, Y.; Wu, S.; Shu, F.; Liu, Z. An MnO₂ Nanosheet as a Label-Free Nanoplatfrom for Homogeneous Biosensing. *Chem. Commun.* **2014**, *50* (9), 1095-1097.
83. Suzuki, H.; Amano, T.; Toyooka, T.; Ibuki, Y. Preparation of DNA-Adsorbed TiO₂ Particles with High Performance for Purification of Chemical Pollutants. *Environ. Sci. Technol.* **2008**, *42* (21), 8076-8082.
84. Pautler, R.; Kelly, E. Y.; Huang, P.-J. J.; Cao, J.; Liu, B.; Liu, J. Attaching DNA to Nanoceria: Regulating Oxidase Activity and Fluorescence Quenching. *ACS Appl. Mater. Interfaces* **2013**, *5* (15), 6820-6825.
85. Fan, H.; Zhao, Z.; Yan, G.; Zhang, X.; Yang, C.; Meng, H.; Chen, Z.; Liu, H.; Tan, W. A Smart DNAzyme-MnO₂ Nanosystem for Efficient Gene Silencing. *Angew. Chem. Int. Ed.* **2015**, *54* (16), 4801-4805.
86. Ali, I. New Generation Adsorbents for Water Treatment. *Chem. Rev.* **2012**, *112* (10), 5073-5091.

87. Hua, M.; Zhang, S.; Pan, B.; Zhang, W.; Lv, L.; Zhang, Q. Heavy Metal Removal from Water/Wastewater by Nanosized Metal Oxides: A Review. *J. Hazard. Mater.* **2012**, *211–212*, 317-331.
88. Mohan, D.; Pittman Jr, C. U. Arsenic Removal from Water/Wastewater Using Adsorbents: A Critical Review. *J. Hazard. Mater.* **2007**, *142* (1–2), 1-53.
89. Pena, M. E.; Korfiatis, G. P.; Patel, M.; Lippincott, L.; Meng, X. Adsorption of As(V) and As(III) by Nanocrystalline Titanium Dioxide. *Water Res.* **2005**, *39* (11), 2327-2337.
90. Zheng, Y.-M.; Yu, L.; Wu, D.; Paul Chen, J. Removal of Arsenite from Aqueous Solution by a Zirconia Nanoparticle. *Chem. Eng. J. (Lausanne)* **2012**, *188*, 15-22.
91. Hristovski, K.; Baumgardner, A.; Westerhoff, P. Selecting Metal Oxide Nanomaterials for Arsenic Removal in Fixed Bed Columns: From Nanopowders to Aggregated Nanoparticle Media. *J. Hazard. Mater.* **2007**, *147* (1–2), 265-274.
92. Mandal, B. K.; Suzuki, K. T. Arsenic Round the World: A Review. *Talanta* **2002**, *58* (1), 201-235.
93. Shen, S.; Li, X.-F.; Cullen, W. R.; Weinfeld, M.; Le, X. C. Arsenic Binding to Proteins. *Chem. Rev.* **2013**, *113* (10), 7769-7792.
94. Charoensuk, V.; Gati, W. P.; Weinfeld, M.; Le, X. C. Differential Cytotoxic Effects of Arsenic Compounds in Human Acute Promyelocytic Leukemia Cells. *Toxicol. Appl. Pharmacol.* **2009**, *239* (1), 64-70.
95. Cohen, S. M.; Ohnishi, T.; Arnold, L. L.; Le, X. C. Arsenic-Induced Bladder Cancer in an Animal Model. *Toxicol. Appl. Pharmacol.* **2007**, *222* (3), 258-263.

96. Smedley, P. L.; Kinniburgh, D. G. A Review of the Source, Behaviour and Distribution of Arsenic in Natural Waters. *Appl. Geochem.* **2002**, *17* (5), 517-568.
97. Le, X. C.; Lu, X.; Li, X.-F. Arsenic Speciation. *Anal. Chem.* **2004**, *76* (1), 26A-33A.
98. Yan, X.-P.; Kerrich, R.; Hendry, M. J. Distribution of Arsenic(III), Arsenic(V) and Total Inorganic Arsenic in Porewaters from a Thick Till and Clay-rich Aquitard Sequence, Saskatchewan, Canada. *Geochim. Cosmochim. Acta* **2000**, *64* (15), 2637-2648.
99. Pierce, M. L.; Moore, C. B. Adsorption of Arsenite on Amorphous Iron Hydroxide from Dilute Aqueous Solution. *Environ. Sci. Technol.* **1980**, *14* (2), 214-216.
100. Pierce, M. L.; Moore, C. B. Adsorption of Arsenite and Arsenate on Amorphous Iron Hydroxide. *Water Res.* **1982**, *16* (7), 1247-1253.
101. Raven, K. P.; Jain, A.; Loeppert, R. H. Arsenite and Arsenate Adsorption on Ferrihydrite: Kinetics, Equilibrium, and Adsorption Envelopes. *Environ. Sci. Technol.* **1998**, *32* (3), 344-349.
102. Mayo, J. T.; Yavuz, C.; Yean, S.; Cong, L.; Shiple, H.; Yu, W.; Falkner, J.; Kan, A.; Tomson, M.; Colvin, V. L. The Effect of Nanocrystalline Magnetite Size on Arsenic Removal. *Sci. Technol. Adv. Mater.* **2007**, *8* (1-2), 71-75.
103. Boujelben, N.; Bouzid, J.; Elouear, Z.; Feki, M. Retention of Nickel from Aqueous Solutions using Iron Oxide and Manganese Oxide Coated Sand: Kinetic and Thermodynamic Studies. *Environ. Technol.* **2010**, *31* (14), 1623-1634.
104. Eren, E. Removal of Lead Ions by Unye (Turkey) Bentonite in Iron and Magnesium Oxide-Coated Forms. *J. Hazard. Mater.* **2009**, *165* (1-3), 63-70.

105. Han, R.; Zou, W.; Li, H.; Li, Y.; Shi, J. Copper(II) and Lead(II) Removal from Aqueous Solution in Fixed-bed Columns by Manganese Oxide Coated Zeolite. *J. Hazard. Mater.* **2006**, *137* (2), 934-942.
106. Yang, J.; Zhang, H.; Yu, M.; Emmanuelawati, I.; Zou, J.; Yuan, Z.; Yu, C. High-Content, Well-Dispersed γ -Fe₂O₃ Nanoparticles Encapsulated in Macroporous Silica with Superior Arsenic Removal Performance. *Adv. Funct. Mater.* **2014**, *24* (10), 1354-1363.
107. Manning, B. A.; Fendorf, S. E.; Goldberg, S. Surface Structures and Stability of Arsenic(III) on Goethite: Spectroscopic Evidence for Inner-Sphere Complexes. *Environ. Sci. Technol.* **1998**, *32* (16), 2383-2388.
108. Goldberg, S.; Johnston, C. T. Mechanisms of Arsenic Adsorption on Amorphous Oxides Evaluated Using Macroscopic Measurements, Vibrational Spectroscopy, and Surface Complexation Modeling. *J. Colloid Interface Sci.* **2001**, *234* (1), 204-216.
109. Fendorf, S.; Eick, M. J.; Grossl, P.; Sparks, D. L. Arsenate and Chromate Retention Mechanisms on Goethite. 1. Surface Structure. *Environ. Sci. Technol.* **1997**, *31* (2), 315-320.
110. Liu, C.-H.; Chuang, Y.-H.; Chen, T.-Y.; Tian, Y.; Li, H.; Wang, M.-K.; Zhang, W. Mechanism of Arsenic Adsorption on Magnetite Nanoparticles from Water: Thermodynamic and Spectroscopic Studies. *Environ. Sci. Technol.* **2015**, *49* (13), 7726-7734.
111. Waychunas, G. A.; Rea, B. A.; Fuller, C. C.; Davis, J. A. Surface Chemistry of Ferrihydrite: Part 1. EXAFS Studies of the Geometry of Coprecipitated and Adsorbed Arsenate. *Geochim. Cosmochim. Acta* **1993**, *57* (10), 2251-2269.

112. Lumsdon, D. G.; Fraser, A. R.; Russell, J. D.; Livesey, N. T. New Infrared Band Assignments for the Arsenate Ion Adsorbed on Synthetic Goethite (α -FeOOH). *Journal of Soil Science* **1984**, *35* (3), 381-386.
113. Jain, A.; Loeppert, R. H. Effect of Competing Anions on the Adsorption of Arsenate and Arsenite by Ferrihydrite. *J. Environ. Qual.* **2000**, *29* (5).
114. Qi, P.; Pichler, T. Closer Look at As(III) and As(V) Adsorption onto Ferrihydrite under Competitive Conditions. *Langmuir* **2014**, *30* (37), 11110-11116.
115. Frau, F.; Addari, D.; Atzei, D.; Biddau, R.; Cidu, R.; Rossi, A. Influence of Major Anions on As(V) Adsorption by Synthetic 2-line Ferrihydrite. Kinetic Investigation and XPS Study of the Competitive Effect of Bicarbonate. *Water Air and Soil Pollution* **2010**, *205* (1-4), 25-41.
116. Manning, B. A.; Goldberg, S. Modeling Competitive Adsorption of Arsenate with Phosphate and Molybdate on Oxide Minerals. *Soil Sci. Soc. Am. J.* **1996**, *60* (1).
117. Hingston, F. J.; Posner, A. M.; Quirk, J. P. Competitive Adsorption of Negatively Charged Ligands on Oxide Surfaces. *Discuss. Faraday Soc.* **1971**, *52* (0), 334-342.
118. Gao, Y.; Mucci, A. Individual and Competitive Adsorption of Phosphate and Arsenate on Goethite in Artificial Seawater. *Chem. Geol.* **2003**, *199* (1-2), 91-109.
119. Liu, F.; De Cristofaro, A.; Violante, A. Effect of pH, Phosphate and Oxalate on the Adsorption/Desorption of Arsenate on/from Goethite. *Soil Sci.* **2001**, *166* (3), 197-208.
120. Zeng, H.; Fisher, B.; Giammar, D. E. Individual and Competitive Adsorption of Arsenate and Phosphate To a High-Surface-Area Iron Oxide-Based Sorbent. *Environ. Sci. Technol.* **2008**, *42* (1), 147-152.

121. Lin, Y.; Ren, J.; Qu, X. Catalytically Active Nanomaterials: A Promising Candidate for Artificial Enzymes. *Acc. Chem. Res.* **2014**, *47* (4), 1097-1105.
122. Wei, H.; Wang, E. Nanomaterials with Enzyme-Like Characteristics (nanozymes): Next-generation Artificial Enzymes. *Chem. Soc. Rev.* **2013**, *42* (14), 6060-6093.
123. Celardo, I.; Pedersen, J. Z.; Traversa, E.; Ghibelli, L. Pharmacological Potential of Cerium Oxide Nanoparticles. *Nanoscale* **2011**, *3* (4), 1411-1420.
124. Comotti, M.; Della Pina, C.; Matarrese, R.; Rossi, M. The Catalytic Activity of “Naked” Gold Particles. *Angew. Chem. Int. Ed.* **2004**, *43* (43), 5812-5815.
125. Luo, W.; Zhu, C.; Su, S.; Li, D.; He, Y.; Huang, Q.; Fan, C. Self-Catalyzed, Self-Limiting Growth of Glucose Oxidase-Mimicking Gold Nanoparticles. *ACS Nano* **2010**, *4* (12), 7451-7458.
126. Gao, L.; Zhuang, J.; Nie, L.; Zhang, J.; Zhang, Y.; Gu, N.; Wang, T.; Feng, J.; Yang, D.; Perrett, S.; Yan, X. Intrinsic Peroxidase-Like Activity of Ferromagnetic Nanoparticles. *Nat. Nanotechnol.* **2007**, *2* (9), 577-583.
127. Asati, A.; Santra, S.; Kaittanis, C.; Nath, S.; Perez, J. M. Oxidase-Like Activity of Polymer-Coated Cerium Oxide Nanoparticles. *Angew. Chem. Int. Ed.* **2009**, *121* (13), 2344-2348.
128. Dong, J.; Song, L.; Yin, J.-J.; He, W.; Wu, Y.; Gu, N.; Zhang, Y. Co₃O₄ Nanoparticles with Multi-Enzyme Activities and Their Application in Immunohistochemical Assay. *ACS Appl. Mater. Interfaces* **2014**, *6* (3), 1959-1970.
129. Ragg, R.; Natalio, F.; Tahir, M. N.; Janssen, H.; Kashyap, A.; Strand, D.; Strand, S.; Tremel, W. Molybdenum Trioxide Nanoparticles with Intrinsic Sulfite Oxidase Activity. *ACS Nano* **2014**, *8* (5), 5182-5189.

130. Song, Y.; Qu, K.; Zhao, C.; Ren, J.; Qu, X. Graphene Oxide: Intrinsic Peroxidase Catalytic Activity and Its Application to Glucose Detection. *Adv. Mater.* **2010**, *22* (19), 2206-2210.
131. Song, Y.; Wang, X.; Zhao, C.; Qu, K.; Ren, J.; Qu, X. Label-Free Colorimetric Detection of Single Nucleotide Polymorphism by Using Single-Walled Carbon Nanotube Intrinsic Peroxidase-Like Activity. *Chem. – Eur. J.* **2010**, *16* (12), 3617-3621.
132. Tokuyama, H.; Yamago, S.; Nakamura, E.; Shiraki, T.; Sugiura, Y. Photoinduced Biochemical Activity of Fullerene Carboxylic Acid. *J. Am. Chem. Soc.* **1993**, *115* (17), 7918-7919.
133. Dugan, L. L.; Gabrielsen, J. K.; Yu, S. P.; Lin, T.-S.; Choi, D. W. Buckminsterfullerenol Free Radical Scavengers Reduce Excitotoxic and Apoptotic Death of Cultured Cortical Neurons. *Neurobiol. Dis.* **1996**, *3* (2), 129-135.
134. Dugan, L. L.; Turetsky, D. M.; Du, C.; Lobner, D.; Wheeler, M.; Almlı, C. R.; Shen, C. K.-F.; Luh, T.-Y.; Choi, D. W.; Lin, T.-S. Carboxyfullerenes as Neuroprotective Agents. *Proc. Natl. Acad. Sci. U. S. A.* **1997**, *94* (17), 9434-9439.
135. Cui, R.; Han, Z.; Zhu, J.-J. Helical Carbon Nanotubes: Intrinsic Peroxidase Catalytic Activity and Its Application for Biocatalysis and Biosensing. *Chem. – Eur. J.* **2011**, *17* (34), 9377-9384.
136. Goran, J. M.; Phan, E. N. H.; Favela, C. A.; Stevenson, K. J. H₂O₂ Detection at Carbon Nanotubes and Nitrogen-Doped Carbon Nanotubes: Oxidation, Reduction, or Disproportionation? *Anal. Chem.* **2015**, *87* (12), 5989-5996.

137. Song, Y.; Chen, Y.; Feng, L.; Ren, J.; Qu, X. Selective and Quantitative Cancer Cell Detection Using Target-Directed Functionalized Graphene and its Synergetic Peroxidase-like Activity. *Chem. Commun.* **2011**, *47* (15), 4436-4438.
138. Liu, M.; Zhao, H.; Chen, S.; Yu, H.; Quan, X. Stimuli-Responsive Peroxidase Mimicking at a Smart Graphene Interface. *Chem. Commun.* **2012**, *48* (56), 7055-7057.
139. Xu, C.; Zhao, C.; Li, M.; Wu, L.; Ren, J.; Qu, X. Artificial Evolution of Graphene Oxide Chemzyme with Enantioselectivity and Near-Infrared Photothermal Effect for Cascade Biocatalysis Reactions. *Small* **2014**, *10* (9), 1841-1847.
140. Zhao, R.; Zhao, X.; Gao, X. Molecular-Level Insights into Intrinsic Peroxidase-Like Activity of Nanocarbon Oxides. *Chem. – Eur. J.* **2015**, *21* (3), 960-964.
141. Shi, W.; Wang, Q.; Long, Y.; Cheng, Z.; Chen, S.; Zheng, H.; Huang, Y. Carbon Nanodots as Peroxidase Mimetics and their Applications to Glucose Detection. *Chem. Commun.* **2011**, *47* (23), 6695-6697.
142. Pasquato, L.; Rancan, F.; Scrimin, P.; Mancin, F.; Frigeri, C. N-Methylimidazole-Functionalized Gold Nanoparticles as Catalysts for Cleavage of a Carboxylic Acid Ester. *Chem. Commun.* **2000**, (22), 2253-2254.
143. Manea, F.; Houillon, F. B.; Pasquato, L.; Scrimin, P. Nanozymes: Gold-Nanoparticle-Based Transphosphorylation Catalysts. *Angew. Chem. Int. Ed.* **2004**, *43* (45), 6165-6169.
144. Pengo, P.; Polizzi, S.; Pasquato, L.; Scrimin, P. Carboxylate–Imidazole Cooperativity in Dipeptide-Functionalized Gold Nanoparticles with Esterase-like Activity. *J. Am. Chem. Soc.* **2005**, *127* (6), 1616-1617.

145. Pengo, P.; Baltzer, L.; Pasquato, L.; Scrimin, P. Substrate Modulation of the Activity of an Artificial Nanoesterase Made of Peptide-Functionalized Gold Nanoparticles. *Angew. Chem. Int. Ed.* **2007**, *46* (3), 400-404.
146. Bonomi, R.; Selvestrel, F.; Lombardo, V.; Sissi, C.; Polizzi, S.; Mancin, F.; Tonellato, U.; Scrimin, P. Phosphate Diester and DNA Hydrolysis by a Multivalent, Nanoparticle-Based Catalyst. *J. Am. Chem. Soc.* **2008**, *130* (47), 15744-15745.
147. Wan, Y.; Qi, P.; Zhang, D.; Wu, J.; Wang, Y. Manganese Oxide Nanowire-Mediated Enzyme-Linked Immunosorbent Assay. *Biosens. Bioelectron.* **2012**, *33* (1), 69-74.
148. Zhang, X.; Huang, Y. Evaluation of the Antioxidant Activity of Phenols and Tannic Acid Determination with Mn₃O₄ Nano-octahedrons as an Oxidase Mimic. *Anal. Methods* **2015**, *7* (20), 8640-8646.
149. Zhang, X.; He, S.; Chen, Z.; Huang, Y. CoFe₂O₄ Nanoparticles as Oxidase Mimic-Mediated Chemiluminescence of Aqueous Luminol for Sulfite in White Wines. *J. Agric. Food Chem.* **2013**, *61* (4), 840-847.
150. Wei, H.; Wang, E. Fe₃O₄ Magnetic Nanoparticles as Peroxidase Mimetics and Their Applications in H₂O₂ and Glucose Detection. *Anal. Chem.* **2008**, *80* (6), 2250-2254.
151. Jiang, Z.; Kun, L.; Ouyang, H.; Liang, A.; Jiang, H. A Simple and Sensitive Fluorescence Quenching Method for the Determination of H₂O₂ Using Rhodamine B and Fe₃O₄ Nanocatalyst. *J. Fluoresc.* **2011**, *21* (5), 2015-2020.
152. Duan, D.; Fan, K.; Zhang, D.; Tan, S.; Liang, M.; Liu, Y.; Zhang, J.; Zhang, P.; Liu, W.; Qiu, X.; Kobinger, G. P.; Fu Gao, G.; Yan, X. Nanozyme-Strip for Rapid Local Diagnosis of Ebola. *Biosens. Bioelectron.* **2015**, *74*, 134-141.

153. Gao, L.; Giglio, K. M.; Nelson, J. L.; Sondermann, H.; Travis, A. J. Ferromagnetic Nanoparticles with Peroxidase-like Activity Enhance the Cleavage of Biological Macromolecules for Biofilm Elimination. *Nanoscale* **2014**, *6* (5), 2588-2593.
154. Natalio, F.; Andre, R.; Hartog, A. F.; Stoll, B.; Jochum, K. P.; Wever, R.; Tremel, W. Vanadium Pentoxide Nanoparticles Mimic Vanadium Haloperoxidases and Thwart Biofilm Formation. *Nat. Nanotechnol.* **2012**, *7* (8), 530-535.
155. Winterbourn, C. C. Reconciling the Chemistry and Biology of Reactive Oxygen Species. *Nat. Chem. Biol.* **2008**, *4* (5), 278-286.
156. Korsvik, C.; Patil, S.; Seal, S.; Self, W. T. Superoxide Dismutase Mimetic Properties Exhibited by Vacancy Engineered Ceria Nanoparticles. *Chem. Commun.* **2007**, (10), 1056-1058.
157. Pirmohamed, T.; Dowding, J. M.; Singh, S.; Wasserman, B.; Heckert, E.; Karakoti, A. S.; King, J. E. S.; Seal, S.; Self, W. T. Nanoceria Exhibit Redox State-Dependent Catalase Mimetic Activity. *Chem. Commun.* **2010**, *46* (16), 2736-2738.
158. Tarnuzzer, R. W.; Colon, J.; Patil, S.; Seal, S. Vacancy Engineered Ceria Nanostructures for Protection from Radiation-Induced Cellular Damage. *Nano Lett.* **2005**, *5* (12), 2573-2577.
159. Chen, Z.; Yin, J.-J.; Zhou, Y.-T.; Zhang, Y.; Song, L.; Song, M.; Hu, S.; Gu, N. Dual Enzyme-like Activities of Iron Oxide Nanoparticles and Their Implication for Diminishing Cytotoxicity. *ACS Nano* **2012**, *6* (5), 4001-4012.
160. Zhang, Y.; Wang, Z.; Li, X.; Wang, L.; Yin, M.; Wang, L.; Chen, N.; Fan, C.; Song, H. Dietary Iron Oxide Nanoparticles Delay Aging and Ameliorate Neurodegeneration in *Drosophila*. *Adv. Mater.* **2016**, *28* (7), 1387-1393.

161. Mu, J.; Zhang, L.; Zhao, M.; Wang, Y. Co₃O₄ Nanoparticles as an Efficient Catalase Mimic: Properties, Mechanism and its Electrocatalytic Sensing Application for Hydrogen Peroxide. *J. Mol. Catal. A: Chem.* **2013**, *378* (0), 30-37.
162. Mu, J.; Zhang, L.; Zhao, M.; Wang, Y. Catalase Mimic Property of Co₃O₄ Nanomaterials with Different Morphology and Its Application as a Calcium Sensor. *ACS Appl. Mater. Interfaces* **2014**, *6* (10), 7090-7098.
163. Liang, M.; Fan, K.; Pan, Y.; Jiang, H.; Wang, F.; Yang, D.; Lu, D.; Feng, J.; Zhao, J.; Yang, L.; Yan, X. Fe₃O₄ Magnetic Nanoparticle Peroxidase Mimetic-Based Colorimetric Assay for the Rapid Detection of Organophosphorus Pesticide and Nerve Agent. *Anal. Chem.* **2013**, *85* (1), 308-312.
164. Chaudhari, K. N.; Chaudhari, N. K.; Yu, J.-S. Peroxidase Mimic Activity of Hematite Iron Oxides (α -Fe₂O₃) with Different Nanostructures. *Catal. Sci. Technol.* **2012**, *2* (1), 119-124.
165. Mu, J.; Wang, Y.; Zhao, M.; Zhang, L. Intrinsic Peroxidase-Like Activity and Catalase-Like Activity of Co₃O₄ Nanoparticles. *Chem. Commun.* **2012**, *48* (19), 2540-2542.
166. Chen, W.; Chen, J.; Feng, Y.-B.; Hong, L.; Chen, Q.-Y.; Wu, L.-F.; Lin, X.-H.; Xia, X.-H. Peroxidase-like Activity of Water-soluble Cupric Oxide Nanoparticles and its Analytical Application for Detection of Hydrogen Peroxide and Glucose. *Analyst* **2012**, *137* (7), 1706-1712.
167. Shi, W.; Zhang, X.; He, S.; Huang, Y. CoFe₂O₄ Magnetic Nanoparticles as a Peroxidase Mimic Mediated Chemiluminescence for Hydrogen Peroxide and Glucose. *Chem. Commun.* **2011**, *47* (38), 10785-10787.

168. Perez, J. M.; Asati, A.; Nath, S.; Kaittanis, C. Synthesis of Biocompatible Dextran-Coated Nanoceria with pH-Dependent Antioxidant Properties. *Small* **2008**, *4* (5), 552-556.
169. Hirst, S. M.; Karakoti, A. S.; Tyler, R. D.; Sriranganathan, N.; Seal, S.; Reilly, C. M. Anti-inflammatory Properties of Cerium Oxide Nanoparticles. *Small* **2009**, *5* (24), 2848-2856.
170. Karakoti, A. S.; Singh, S.; Kumar, A.; Malinska, M.; Kuchibhatla, S. V. N. T.; Wozniak, K.; Self, W. T.; Seal, S. PEGylated Nanoceria as Radical Scavenger with Tunable Redox Chemistry. *J. Am. Chem. Soc.* **2009**, *131* (40), 14144-14145.
171. Mandoli, C.; Pagliari, F.; Pagliari, S.; Forte, G.; Di Nardo, P.; Licoccia, S.; Traversa, E. Stem Cell Aligned Growth Induced by CeO₂ Nanoparticles in PLGA Scaffolds with Improved Bioactivity for Regenerative Medicine. *Adv. Funct. Mater.* **2010**, *20* (10), 1617-1624.
172. Celardo, I.; De Nicola, M.; Mandoli, C.; Pedersen, J. Z.; Traversa, E.; Ghibelli, L. Ce³⁺ Ions Determine Redox-Dependent Anti-apoptotic Effect of Cerium Oxide Nanoparticles. *ACS Nano* **2011**, *5* (6), 4537-4549.
173. Ornatska, M.; Sharpe, E.; Andreescu, D.; Andreescu, S. Paper Bioassay Based on Ceria Nanoparticles as Colorimetric Probes. *Anal. Chem.* **2011**, *83* (11), 4273-4280.
174. Muhammad, F.; Wang, A.; Qi, W.; Zhang, S.; Zhu, G. Intracellular Antioxidants Dissolve Man-Made Antioxidant Nanoparticles: Using Redox Vulnerability of Nanoceria to Develop a Responsive Drug Delivery System. *ACS Appl. Mater. Interfaces* **2014**, *6* (21), 19424-19433.

175. Vernekar, A. A.; Das, T.; Mugesh, G. Vacancy-Engineered Nanocerium: Enzyme Mimetic Hotspots for the Degradation of Nerve Agents. *Angew. Chem. Int. Ed.* **2016**, *55* (4), 1412-1416.
176. Wang, H.; Yang, R.; Yang, L.; Tan, W. Nucleic Acid Conjugated Nanomaterials for Enhanced Molecular Recognition. *ACS Nano* **2009**, *3* (9), 2451-2460.
177. Song, S.; Qin, Y.; He, Y.; Huang, Q.; Fan, C.; Chen, H.-Y. Functional Nanoprobes for Ultrasensitive Detection of Biomolecules. *Chem. Soc. Rev.* **2010**, *39* (11), 4234-4243.
178. Zhao, W.; Brook, M. A.; Li, Y. Design of Gold Nanoparticle-Based Colorimetric Biosensing Assays. *ChemBioChem* **2008**, *9* (15), 2363-2371.
179. Giljohann, D. A.; Seferos, D. S.; Daniel, W. L.; Massich, M. D.; Patel, P. C.; Mirkin, C. A. Gold Nanoparticles for Biology and Medicine. *Angew. Chem. Int. Ed.* **2010**, *49* (19), 3280-3294.
180. Park, S. Y.; Lytton-Jean, A. K. R.; Lee, B.; Weigand, S.; Schatz, G. C.; Mirkin, C. A. DNA-Programmable Nanoparticle Crystallization. *Nature* **2008**, *451* (7178), 553-556.
181. Nykypanchuk, D.; Maye, M. M.; van der Lelie, D.; Gang, O. DNA-Guided Crystallization of Colloidal Nanoparticles. *Nature* **2008**, *451* (7178), 549-552.
182. Katz, E.; Willner, I. Integrated Nanoparticle-Biomolecule Hybrid Systems: Synthesis, Properties, and Applications. *Angew. Chem. Int. Ed.* **2004**, *43* (45), 6042-6108.
183. Cheng, W.; Campolongo, M. J.; Cha, J. J.; Tan, S. J.; Umbach, C. C.; Muller, D. A.; Luo, D. Free-standing Nanoparticle Superlattice Sheets Controlled by DNA. *Nat. Mater.* **2009**, *8* (6), 519-525.
184. Pinheiro, A. V.; Han, D.; Shih, W. M.; Yan, H. Challenges and Opportunities for Structural DNA Nanotechnology. *Nat. Nanotechnol.* **2011**, *6* (12), 763-772.

185. Lu, Y.; Liu, J. Smart Nanomaterials Inspired by Biology: Dynamic Assembly of Error-Free Nanomaterials in Response to Multiple Chemical and Biological Stimuli. *Acc. Chem. Res.* **2007**, *40* (5), 315-323.
186. Mitchell, G. P.; Mirkin, C. A.; Letsinger, R. L. Programmed Assembly of DNA Functionalized Quantum Dots. *J. Am. Chem. Soc.* **1999**, *121* (35), 8122-8123.
187. Lu, C.-H.; Yang, H.-H.; Zhu, C.-L.; Chen, X.; Chen, G.-N. A Graphene Platform for Sensing Biomolecules. *Angew. Chem. Int. Ed.* **2009**, *48* (26), 4785-4787.
188. Liu, B.; Sun, Z.; Zhang, X.; Liu, J. Mechanisms of DNA Sensing on Graphene Oxide. *Anal. Chem.* **2013**, *85* (16), 7987-7993.
189. Zhang, X.; Liu, B.; Dave, N.; Servos, M. R.; Liu, J. Instantaneous Attachment of an Ultrahigh Density of Nonthiolated DNA to Gold Nanoparticles and Its Applications. *Langmuir* **2012**, *28* (49), 17053-17060.
190. Liu, H.; Avrutin, V.; Izyumskaya, N.; Özgür, Ü.; Morkoç, H. Transparent Conducting Oxides for Electrode Applications in Light Emitting and Absorbing Devices. *Superlattices Microstruct.* **2010**, *48* (5), 458-484.
191. Paleček, E.; Bartošík, M. Electrochemistry of Nucleic Acids. *Chem. Rev.* **2012**, *112* (6), 3427-3481.
192. Zhao, W.-W.; Xu, J.-J.; Chen, H.-Y. Photoelectrochemical DNA Biosensors. *Chem. Rev.* **2014**, *114* (15), 7421-7441.
193. Gao, Z.; Tansil, N. C. An Ultrasensitive Photoelectrochemical Nucleic Acid Biosensor. *Nucleic Acids Res.* **2005**, *33* (13), e123.
194. Wei, X.; Ma, X.; Sun, J.-j.; Lin, Z.; Guo, L.; Qiu, B.; Chen, G. DNA Methylation Detection and Inhibitor Screening Based on the Discrimination of the Aggregation of Long

- and Short DNA on a Negatively Charged Indium Tin Oxide Microelectrode. *Anal. Chem.* **2014**, *86* (7), 3563-3567.
195. Patel, M. K.; Singh, J.; Singh, M. K.; Agrawal, V. V.; Ansari, S. G.; Malhotra, B. D. Tin Oxide Quantum Dot Based DNA Sensor for Pathogen Detection. *J. Nanosci. Nanotechnol.* **2013**, *13* (3), 1671-1678.
196. Lee, J.; Lee, S.; Li, G.; Petruska, M. A.; Paine, D. C.; Sun, S. A Facile Solution-Phase Approach to Transparent and Conducting ITO Nanocrystal Assemblies. *J. Am. Chem. Soc.* **2012**, *134* (32), 13410-13414.
197. Fan, Y.; Chen, X.; Kong, J.; Tung, C.-h.; Gao, Z. Direct Detection of Nucleic Acids by Tagging Phosphates on Their Backbones with Conductive Nanoparticles. *Angew. Chem.* **2007**, *119* (12), 2097-2100.
198. He, S.; Song, B.; Li, D.; Zhu, C.; Qi, W.; Wen, Y.; Wang, L.; Song, S.; Fang, H.; Fan, C. A Graphene Nanoprobe for Rapid, Sensitive, and Multicolor Fluorescent DNA Analysis. *Adv. Funct. Mater.* **2010**, *20* (3), 453-459.
199. Miller, W. H.; Schipper, H. M.; Lee, J. S.; Singer, J.; Waxman, S. Mechanisms of Action of Arsenic Trioxide. *Cancer Res.* **2002**, *62* (14), 3893-3903.
200. Le, X. C.; Ma, M. S.; Wong, N. A. Speciation of Arsenic Compounds Using High-Performance Liquid Chromatography at Elevated Temperature and Selective Hydride Generation Atomic Fluorescence Detection. *Anal. Chem.* **1996**, *68* (24), 4501-4506.
201. Welz, B.; Sucmanova, M. L-Cysteine as a Reducing and Releasing Agent for the Determination of Antimony and Arsenic using Flow Injection Hydride Generation Atomic Absorption Spectrometry-Part 1. Optimization of the Analytical Parameters. *Analyst* **1993**, *118* (11), 1417-1423.

202. Larsen, E. H.; Sturup, S. Carbon-Enhanced Inductively Coupled Plasma Mass Spectrometric Detection of Arsenic and Selenium and its Application to Arsenic Speciation. *J. Anal. At. Spectrom.* **1994**, *9* (10), 1099-1105.
203. Li, C.; Basaran, A. E.; Tyson, J. F. Determination of Inorganic Arsenic in Water by a Quartz Crystal Microbalance. *Anal. Methods* **2013**, *5* (22), 6286-6291.
204. Dai, X.; Compton, R. G. Detection of As(III) via Oxidation to As(V) Using Platinum Nanoparticle Modified Glassy Carbon Electrodes: Arsenic Detection without Interference from Copper. *Analyst* **2006**, *131* (4), 516-521.
205. Yogarajah, N.; Tsai, S. S. H. Detection of Trace Arsenic in Drinking Water: Challenges and Opportunities for Microfluidics. *Environ. Sci.: Water Res. Technol.* **2015**, *1* (4), 426-447.
206. Merulla, D.; Buffi, N.; Beggah, S.; Truffer, F.; Geiser, M.; Renaud, P.; van der Meer, J. R. Bioreporters and Biosensors for Arsenic Detection. Biotechnological Solutions for a World-wide Pollution Problem. *Curr. Opin. Biotechnol.* **2013**, *24* (3), 534-541.
207. Sanllorente-Mendez, S.; DomÁnguez-Renedo, O.; Arcos-MartÁñez, M. J. Immobilization of Acetylcholinesterase on Screen-Printed Electrodes. Application to the Determination of Arsenic(III). *Sensors* **2010**, *10* (3), 2119-2128.
208. Fuku, X.; Iftikar, F.; Hess, E.; Iwuoha, E.; Baker, P. Cytochrome c Biosensor for Determination of Trace Levels of Cyanide and Arsenic Compounds. *Anal. Chim. Acta* **2012**, *730* (0), 49-59.
209. Davis, S. N.; DeWiest, R. J. M. *Hydrogeology*; John Wiley & Sons, Inc.: New York, 1966.

210. Yang, R.; Jin, J.; Chen, Y.; Shao, N.; Kang, H.; Xiao, Z.; Tang, Z.; Wu, Y.; Zhu, Z.; Tan, W. Carbon Nanotube-Quenched Fluorescent Oligonucleotides: Probes that Fluoresce upon Hybridization. *J. Am. Chem. Soc.* **2008**, *130* (26), 8351-8358.
211. Maxwell, D. J.; Taylor, J. R.; Nie, S. Self-Assembled Nanoparticle Probes for Recognition and Detection of Biomolecules. *J. Am. Chem. Soc.* **2002**, *124* (32), 9606-9612.
212. Liu, J.; Brown, A. K.; Meng, X.; Cropek, D. M.; Istok, J. D.; Watson, D. B.; Lu, Y. A Catalytic Beacon Sensor for Uranium with Parts-per-trillion Sensitivity and Millionfold Selectivity. *Proc. Natl. Acad. Sci. U. S. A.* **2007**, *104* (7), 2056-2061.
213. Nutiu, R.; Li, Y. Structure-Switching Signaling Aptamers. *J. Am. Chem. Soc.* **2003**, *125* (16), 4771-4778.
214. Yang, C. J.; Lin, H.; Tan, W. Molecular Assembly of Superquenchers in Signaling Molecular Interactions. *J. Am. Chem. Soc.* **2005**, *127* (37), 12772-12773.
215. Dey, B.; Mukherjee, P.; Mondal, R. K.; Chattopadhyay, A. P.; Hauli, I.; Mukhopadhyay, S. K.; Fleck, M. Femtomolar Level Sensing of Inorganic Arsenic(III) in Water and in Living-Systems Using a Non-toxic Fluorescent Probe. *Chem. Commun.* **2014**, *50* (96), 15263-15266.
216. Mulvihill, M.; Tao, A.; Benjauthrit, K.; Arnold, J.; Yang, P. Surface-Enhanced Raman Spectroscopy for Trace Arsenic Detection in Contaminated Water. *Angew. Chem. Int. Ed.* **2008**, *47* (34), 6456-6460.
217. Kalluri, J. R.; Arbnesi, T.; Afrin Khan, S.; Neely, A.; Candice, P.; Varisli, B.; Washington, M.; McAfee, S.; Robinson, B.; Banerjee, S.; Singh, A. K.; Senapati, D.; Ray, P. C. Use of Gold Nanoparticles in a Simple Colorimetric and Ultrasensitive Dynamic

Light Scattering Assay: Selective Detection of Arsenic in Groundwater. *Angew. Chem. Int. Ed.* **2009**, *48* (51), 9668-9671.

218. Zhang, X.-B.; Kong, R.-M.; Lu, Y. Metal Ion Sensors Based on DNAzymes and Related DNA Molecules. *Annu. Rev. Anal. Chem.* **2011**, *4* (1), 105-128.

219. Kim, M.; Um, H. J.; Bang, S.; Lee, S. H.; Oh, S. J.; Han, J. H.; Kim, K. W.; Min, J.; Kim, Y. H. Arsenic Removal from Vietnamese Groundwater Using the Arsenic-Binding DNA Aptamer. *Environ. Sci. Technol.* **2009**, *43* (24), 9335-9340.

220. Wu, Y.; Zhan, S.; Xing, H.; He, L.; Xu, L.; Zhou, P. Nanoparticles Assembled by Aptamers and Crystal Violet for Arsenic(III) Detection in Aqueous Solution Based on a Resonance Rayleigh Scattering Spectral Assay. *Nanoscale* **2012**, *4* (21), 6841-6849.

221. Li, D.; Song, S.; Fan, C. Target-Responsive Structural Switching for Nucleic Acid-Based Sensors. *Acc. Chem. Res.* **2010**, *43* (5), 631-641.

222. Katz, E.; Willner, I. Nanobiotechnology: Integrated Nanoparticle-Biomolecule Hybrid Systems: Synthesis, Properties, and Applications. *Angew. Chem. Int. Ed.* **2004**, *43* (45), 6042-6108.

223. Tan, W.; Donovan, M. J.; Jiang, J. Aptamers from Cell-Based Selection for Bioanalytical Applications. *Chem. Rev.* **2013**, *113* (4), 2842-2862.

224. Li, F.; Pei, H.; Wang, L.; Lu, J.; Gao, J.; Jiang, B.; Zhao, X.; Fan, C. Nanomaterial-Based Fluorescent DNA Analysis: A Comparative Study of the Quenching Effects of Graphene Oxide, Carbon Nanotubes, and Gold Nanoparticles. *Adv. Funct. Mater.* **2013**, *23* (33), 4140-4148.

225. Liu, B.; Liu, J. DNA Adsorption by Indium Tin Oxide Nanoparticles. *Langmuir* **2015**, *31* (1), 371-377.

226. Liu, B.; Liu, J. DNA Adsorption by Magnetic Iron Oxide Nanoparticles and Its Application for Arsenate Detection. *Chem. Commun.* **2014**, *50* (62), 8568-8570.
227. Liu, B.; Sun, Z.; Huang, P.-J. J.; Liu, J. Hydrogen Peroxide Displacing DNA from Nanoceria: Mechanism and Detection of Glucose in Serum. *J. Am. Chem. Soc.* **2015**, *137* (3), 1290-1295.
228. Feuillie, C.; Sverjensky, D. A.; Hazen, R. M. Attachment of Ribonucleotides on α -Alumina as a Function of pH, Ionic Strength, and Surface Loading. *Langmuir* **2015**, *31* (1), 240-248.
229. Fahrenkopf, N. M.; Rice, P. Z.; Bergkvist, M.; Deskins, N. A.; Cady, N. C. Immobilization Mechanisms of Deoxyribonucleic Acid (DNA) to Hafnium Dioxide (HfO₂) Surfaces for Biosensing Applications. *ACS Appl. Mater. Interfaces* **2012**, *4* (10), 5360-5368.
230. Diehl, K. L.; Anslyn, E. V. Array Sensing using Optical Methods for Detection of Chemical and Biological Hazards. *Chem. Soc. Rev.* **2013**, *42* (22), 8596-8611.
231. Clancy, T. M.; Hayes, K. F.; Raskin, L. Arsenic Waste Management: A Critical Review of Testing and Disposal of Arsenic-Bearing Solid Wastes Generated during Arsenic Removal from Drinking Water. *Environ. Sci. Technol.* **2013**, *47* (19), 10799-10812.
232. Warwick, C.; Guerreiro, A.; Soares, A. Sensing and Analysis of Soluble Phosphates in Environmental Samples: A Review. *Biosens. Bioelectron.* **2013**, *41*, 1-11.
233. Rakow, N. A.; Suslick, K. S. A Colorimetric Sensor Array for Odour Visualization. *Nature* **2000**, *406* (6797), 710-713.

234. Carey, J. R.; Suslick, K. S.; Hulkower, K. I.; Imlay, J. A.; Imlay, K. R. C.; Ingison, C. K.; Ponder, J. B.; Sen, A.; Wittrig, A. E. Rapid Identification of Bacteria with a Disposable Colorimetric Sensing Array. *J. Am. Chem. Soc.* **2011**, *133* (19), 7571-7576.
235. De, M.; Rana, S.; Akpınar, H.; Miranda, O. R.; Arvizo, R. R.; Bunz, U. H. F.; Rotello, V. M. Sensing of Proteins in Human Serum Using Conjugates of Nanoparticles and Green Fluorescent Protein. *Nat. Chem.* **2009**, *1* (6), 461-465.
236. Tan, S. S.; Kim, S. J.; Kool, E. T. Differentiating between Fluorescence-Quenching Metal Ions with Polyfluorophore Sensors Built on a DNA Backbone. *J. Am. Chem. Soc.* **2011**, *133* (8), 2664-2671.
237. Kwon, H.; Jiang, W.; Kool, E. T. Pattern-Based Detection of Anion Pollutants in Water with DNA Polyfluorophores. *Chem. Sci.* **2015**, *6* (4), 2575-2583.
238. Tao, Y.; Ran, X.; Ren, J.; Qu, X. Array-Based Sensing of Proteins and Bacteria By Using Multiple Luminescent Nanodots as Fluorescent Probes. *Small* **2014**, *10* (18), 3667-3671.
239. Pei, H.; Li, J.; Lv, M.; Wang, J.; Gao, J.; Lu, J.; Li, Y.; Huang, Q.; Hu, J.; Fan, C. A Graphene-Based Sensor Array for High-Precision and Adaptive Target Identification with Ensemble Aptamers. *J. Am. Chem. Soc.* **2012**, *134* (33), 13843-13849.
240. Ran, X.; Pu, F.; Ren, J.; Qu, X. A CuS-Based Chemical Tongue Chip for Pattern Recognition of Proteins and Antibiotic-Resistant Bacteria. *Chem. Commun.* **2015**, *51* (13), 2675-2678.
241. Zhang, H.; Ji, Z.; Xia, T.; Meng, H.; Low-Kam, C.; Liu, R.; Pokhrel, S.; Lin, S.; Wang, X.; Liao, Y.-P.; Wang, M.; Li, L.; Rallo, R.; Damoiseaux, R.; Telesca, D.; Mädler, L.; Cohen, Y.; Zink, J. I.; Nel, A. E. Use of Metal Oxide Nanoparticle Band Gap To

Develop a Predictive Paradigm for Oxidative Stress and Acute Pulmonary Inflammation. *ACS Nano* **2012**, *6* (5), 4349-4368.

242. Koziej, D.; Lauria, A.; Niederberger, M. 25th Anniversary Article: Metal Oxide Particles in Materials Science: Addressing All Length Scales. *Adv. Mater.* **2014**, *26* (2), 235-257.

243. Herne, T. M.; Tarlov, M. J. Characterization of DNA Probes Immobilized on Gold Surfaces. *J. Am. Chem. Soc.* **1997**, *119* (38), 8916-8920.

244. Tu, X.; Manohar, S.; Jagota, A.; Zheng, M. DNA Sequence Motifs for Structure-Specific Recognition and Separation of Carbon Nanotubes. *Nature* **2009**, *460* (7252), 250-253.

245. Lin, Y.; Xu, C.; Ren, J.; Qu, X. Using Thermally Regenerable Cerium Oxide Nanoparticles in Biocomputing to Perform Label-free, Resettable, and Colorimetric Logic Operations. *Angew. Chem. Int. Ed.* **2012**, *51* (50), 12579-12583.

246. Xu, C.; Liu, Z.; Wu, L.; Ren, J.; Qu, X. Nucleoside Triphosphates as Promoters to Enhance Nanoceria Enzyme-like Activity and for Single-Nucleotide Polymorphism Typing. *Adv. Funct. Mater.* **2014**, *24* (11), 1624-1630.

247. Xu, C.; Qu, X. Cerium Oxide Nanoparticle: a Remarkably Versatile Rare Earth Nanomaterial for Biological Applications. *NPG Asia Mater.* **2014**, *6*, e90.

248. Ujjain, S. K.; Das, A.; Srivastava, G.; Ahuja, P.; Roy, M.; Arya, A.; Bhargava, K.; Sethy, N.; Singh, S. K.; Sharma, R. K.; Das, M. Nanoceria Based Electrochemical Sensor for Hydrogen Peroxide Detection. *Biointerphases* **2014**, *9* (3), 031011.

249. Peng, Y.; Chen, X.; Yi, G.; Gao, Z. Mechanism of the Oxidation of Organic Dyes in the Presence of Nanoceria. *Chem. Commun.* **2011**, *47* (10), 2916-2918.

250. Chen, J.; Patil, S.; Seal, S.; McGinnis, J. F. Rare Earth Nanoparticles Prevent Retinal Degeneration Induced by Intracellular Peroxides. *Nat. Nanotechnol.* **2006**, *1* (2), 142-150.
251. Menchón, C.; Martín, R.; Apostolova, N.; Victor, V. M.; Álvaro, M.; Herance, J. R.; García, H. Gold Nanoparticles Supported on Nanoparticulate Ceria as a Powerful Agent against Intracellular Oxidative Stress. *Small* **2012**, *8* (12), 1895-1903.
252. Lee, S. S.; Song, W. S.; Cho, M. J.; Puppala, H. L.; Nguyen, P.; Zhu, H. G.; Segatori, L.; Colvin, V. L. Antioxidant Properties of Cerium Oxide Nanocrystals as a Function of Nanocrystal Diameter and Surface Coating. *ACS Nano* **2013**, *7* (11), 9693-9703.
253. Rhee, S. G. H₂O₂, a Necessary Evil for Cell Signaling. *Science* **2006**, *312* (5782), 1882-1883.
254. Gomes, A.; Fernandes, E.; Lima, J. L. F. C. Fluorescence Probes Used for Detection of Reactive Oxygen Species. *J. Biochem. Biophys. Methods* **2005**, *65* (2-3), 45-80.
255. Lippert, A. R.; Van de Bittner, G. C.; Chang, C. J. Boronate Oxidation as a Bioorthogonal Reaction Approach for Studying the Chemistry of Hydrogen Peroxide in Living Systems. *Acc. Chem. Res.* **2011**, *44* (9), 793-804.
256. Hayat, A.; Andreescu, D.; Bulbul, G.; Andreescu, S. Redox Reactivity of Cerium Oxide Nanoparticles Against Dopamine. *J. Colloid Interface Sci.* **2014**, *418*, 240-245.
257. Lang, N. J.; Liu, B.; Liu, J. Characterization of Glucose Oxidation by Gold Nanoparticles Using Nanoceria. *J. Colloid Interface Sci.* **2014**, *428* (0), 78-83.
258. Xue, Y.; Zhai, Y. W.; Zhou, K. B.; Wang, L.; Tan, H. N.; Luan, Q. F.; Yao, X. The Vital Role of Buffer Anions in the Antioxidant Activity of CeO₂ Nanoparticles. *Chem.--Eur. J.* **2012**, *18* (35), 11115-11122.

259. Cafun, J.-D.; Kvashnina, K. O.; Casals, E.; Puentes, V. F.; Glatzel, P. Absence of Ce³⁺ Sites in Chemically Active Colloidal Ceria Nanoparticles. *ACS Nano* **2013**, *7* (12), 10726-10732.
260. Sardesai, N. P.; Andreescu, D.; Andreescu, S. Electroanalytical Evaluation of Antioxidant Activity of Cerium Oxide Nanoparticles by Nanoparticle Collisions at Microelectrodes. *J. Am. Chem. Soc.* **2013**, *135* (45), 16770-16773.
261. Wang, G.-C.; Sung, H. H. Y.; Williams, I. D.; Leung, W.-H. Tetravalent Titanium, Zirconium, and Cerium Oxo and Peroxo Complexes Containing an Imidodiphosphate Ligand. *Inorg. Chem.* **2012**, *51* (6), 3640-3647.
262. McCormack, R. N.; Mendez, P.; Barkam, S.; Neal, C. J.; Das, S.; Seal, S. Inhibition of Nanoceria's Catalytic Activity due to Ce³⁺ Site-Specific Interaction with Phosphate Ions. *J. Phys. Chem. C* **2014**, *118* (33), 18992-19006.
263. Dong, Y.-l.; Zhang, H.-g.; Rahman, Z. U.; Su, L.; Chen, X.-j.; Hu, J.; Chen, X.-g. Graphene Oxide-Fe₃O₄ Magnetic Nanocomposites with Peroxidase-like Activity for Colorimetric Detection of Glucose. *Nanoscale* **2012**, *4* (13), 3969-3976.
264. Yu, F.; Huang, Y.; Cole, A. J.; Yang, V. C. The Artificial Peroxidase Sctivity of Magnetic Iron Oxide Nanoparticles and its Application to Glucose Detection. *Biomaterials* **2009**, *30* (27), 4716-4722.
265. Zhang, X.-Q.; Gong, S.-W.; Zhang, Y.; Yang, T.; Wang, C.-Y.; Gu, N. Prussian Blue Modified Iron Oxide Magnetic Nanoparticles and their High Peroxidase-like Activity. *J. Mater. Chem.* **2010**, *20* (24), 5110-5116.
266. Liu, S.; Lu, F.; Xing, R.; Zhu, J.-J. Structural Effects of Fe₃O₄ Nanocrystals on Peroxidase-Like Activity. *Chem. – Eur. J.* **2011**, *17* (2), 620-625.

267. Storhoff, J. J.; Mirkin, C. A. Programmed Materials Synthesis with DNA. *Chem. Rev.* **1999**, *99* (7), 1849-1862.
268. Park, K. S.; Kim, M. I.; Cho, D.-Y.; Park, H. G. Label-Free Colorimetric Detection of Nucleic Acids Based on Target-Induced Shielding Against the Peroxidase-Mimicking Activity of Magnetic Nanoparticles. *Small* **2011**, *7* (11), 1521-1525.
269. Yang, K.-A.; Barbu, M.; Halim, M.; Pallavi, P.; Kim, B.; Kolpashchikov, D. M.; Pecic, S.; Taylor, S.; Worgall, T. S.; Stojanovic, M. N. Recognition and Sensing of Low-Epitope Targets via Ternary Complexes with Oligonucleotides and Synthetic Receptors. *Nat. Chem.* **2014**, *6* (11), 1003-1008.
270. Lin, Y.; Wu, L.; Huang, Y.; Ren, J.; Qu, X. Positional assembly of hemin and gold nanoparticles in graphene-mesoporous silica nanohybrids for tandem catalysis. *Chem. Sci.* **2015**, *6* (2), 1272-1276.
271. Coffey, J. L.; Bigham, S. R.; Pinizzotto, R. F.; Yang, H. Characterization of Quantum-Confined CdS Nanocrystallites Stabilized by Deoxyribonucleic Acid (DNA). *Nanotechnology* **1992**, *3* (2), 69.
272. Houlton, A.; Pike, A. R.; Angel Galindo, M.; Horrocks, B. R. DNA-based Routes to Semiconducting Nanomaterials. *Chem. Commun.* **2009**, (14), 1797-1806.
273. Petia, A.; Weitz, R. T.; Peter, G.; Vesna, S.; Peter, K.; Peter, A. v. A.; Marko, B.; Joachim, B. DNA-Templated Synthesis of ZnO Thin Layers and Nanowires. *Nanotechnology* **2009**, *20* (36), 365302.